Understanding the Influence of Side Reactions during Electrochemical CO2 Reduction

Yang, K.

DOI
10.4233/uuid:19555603-433b-4207-8ba6-f6a83dd68d8d

Publication date
2022

Document Version
Final published version

Citation (APA)
Yang, K. (2022). *Understanding the Influence of Side Reactions during Electrochemical CO2 Reduction*. [Dissertation (TU Delft), Delft University of Technology]. https://doi.org/10.4233/uuid:19555603-433b-4207-8ba6-f6a83dd68d8d

Important note
To cite this publication, please use the final published version (if applicable).
Please check the document version above.

Understanding the Influence of Side Reactions during Electrochemical CO_2 Reduction

Understanding the Influence of Side Reactions during Electrochemical CO_2 Reduction

Proefschrift

ter verkrijging van de graad van doctor
aan de Technische Universiteit Delft,
op gezag van de Rector Magnificus
Prof.dr.ir. T.H.J.J. van der Hagen,
voorzitter van het College voor Promoties,
in het openbaar te verdedigen op 21 maart 2022 om 15:00 uur

door

Kailun YANG

Master of Engineering in Applied Chemistry,
Renmin University of China, China,
Geboren te Handan, China.

Dit proefschrift is goedgekeurd door de

promotor: Dr. W.A. Smith
copromotor: Dr. T. Burdyny

Samenstelling promotiecommissie:

Rector Magnificus	voorzitter
Dr. W.A. Smith	Technische Universiteit Delft, promotor
Dr. T. Burdyny	Technische Universiteit Delft, copromotor

Onafhankelijke leden:

Prof.dr. B. Dam	Technische Universiteit Delft
Dr. C.T. Dinh	Queen's University, Canada
Dr. C. Janáky	University of Szeged, Hungary
Dr. S. Haussener	École Polytechnique Fédérale de Lausanne, Switzerland
Prof.dr. A. Urakawa	Technische Universiteit Delft, reservelid

The work described in this thesis was carried out in the Materials for Energy Conversion and Storage (MECS) group, Department of Chemical Engineering, Faculty of Applied Sciences, Delft University of Technology. This work was funded by China Scholarship Council.

Printed by: Ridderprint | www.ridderprint.nl

Cover design by: uniquepixel

ISBN 978-94-6366-512-4

An electronic version of this dissertation is available at
http://repository.tudelft.nl/.

Contents

1

Introduction

"If all the insects were to disappear from the earth, within fifty years all life on earth would end. If all human beings disappeared from the earth, within fifty years all forms of life would flourish." - Jonas Salk

1.1. Negative emissions

The greenhouse effect has been a non-anthropogenic phenomenon that has warmed the earth throughout millions of years of history. However, the anthropogenic-driven greenhouse effects have accelerated in the past 200 hundred years, and now threaten humanity and the global ecosystem.[1, 2] As the largest part in the greenhouse gas compositions, carbon dioxide (CO_2) concentration has been increased from the pre-industrial level around 280 ppm to the current 410 ppm in the atmosphere. At present, the CO_2 equivalent greenhouse gas emission is around 51 billion tons annually (Figure 1.1).[3] Such excessive emis-

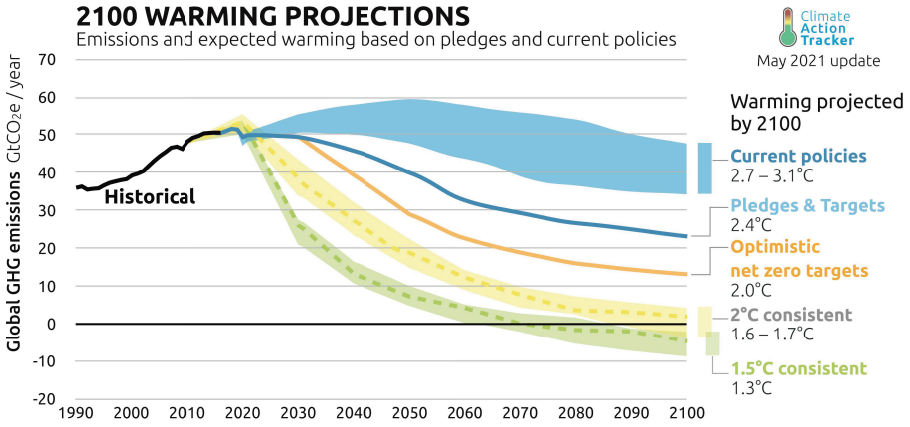

Figure 1.1: Emissions and expected warming based on pledges and current policies. [3].

1

sion is caused by burning of fossil fuels for energy, which humans have simultaneously heralded for numerous improvements in the quality of life and scientific advancements.

One of the major consequences of the over usage of fossil fuels is global warming. The global temperature has increased by around 1 degree Celsius compared to its pre-industrial period. The warming has caused regional and seasonal climate changes worldwide, resulting in natural disasters such as extreme weather, increase in sea level, droughts, floods, hurricanes, wildfires, extinction of spices, etc. Unfortunately, these effects do not come alone. They tend to come along with one or another, causing unbearable severe consequences across the entire planet.[4, 5]

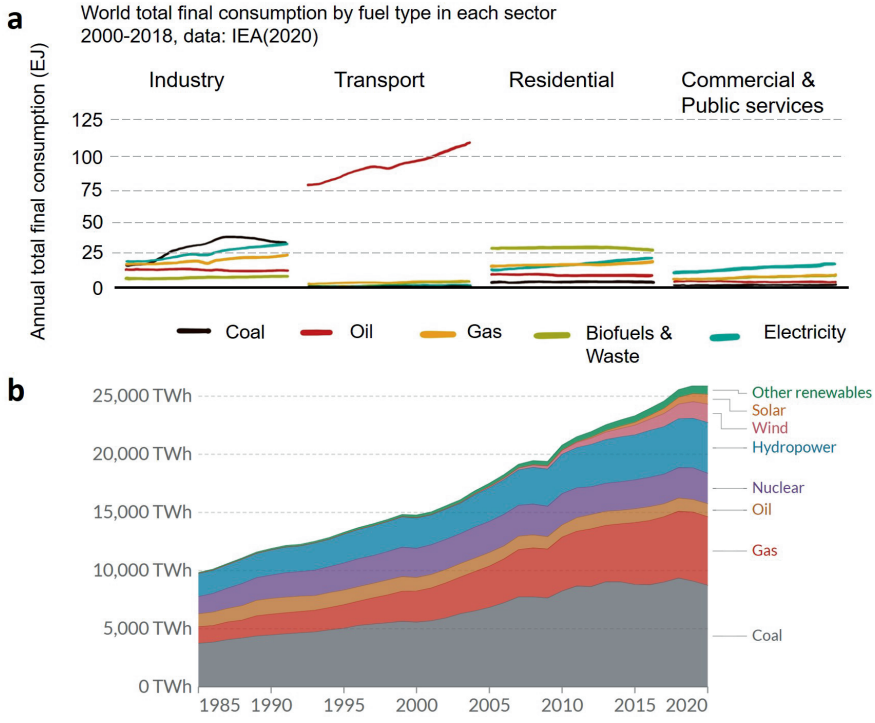

Figure 1.2: (a) World total final consumption by fuel type in each sector.[6] (b) World electricity production by source. Data based on BP Statistical Review of World Energy & Ember (2021). "Other renewables" includes biomass and waste, geothermal, wave and tidal.[7]

In the special IPCC report "Global Warming of 1.5°C ", it has been shown that such warming effect should be kept well below 1.5°C instead of previously predicted 2°C.[8] Going beyond 1.5°C is apparently gambling with earth's liveability, at the risk of lives of all the living creatures on earth.[9] As shown in Figure 1.1, with current policies, the emission would go above 60 billion tons per year, raising the global temperature by 2.7-3.1°C by 2100. With the target of "net zero", the temperature will increase by 2°C instead. However, our goal is to maintain

the temperature increase below 1.5°C to avoid reaching the critical point, which causes disasters and threatens the existence of lives. This means we not only need to cut down the emissions, but also to remove the already existing greenhouse gases from the atmosphere. "Net negative" is the only pathway we should take to save the life as we have come to know it in the past few hundred years.

Due to COVID-19 pandemic, global emissions dropped by around 5% in 2020.[4] However, this little drop is at the cost of the severe setback of the global economy and loss of millions of human lives. To reduce emissions in a sustainable way, we should work on two aspects simultaneously: (i) decarbonize traditional industrial sectors– using renewable energy instead of fossil fuels and (ii) decarbonize the atmosphere – removing the excess CO_2 in the air.

Figure 1.2(a) shows that the energy supplies in major sectors are still mostly based on coal, oil and natural gas, with electricity taking an increasingly important part.[6] It should be mentioned that the largest sources for electricity generation are still fossil fuels, which take about 60% (Figure 1.2(b)).[7] Meanwhile, electricity from renewable sources such as hydropower, wind, solar etc. only takes less than 30%. To decarbonize those sectors, the electricity should first come from renewable energy, then take over fossil fuels. Fortunately, with fast development and advances in science and technology, the cost of renewable energy has declined sharply since 2010 as shown in Figure 1.3.[10] In 2019, the price of electricity generated from onshore wind and solar photovoltaics can already compete with fossil fuel fired power plants, which is between \$0.05/kWh and \$0.18/kWh.

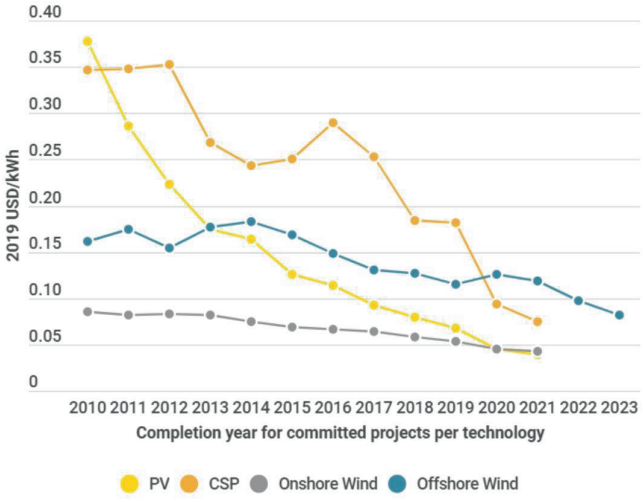

Figure 1.3: Power generation cost in 2019.[10]

Undoubtedly, fossil fuels are destined to totally be cut out from the electricity generation sector and replaced by renewable sources in the near future. Yet, it has far more implications than just on the electricity sector. Cheap and reliable renewable electricity can also power other energy-intensive sectors such as industry, transportation, residential, agricul-

1

ture etc. Electrifying every process possible is one of the most promising ways to complete the energy transition. Certainly, there are also drawbacks and challenges we should consider while proceeding with this path. Because of the seasonal and regional intermittency property of renewable energy sources, transmission and distribution of electricity are responsible for 1/3 of the final cost.[4] Thus transferring electricity and storing it in a more stable and safe chemical form is necessary and needs to be solved in urgent.

While taking the energy de-carbonation and transition path, focuses should be put on carbon removal, reuse and storage as well. As discussed above, "net negative" is the goal to cope with the global warming issue, not "net zero". Promising approaches for carbon removal and storage we have so far are: maintaining and restoring forests; building soil carbon in farms; bio-energy with carbon capture and storage; direct air capture; carbon mineralization or enhanced weathering; ocean based carbon removal concepts, etc.[11–13] It is worth mentioning that all these and other possible solutions to remove CO_2 from air should be developed in tandem to avoid catastrophic climate disasters.

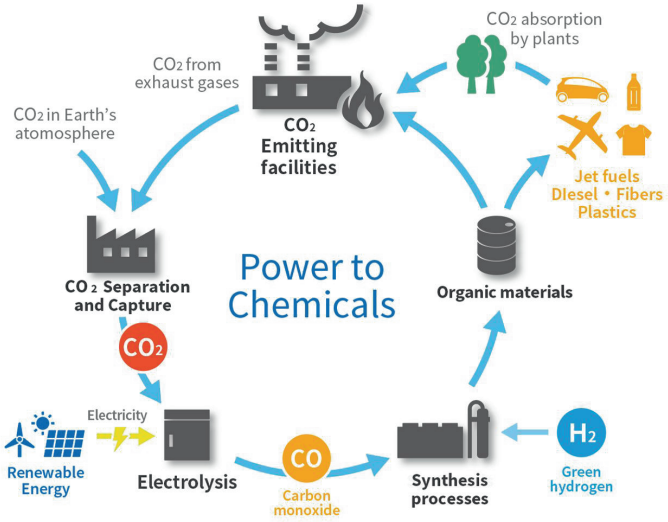

Figure 1.4: Pathways for CO_2 utilization and conversion.[14]

1.2. Energy conversion and storage by electrochemical CO_2 reduction

One approach which can solve renewable electricity storage together with CO_2 elimination issues simultaneously, has attracted considerable attentions in recent years – electrochemical CO_2 reduction (ECO2R) as shown in Figure 1.4.[14–20] It functions to reduce the CO_2 captured from point source or air directly, to chemicals or fuels, using the electricity from renewable energy.[21–26] The chemicals and fuels can be stored and transported more fea-

sibly than electricity. Once being consumed, CO_2 will be released to the atmosphere and later again captured. Thus the carbon cycle can be closed.

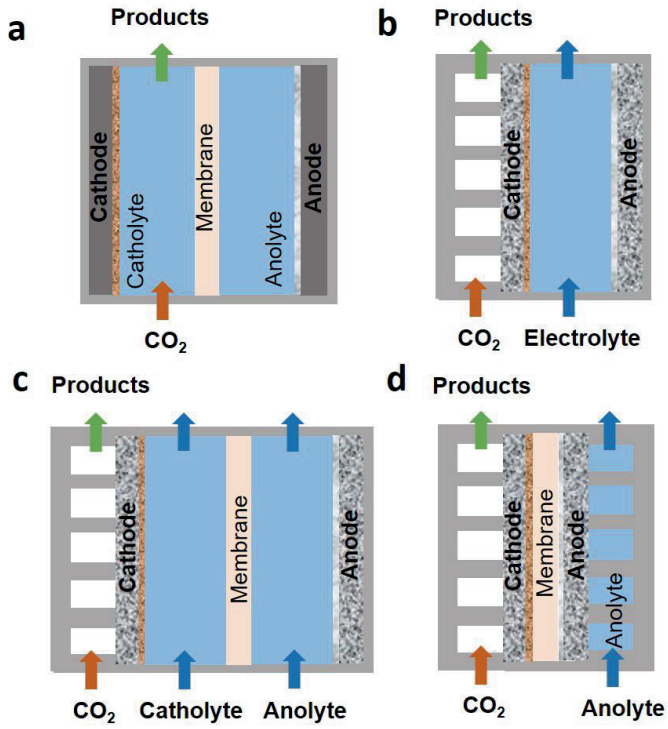

Figure 1.5: Schematic illustration of designs of (a) H-cell, (b) microfluidic cell, (c) gas diffusion flow cell and (d) membrane electrode assembly cell.

The electrochemical CO_2 reduction field has made major progress in the past decade.[27–29] Reactors employed for ECO2R have shifted from conventional liquid cells (Figure 1.5(a)) to gas diffusion electrodes based flow cells (Figure 1.5(b-c))and zero gap membrane electrode assemblies (Figure 1.5(d)). With science and technology advances in catalysts and reactors, the performance of ECO2R has been improved significantly. Activity has been improved by more than one order of magnitude over the past decade, with high selectivity and hundreds of hours stability.[30–34] Despite such improvement, ECO2R still faces lots of difficulties. There are two main challenges (i) competing hydrogen reduction reaction (HER) during ECO2R;[35–37] and (ii) high local pH caused by both ECO2R and HER, thus (bi)carbonate salt formation issue[38–42]. These two factors have imposed major obstacles in upgrading the performance of ECO2R electrolyzers, which need to be well understood and solved. In the next chapter, the theory of intrinsic property of ECO2R and HER, together with high local pH induced by these electrochemical reactions and salt formation issues will be introduced. Furthermore, their influences on current CO_2 electrolyzers, together with potential solutions to solve the challenges will be discussed.

1

1.3. Thesis outline

The organization of the thesis is given below.

Chapter 2 provides an overview of fundamentals in the electrochemical CO_2 reduction field, with focuses on addressing the competition between HER and ECO2R reactions, and high local pH induced (bi)carbonate formation issues. Following that, the effect of competing HER and (bi)carbonate precipitation on activity, selectivity, stability and energy efficiency are discussed in detail. Challenges and recent advances in solving the problems are also given. Note that the theory introduced is required to explain the presented technical chapters, and is not a full representation of the rapidly expanding field of CO_2 electrolysis.

Chapter 3 attempts to lower local pH and increase the local CO_2 concentration in an H-cell during ECO2R by using phosphate buffer solutions (K_2HPO_4: KH_2PO_4 = 1:1). In situ surface enhanced infrared absorption spectroscopy (SEIRAS) is used to measure the local pH during ECO2R, and a model is introduced to calculate and verify the results as well. Electrochemical ECO2R tests are conducted on smooth polycrystalline Cu and Cu nanowires respectively to measure the actual ECO2R performance in the highly buffered solution. SEIRAS, modelling and ECO2R tests all show that the local pH remains high (5 pH units higher than bulk pH) and local CO_2 concentration stays low, which leads to similar ECO2R activity in all buffer concentrations. This work emphasizes the competing effect of HER and ECO2R in a liquid cell, which unavoidably results in high local pH and low CO_2 concentration. It also addresses the importance of mass transport while interpreting kinetics and drawing mechanistic conclusions for electrochemical CO_2 reduction.

Chapter 4 investigates the well-recognized flooding issue in gas diffusion electrodes, especially for electrochemical CO_2 reduction purposes. We hypothesize that flooding is caused by the carbon based gas diffusion layer (GDL), which is relatively active for HER at the potential window where ECO2R happens. Electrochemical tests on different catalysts (Ag, Pt, Au ,Cu) coated carbon GDL and blank carbon GDL are performed in both CO_2 and N_2 atmosphere. This work shows that potential plays an extremely important role in causing flooding. Systematic design of catalysts and gas diffusion layers specifically for ECO2R purposes are necessary to achieve long stability while moving to gas diffusion electrodes for boosting activity.

Chapter 5 attempts to solve the low gaseous CO_2 utilization problem which has attracted major attention in the past 3 years. We try to neutralize local OH^- concentration by introducing protons to catalyst surface. This is achieved by using a membrane electrode assembly together with a bipolar membrane. However the competing effect between HER and ECO2R due to high proton concentration from membrane leads to primarily H_2 production in such a system. By promoting the cation available at the catalyst surface, CO_2 reduction can be more favoured over HER. Further comparing with anion exchange membrane in the cell shows that CO_2 parasitic loss has been decreased by around 5 times, and utilization efficiency is increased by 2-3 times. This work provides insights into engineering bipolar membrane to CO_2 electrolyzers with highly improved ECO2R activity and CO_2 gas utilization. Future studies on such system are encouraged to achieve higher energy efficiency.

This thesis is concluded by a summary of all the chapters mentioned above.

References

[1] Lindsey Rebecca and Dahlman LuAnn, *Climate change: Global temperature,* https://www.climate.gov/news-features/understanding-climate/climate-change-global-temperature (2021).

[2] M. Meinshausen, Z. R. J. Nicholls, J. Lewis, M. J. Gidden, E. Vogel, M. Freund, U. Beyerle, C. Gessner, A. Nauels, N. Bauer, J. G. Canadell, J. S. Daniel, A. John, P. B. Krummel, G. Luderer, N. Meinshausen, S. A. Montzka, P. J. Rayner, S. Reimann, S. J. Smith, M. van den Berg, G. J. M. Velders, M. K. Vollmer, and R. H. J. Wang, *The shared socioeconomic pathway (SSP) greenhouse gas concentrations and their extensions to 2500,* Geoscientific Model Development **13**, 3571 (2020).

[3] Climate Action Tracker, *Addressing global warming,* https://www.climateactiontracker.org/global/temperatures/ (2021).

[4] Gates, Bill, *How to Avoid a Climate Disaster: The Solutions We Have and the Breakthroughs We Need* (2021).

[5] Live Science, *Effects of global warming,* https://www.livescience.com/37057-global-warming-effects.html (2017).

[6] World Energy Data, *World total final consumption,* https://www.worldenergydata.org/world-total-final-consumption/ (2021).

[7] Our World in Data, *Electricity production by source,* https://ourworldindata.org/grapher/electricity-prod-source-stacked (2020).

[8] IPCC, *Global warming of 1.5°c,* https://www.ipcc.ch/sr15/ (2018).

[9] World Wide Fund for Nature, *Our warming world: How much difference will half-a-degree really make?* https://www.wwf.org.uk/updates/our-warming-world-how-much-difference-will-half-degree-really-make (2018).

[10] Douglas Broom, *5 charts show the rapid fall in costs of renewable energy,* https://energypost.eu/5-charts-show-the-rapid-fall-in-costs-of-renewable-\energy/ (2020).

[11] James Mulligan, Gretchen Ellison, Kelly Levin, Katie Lebling and Alex Rudee, *6 ways to remove carbon pollution from the sky,* https://www.wri.org/insights/6-ways-remove-carbon-pollution-sky (2020).

[12] R. Norhasyima and T. Mahlia, *Advances in CO_2 utilization technology: A patent landscape review,* Journal of CO_2 Utilization **26**, 323 (2018).

[13] E. I. Koytsoumpa, C. Bergins, and E. Kakaras, *The CO_2 economy: Review of CO_2 capture and reuse technologies,* The Journal of Supercritical Fluids **132**, 3 (2018).

[14] Chemical Engineering, *Toshiba, ana, toyo and idemitsu kosan partner on power-to-chemicals strategy,* https://www.chemengonline.com/toshiba-ana-toyo-and-idemitsu-kosan-partner-on-power-to-chemicals-\strategy/ (2020).

[15] M. Aresta, A. Dibenedetto, and A. Angelini, *The changing paradigm in CO_2 utilization,* Journal of CO_2 Utilization **3-4**, 65 (2013).

[16] R. Lin, J. Guo, X. Li, P. Patel, and A. Seifitokaldani, *Electrochemical reactors for CO_2 conversion,* Catalysts **10**, 473 (2020).

[17] J. Resasco and A. T. Bell, *Electrocatalytic CO_2 reduction to fuels: Progress and opportunities,* Trends in Chemistry **2**, 825 (2020).

[18] P. D. Luna, C. Hahn, D. Higgins, S. A. Jaffer, T. F. Jaramillo, and E. H. Sargent, *What would it take for renewably powered electrosynthesis to displace petrochemical processes?* Science **364**, 3506 (2019).

[19] O. S. Bushuyev, P. D. Luna, C. T. Dinh, L. Tao, G. Saur, J. van de Lagemaat, S. O. Kelley, and E. H. Sargent, *What should we make with CO_2 and how can we make it?* Joule **2**, 825 (2018).

[20] W. A. Smith, T. Burdyny, D. A. Vermaas, and H. Geerlings, *Pathways to industrial-scale fuel out of thin air from CO_2 electrolysis,* Joule **3**, 1822 (2019).

[21] S. Verma, B. Kim, H.-R. ". Jhong, S. Ma, and P. J. A. Kenis, *A gross-margin model for defining technoeconomic benchmarks in the electroreduction of CO_2,* ChemSusChem **9**, 1972 (2016).

[22] M. Jouny, W. Luc, and F. Jiao, *General techno-economic analysis of CO_2 electrolysis systems,* Industrial & Engineering Chemistry Research **57**, 2165 (2018).

[23] Z. W. Seh, J. Kibsgaard, C. F. Dickens, I. Chorkendorff, J. K. Nørskov, and T. F. Jaramillo, *Combining theory and experiment in electrocatalysis: Insights into materials design,* Science **355**, eaad4998 (2017).

[24] M. G. Kibria, J. P. Edwards, C. M. Gabardo, C.-T. Dinh, A. Seifitokaldani, D. Sinton, and E. H. Sargent, *Electrochemical CO_2 reduction into chemical feedstocks: From mechanistic electrocatalysis models to system design,* Advanced Materials **31**, 1807166 (2019).

[25] H. Rabiee, L. Ge, X. Zhang, S. Hu, M. Li, and Z. Yuan, *Gas diffusion electrodes (GDEs) for electrochemical reduction of carbon dioxide, carbon monoxide, and dinitrogen to value-added products: a review,* Energy & Environmental Science **14**, 1959 (2021).

[26] R. G. Grim, Z. Huang, M. T. Guarnieri, J. R. Ferrell, L. Tao, and J. A. Schaidle, *Transforming the carbon economy: challenges and opportunities in the convergence of low-cost electricity and reductive CO_2 utilization,* Energy & Environmental Science **13**, 472 (2020).

[27] C.-T. Dinh, T. Burdyny, M. G. Kibria, A. Seifitokaldani, C. M. Gabardo, F. P. G. de Arquer, A. Kiani, J. P. Edwards, P. D. Luna, O. S. Bushuyev, C. Zou, R. Quintero-Bermudez, Y. Pang, D. Sinton, and E. H. Sargent, *CO_2 electroreduction to ethylene via hydroxide-mediated copper catalysis at an abrupt interface,* Science **360**, 783 (2018).

[28] T. Burdyny and W. A. Smith, *CO_2 reduction on gas-diffusion electrodes and why catalytic performance must be assessed at commercially-relevant conditions,* Energy & Environmental Science **12**, 1442 (2019).

[29] D. Higgins, C. Hahn, C. Xiang, T. F. Jaramillo, and A. Z. Weber, *Gas-diffusion electrodes for carbon dioxide reduction: A new paradigm,* ACS Energy Letters **4**, 317 (2018).

[30] J. J. Kaczur, H. Yang, Z. Liu, S. D. Sajjad, and R. I. Masel, *Carbon dioxide and water electrolysis using new alkaline stable anion membranes,* Frontiers in Chemistry **6** (2018), 10.3389/fchem.2018.00263.

[31] B. Endrődi, E. Kecsenovity, A. Samu, F. Darvas, R. V. Jones, V. Török, A. Danyi, and C. Janáky, *Multilayer electrolyzer stack converts carbon dioxide to gas products at high pressure with high efficiency,* ACS Energy Letters **4**, 1770 (2019).

[32] B. Endrődi, E. Kecsenovity, A. Samu, T. Halmágyi, S. Rojas-Carbonell, L. Wang, Y. Yan, and C. Janáky, *High carbonate ion conductance of a robust PiperION membrane allows industrial current density and conversion in a zero-gap carbon dioxide electrolyzer cell,* Energy & Environmental Science **13**, 4098 (2020).

[33] B. Endrődi, A. Samu, E. Kecsenovity, T. Halmágyi, D. Sebők, and C. Janáky, *Operando cathode activation with alkali metal cations for high current density operation of water-fed zero-gap carbon dioxide electrolysers,* Nature Energy **6**, 439 (2021).

[34] F. P. G. de Arquer, C.-T. Dinh, A. Ozden, J. Wicks, C. McCallum, A. R. Kirmani, D.-H. Nam, C. Gabardo, A. Seifitokaldani, X. Wang, Y. C. Li, F. Li, J. Edwards, L. J. Richter, S. J. Thorpe, D. Sinton, and E. H. Sargent, *CO_2 electrolysis to multicarbon products at activities greater than 1 a cm-2,* Science **367**, 661 (2020).

[35] Y. Wang, J. Liu, Y. Wang, A. M. Al-Enizi, and G. Zheng, *Tuning of CO_2 reduction selectivity on metal electrocatalysts,* Small **13**, 1701809 (2017).

[36] M. Valenti, N. P. Prasad, R. Kas, D. Bohra, M. Ma, V. Balasubramanian, L. Chu, S. Gimenez, J. Bisquert, B. Dam, and W. A. Smith, *Suppressing H_2 evolution and promoting selective CO_2 electroreduction to CO at low overpotentials by alloying Au with Pd,* ACS Catalysis **9**, 3527 (2019).

[37] A. Goyal, G. Marcandalli, V. A. Mints, and M. T. M. Koper, *Competition between CO_2 reduction and hydrogen evolution on a gold electrode under well-defined mass transport conditions,* Journal of the American Chemical Society **142**, 4154 (2020).

[38] D. Raciti, M. Mao, J. H. Park, and C. Wang, *Local pH effect in the CO_2 reduction reaction on high-surface-area copper electrocatalysts,* Journal of The Electrochemical Society **165**, F799 (2018).

[39] A. S. Varela, M. Kroschel, T. Reier, and P. Strasser, *Controlling the selectivity of CO_2 electroreduction on copper: The effect of the electrolyte concentration and the importance of the local pH,* Catalysis Today **260**, 8 (2016).

[40] K. Yang, R. Kas, and W. A. Smith, *In situ infrared spectroscopy reveals persistent alkalinity near electrode surfaces during CO_2 electroreduction,* Journal of the American Chemical Society **141**, 15891 (2019).

[41] X. Lu, C. Zhu, Z. Wu, J. Xuan, J. S. Francisco, and H. Wang, *In situ observation of the pH gradient near the gas diffusion electrode of CO_2 reduction in alkaline electrolyte,* Journal of the American Chemical Society **142**, 15438 (2020).

[42] A. S. Varela, *The importance of pH in controlling the selectivity of the electrochemical CO_2 reduction,* Current Opinion in Green and Sustainable Chemistry **26**, 100371 (2020).

2

Understanding electrochemical CO_2 reduction and its side reactions

The first section of this chapter introduces the concept of electrochemical CO_2 reduction (ECO2R), as well as the advancement achieved in this research field in the past decades. Following the brief introduction, the primary focus of this chapter is addressed. Namely two side reactions that occur during ECO2R which reduce the activity, selectivity, and efficiency of the targeted reactions. These are the hydrogen evolution reaction (HER) and (bi)carbonate formation, which will be discussed in Sections 2.2 and 2.3 respectively. Section 2.2 provides context for the factors influencing the primary competing reaction to ECO2R: the HER. We discuss how proton sources: water or proton influence activity and selectivity for CO_2 reduction. To decouple the competing HER from ECO2R, gas diffusion electrodes (GDEs) are employed, which have boosted the reaction rate of CO_2 electrolysis substantially. Section 2.3 explains the high local pH, thus (bi)carbonate formation issue, followed by their implications on stability and CO_2 utilization of current CO_2 electrolyzers. Accordingly, major considerations and improvements attempted to solve the existing problems are discussed. At the end of this chapter, section 2.4 briefly addresses the multiple complexity and challenges of commercializing CO_2 electrolyzers in industry. Note that there is much more extensive literature in this field that covers more subjects besides these investigated in this thesis. Nevertheless, the literature cited in this chapter mainly serves to provide essential information to understand the basics of electrochemical CO_2 reduction and its competing reactions, thus laying a foundation for the work presented in chapter 3, 4 and 5.

2.1. Introduction of electrochemical CO_2 reduction.

Electrochemical CO_2 reduction has received great attention nowadays due to the urgency of energy transition and de-carbonation.[1–4] By applying suitable catalysts, CO_2 can be electrochemically reduced to multiple products: carbon monoxide(CO), formic acid(HCOOH), methanol (CH_3OH), methane (CH_4), ethylene (C_2H_4), ethanol (C_2H_5OH), n-propanol (n-PrOH), etc. [5–7] Since the pioneering work by Hori in 1980s,[5, 8] ECO2R research field has achieved considerable accomplishments.

Among those products, CO and C_2H_4 have been the two most researched in literature as shown in Equations (1,2).[5] CO can be used as fuel and reducing agent, it can also form syngas together with H_2, which is used in a variety of industrial synthesis processes. While C_2H_4 is known as the key building block for materials such as plastics, fibers and other value-added products.[9] In the past decades, partial current densities of these targeted products (JCO, JC_2H_4) have increased from less than 50 mA/cm^2 to more than 1000 mA/cm^2.[10–13] Such progress is achieved by a deeper understanding of catalyst properties and improved design of cathodes and electrolyzer systems.[9, 14, 15] However, the common need for protons from water, as well as with hydroxide as a byproduct of ECO2R in neutral and alkaline media as shown in Equations (1,2), have been major challenges which result the two primary side reactions as we shall discuss later throughout this thesis.

$$CO_2 + H_2O + 2e^- \Rightarrow CO + 2OH^- \quad (-0.11\ \text{V vs RHE}) \quad (1)$$

$$2CO_2 + 8H_2O + 12e^- \Rightarrow C_2H_4 + 12OH^- \quad (-0.08\ \text{V vs RHE}) \quad (2)$$

2.2. Hydrogen evolution reaction and high local pH

2.2.1. HER during CO_2 electrolysis

Majority of electrochemical CO_2 reduction studies have been done in conventional H-cells in the past decades.[5, 16] Those studies provided a in-depth understanding of the mechanisms, activity and selectivity properties of ECO2R, but were challenged to achieve high selectivity towards CO_2 reduction products at both low (< 1 mA/cm^2) and high (> 30 mA/cm^2) current densities due to the HER reaction. The reasons for this are multi-fold. Firstly, hydrogen evolution reaction from either water or proton is thermodynamically more favourable than ECO2R, which makes HER an unavoidable side reaction as shown in Equations (3,4).[5]

$$2H_2O + 2e^- \Rightarrow H_2 + 2OH^- \quad (0\ \text{V vs RHE}) \quad (3)$$

$$2H^+ + 2e^- \Rightarrow H_2 \quad (0\ \text{V vs RHE}) \quad (4)$$

Secondly, the competing reactions of ECO2R and HER are influenced by many factors, the most prominent being both the bulk pH of the electrolyte, and the pH surrounding a catalytic surface during operation as shown in Figure 2.1.[17]. These constraints make it challenging to optimize ECO2R over a broad operating range when all of these factors depend on performance metrics such as current density. For example, HER is most favored in acidic solutions where there is easy access to protons in the electrolyte. Alkaline condition on the

contrary favours the kinetics of ECO2R. Most ECO2R studies have been done in a neutral or alkaline environment in literature.[18] At pH above 3, water is proved to be the primary proton donor for ECO2R.[19–21]. Such competing HER especially influences ECO2R in H-cells since CO_2 concentration saturates at only 34 mM in water, much lower than the concentration of water which is close to unity. In addition, due to the large amount of OH^- produced (high local pH) during both CO_2 and water reduction, CO_2 concentration in the vicinity of the catalyst surface is even lower. As a result, ECO2R only has a very small window to efficiently compete with HER.[22]

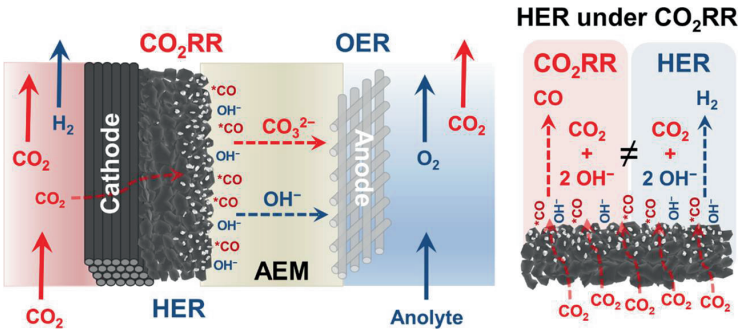

Figure 2.1: Hydrogen evolution reaction and high local pH during CO_2 reduction. Reprinted with permission from [17]. Copyright 2021. American Chemical Society.

2.2.2. Influence of HER and high local pH on activity and selectivity

As mentioned above, the thermodynamic potential of HER overlaps with ECO2R, and the concentration of CO_2 in liquid electrolytes is limited by its solubility, especially under aforementioned high local pH conditions, thus ECO2R suffers from low activity and selectivity.[5, 23].

The typical curves of CO_2 reduction activity in a H-cell are shown in Figure 2.2 (a) and (b) for Cu catalyst and (c) and (d) for Ag catalyst.[22, 24] H_2 Faradaic efficiency (FE) has a "V" shape trend. Only at the potential window corresponding to the bottom of the "V", can ECO2R possibly take over HER. As for partial current density which indicates overall reaction rates, H_2 typically keeps increasing as potential increases. Whereas, for ECO2R, current density usually first increases then plateaus due to mass transport limitation. This limitation not only results from low CO_2 concentration in the bulk electrolyte, but also from the high local OH^- concentration produced during HER and ECO2R as discussed above. Thus the overall activity and selectivity have not been desirable.[25] Separating CO_2 gas from the electrolyte by employing gas diffusion electrodes has brought major breakthroughs in this aspect and is discussed in the following section.[9, 14, 15, 26, 27]

2.2.3. Employment of gas diffusion electrode

By separating gas and liquid feeds, gas diffusion electrode (GDE) has shortened the CO_2 gas diffusion pathways from around 100 µm to less than 100 nm, which increases the availability of CO_2 on the catalyst layer surface.[9, 10, 15] With this enhanced availability of CO_2 on the

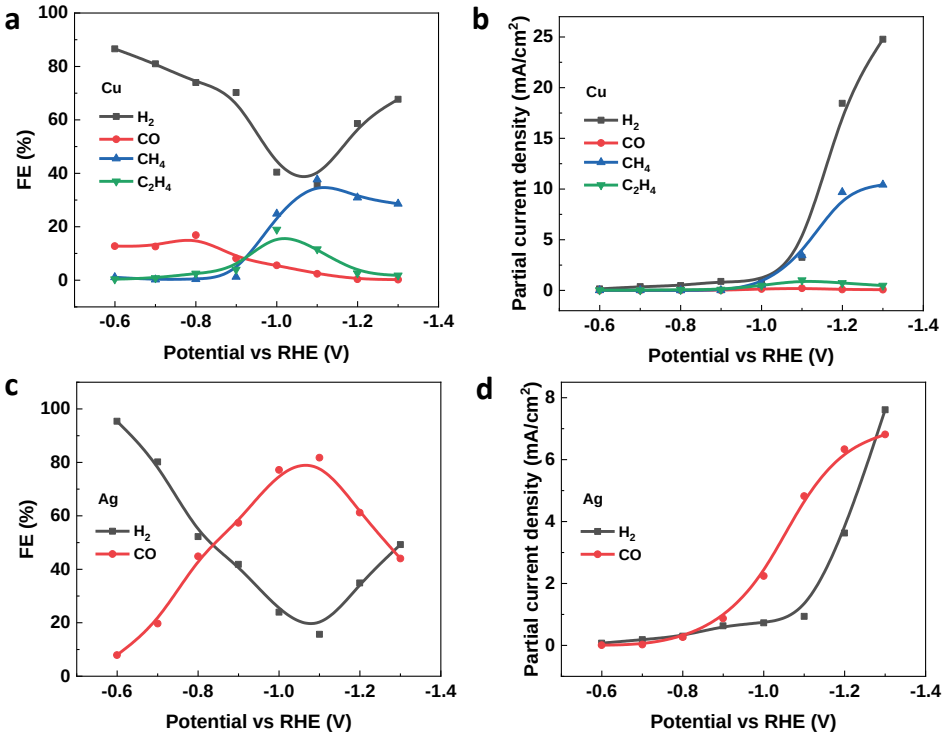

Figure 2.2: Faradaic efficiency (a) and partial current density (b) of CO_2 electrolysis products on a bare polycrystalline Cu surface. Faradaic efficiency (c) and partial current density (d) of CO_2 electrolysis products on a bare polycrystalline Ag surface. Figure reproduced from data obtained in reference[22].

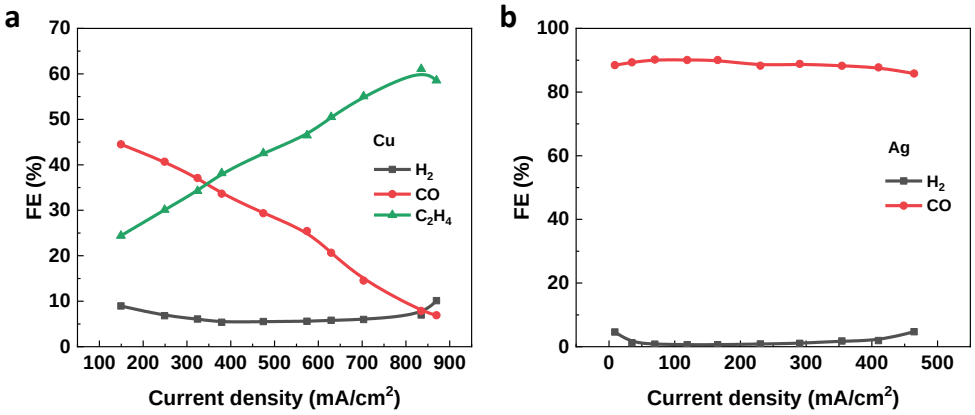

Figure 2.3: Faradaic efficiency of Cu (a) and Ag (b) GDEs under CO_2 reduction operation in 5 M KOH electrolytes as a function of current density. Figure reproduced from data obtained in reference[11].

catalyst surface and capability of using alkaline electrolytes, ECO2R can outperform HER in both activity and selectivity as shown in Figure 2.3.[11] Partial current densities of CO and C_2H_4 have been increased by more than one order of magnitude. Faradaic efficiency of C_2H_4 has been improved to 60% in GDE flow cells compared with the 20% FE in H-cells. The Faradaic efficiencies of CO on Ag and C_2H_4 on Cu are also very stable in a wide range of potentials and current densities.[10, 12, 13] The "V" shape trend is thus broken down while using GDEs. Nowadays lots of attention has been focused on further improvements of GDE engineering, membranes and cell configurations.[28, 29] With such endeavour, CO_2 electrolyzers are expected to reach the reaction rate and product selectivity required for industrial commercialization.

2.3. High local pH and (bi)carbonate formation reactions

2.3.1. (Bi)carbonate formation during CO_2 electrolysis

Aside from the competing HER reaction, ECO2R is heavily challenged by the unwanted production of OH^- in neutral and alkaline electrolyte conditions as a result of water-splitting to provide protons. A large amount of OH^- is produced during electrochemical reactions and then chemically reacts with CO_2 to form bicarbonate and carbonate ions (Equations 5-7). Since the reaction rate between bicarbonate and OH^- is very fast,[30–32] carbonate is hypothesized as the main anion which crosses the membrane in the case where an anion exchange membrane is used, which is later confirmed by experimental measurements.[33, 34]

$$CO_2 + OH^- \Leftrightarrow HCO_3^- \quad (5)$$

$$HCO_3^- + OH^- \Leftrightarrow CO_3^{2-} + H_2O \quad (6)$$

$$CO_2 + 2OH^- \Leftrightarrow CO_3^{2-} + H_2O \quad (7)$$

Table 2.1: Maximum CO_2 utilization in scenarios targeting at different products

CO_2	Product	OH^-	Conversion/ Lost	Maximum utilization
1	1 CO	2	1: 1	50%
1	1 C_2H_4	6	1: 3	25%

The loss of CO_2 to carbonates causes a substantial amount of reagent to be consumed, which affects the CO_2 utilization of the device. Table 2.1 demonstrates the CO_2 utilization in processes targeting at different products (considering all the CO_2 feed is used in the cell). In CO production scenario, when 1 CO_2 is reduced to CO, 2 OH^- is produced. Which again consumes another 1 CO_2 molecule. The ratio between conversion and lost is 1:1, corresponding to maximum 50% utilization of CO_2 feed. While, in C_2H_4 production scenario, the maximum utilization is only 25%.[35–37] As the industrial CO_2 capture, regeneration and further pressurization for transportation are extremely energy-intensive processes,[38]

such low CO_2 utilization makes commercializing CO_2 electrolyzers infeasible due to the low energy efficiency.[39, 40]

2.3.2. Influence of salt formation on stability and CO_2 utilization

Even though with the improvement achieved in activity and selectivity, two problems still need to be solved before scaling up the CO_2 electrolyzers. One is stability and another one is CO_2 utilization. Despite the hundreds of hours stability reached after employing GDEs, current electrolyzers still can not fulfill the requirement for an actual running system in industry.[9, 41, 42] At least thousands of hours' continuous operation with good stability, high CO_2 utilization and energy efficiency is needed.

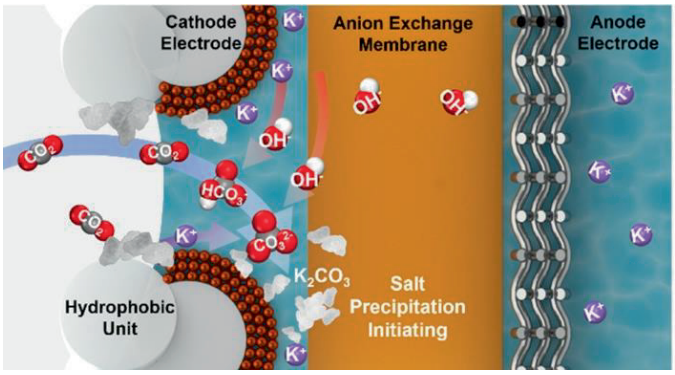

Figure 2.4: Illustration of salt precipitation on cathode during electrochemical CO_2 reduction. Figure reprinted with permission from [43]. Copyright 2021 American Chemical Society.

Two factors have been the major cause for the failure of GDEs: flooding and salt precipitation. These two factors are interconnected as well. Flooding has major influence on a GDE flow cell.[44] For instance, it can be due to the pressure difference between catholyte and feeding gas.[45–48] This can be solved by using pressure regulators. However, common flooding is caused by the high local OH^- concentration and competing HER, hence is hard to avoid. As shown in Equations (5-7), lots of bicarbonate and carbonate anions are produced during electrochemical reactions. Combining with cations, they form salts with low solubility which precipitate easily as shown in Figure 2.4. The salts formed can enter and cover the hydrophobic pores inside of GDE, making liquid easier to penetrate. The accumulation of salts inside the pores can also fully block the transport pathway of gases, resulting in quick failure of the entire system.[48, 49]

In the meanwhile, the side reaction - HER also plays an important role in causing flooding. It has been shown that electrowetting induces initial wetting of the surface, which allows electrolyte to fill the pores more easily.[45, 47, 49, 50] Once wetted, the underneath carbon based GDL can perform hydrogen evolution, which causes a quick failure of the systems as a result. Some groups have used PTFE based GDLs, which showed excellent resistance to flooding. But conductivity is the another obstacle to scale up this non-conductive PTFE

based GDE systems[10, 11, 51]. Further work in this field should also focus on designing GDLs which are suitable for CO_2 purpose, with proper design of porous size, thickness, hydrophobicity, etc.

The utilization of CO_2 is not addressed until recent years.[39, 40, 52, 53] Due to the high capital cost of CO_2 gas capture and regeneration for CO_2 reduction purpose, and low single pass conversion efficiency caused by (bi)carbonate formation (lower than 20% in most literature),[35, 54] the overall energy efficiencies of CO_2 electrolyzers reported are very low. Regenerating CO_2 from those (bi)carbonate salts to recover the electrolyte accounts for more than half of the capital cost.[37] Thus many efforts have been put into increasing CO_2 utilization and energy efficiency at this moment.[21, 37, 55]

2.3.3. Improving CO_2 utilization

Direct (bi)carbonate reduction in a membrane electrode assembly (MEA) cell integrated with a BPM has been a new research direction as shown in Figure 2.5(a). By by-passing the CO_2 gas regeneration and pressurization process, the direct reduction of CO_2 in the capture medium seems promising in increasing energy efficiency.[38] However, the perfor-

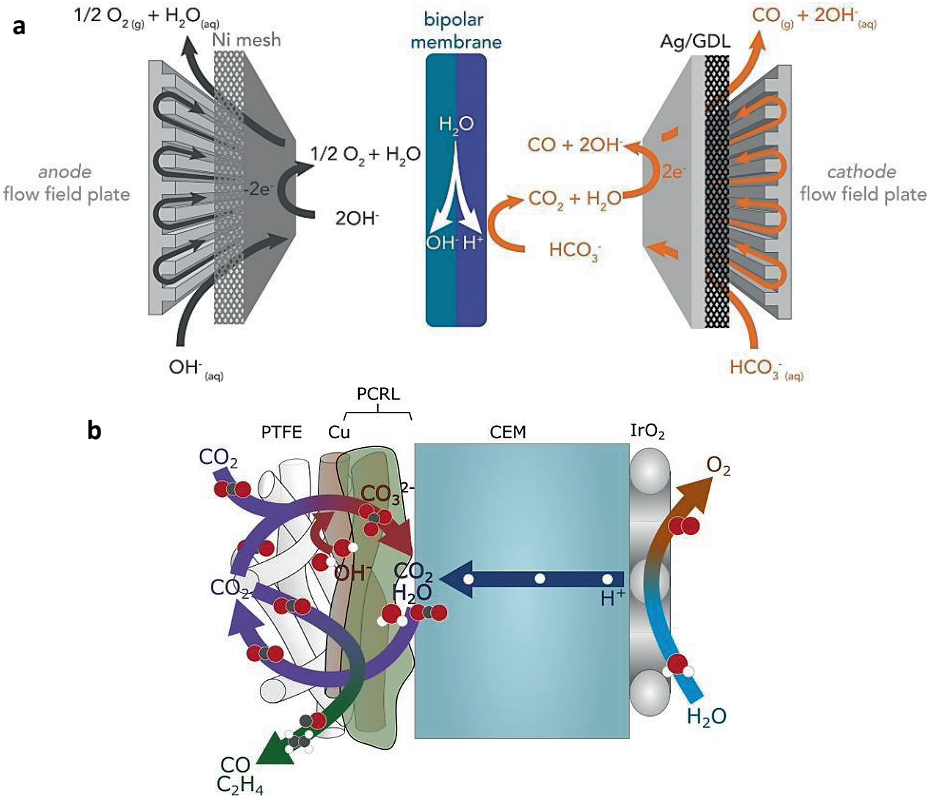

Figure 2.5: Improving CO_2 utilization by introducing H^+ to cathode. Figure a reprinted with permission from [56]. Copyright 2019 Elsevier. Figure b reprinted with permission from [55]. Copyright 2021 American Chemical Society.

mance for CO_2 reduction plateaus at only around 100 mA/cm^2 for the targeted product CO in those systems.[56–59] To achieve the goal which this system advertised for and compete with gaseous CO_2 reduction, it still needs to be further improved in the ECO2R activity.

Efforts have also been put into gaseous CO_2 reduction cells in tackling the salt formation induced instability and low CO_2 utilization issues. One strategy is to eliminate cations from electrolyte. In this way, the formed (bi)carbonate ions can not combine with cations and precipitate.[60, 61] Janaky group used pure water as anolyte in an MEA cell with most commonly used AEM. After activating the catalyst by infusion with cation-containing solution, ECO2R could reach the same performance as with electrolyte contains cations. In the meantime, stability was much higher. The cell could run at CO partial current density higher than 400 mA/cm^2 for more than 200 hours.[61]

Another strategy, which involves ECO2R in acid media, has also attracted researchers' attention. Protons can both come from catholyte or membranes.[21, 37] Ted Sargent group reported CO_2 reduction on Cu in strong acid catholyte conditions, which achieved 77% single-pass utilization.[37] In their another recently published paper, they used cation exchange membrane and water as anolyte in an MEA cell to provide the proton needed to regulate the local environment of CO_2 reduction interfaces. With fast CO_2 regeneration by H^+ reacting with the formed (bi)carbonate ions, CO_2 utilization was improved significantly (Figure 2.5(b)).[55]

Integrating bipolar membranes (BPMs) in an MEA cell also stands out as a promising solution. BPM can provide the proton to the catalyst surface to maintain a neutral or acidic environment, thus decreasing CO_2 loss and increasing CO_2 utilization. Moreover, BPM can also provide OH^- to anolyte, which allows the usage of non-noble catalysts for oxygen evolution reactions. BPM also has the advantage of maintaining the pH at the cathode and anode parts stable, thus a stable cell potential. Such configurations have been reported in literature, but overall CO_2 reduction activity is very low compared to HER.[53, 62, 63] In the meantime, higher potential is required for water dissociation inside of the membrane (minimum 0.83V).[64, 65] However, with further endeavors on improving the ECO2R activity in such a system, thus high CO_2 utilization efficiency, the high potential required could be compensated.[66, 67]

2.4. Complexity of CO_2 electrolyzers

To conclude, CO_2 electrolyzer is a complex electrochemical system encompassing limited mass transport regimes, heterogenous and homogeneous reactions, and multi-phase transport in porous media, which needs to be designed carefully.[45] Many parameters directly influence the measured performance of systems and thus need to be account for to ensure repeatability between groups, and to reach optimal performance. Factors that need to be considered include such as pressure, temperature, flow field, flow rate, choice of GDL, hydrophobicity, hydrophilicity, catalyst morphology, membrane, electrolyte, etc.[68] Such open problems have brought thousands of researchers from different backgrounds into this research field to chip away at the many research questions of interest. With different labs worldwide collectively working and contributing their knowledge together, I am positive that a first CO_2 electrolyzer pilot would come into reality in near future.

References

[1] P. D. Luna, C. Hahn, D. Higgins, S. A. Jaffer, T. F. Jaramillo, and E. H. Sargent, *What would it take for renewably powered electrosynthesis to displace petrochemical processes?* Science **364**, 3506 (2019).

[2] R. Lin, J. Guo, X. Li, P. Patel, and A. Seifitokaldani, *Electrochemical reactors for CO_2 conversion,* Catalysts **10**, 473 (2020).

[3] J. Resasco and A. T. Bell, *Electrocatalytic CO_2 reduction to fuels: Progress and opportunities,* Trends in Chemistry **2**, 825 (2020).

[4] H. Rabiee, L. Ge, X. Zhang, S. Hu, M. Li, and Z. Yuan, *Gas diffusion electrodes (GDEs) for electrochemical reduction of carbon dioxide, carbon monoxide, and dinitrogen to value-added products: a review,* Energy & Environmental Science **14**, 1959 (2021).

[5] Y. Hori, *Electrochemical CO_2 reduction on metal electrodes,* in *Modern Aspects of Electrochemistry* (Springer New York) pp. 89–189.

[6] J. Lee, J. Lim, C.-W. Roh, H. S. Whang, and H. Lee, *Electrochemical CO_2 reduction using alkaline membrane electrode assembly on various metal electrodes,* Journal of CO_2 Utilization **31**, 244 (2019).

[7] Y. Y. Birdja, E. Pérez-Gallent, M. C. Figueiredo, A. J. Göttle, F. Calle-Vallejo, and M. T. M. Koper, *Advances and challenges in understanding the electrocatalytic conversion of carbon dioxide to fuels,* Nature Energy **4**, 732 (2019).

[8] Y. Hori, K. Kikuchi, and S. Suzuki, *PRODUCTION OF CO AND CH4in ELECTROCHEMICAL REDUCTION OF CO_2at METAL ELECTRODES IN AQUEOUS HYDROGENCARBONATE SOLUTION,* Chemistry Letters **14**, 1695 (1985).

[9] S. Hernandez-Aldave and E. Andreoli, *Fundamentals of gas diffusion electrodes and electrolysers for carbon dioxide utilisation: Challenges and opportunities,* Catalysts **10**, 713 (2020).

[10] C.-T. Dinh, T. Burdyny, M. G. Kibria, A. Seifitokaldani, C. M. Gabardo, F. P. G. de Arquer, A. Kiani, J. P. Edwards, P. D. Luna, O. S. Bushuyev, C. Zou, R. Quintero-Bermudez, Y. Pang, D. Sinton, and E. H. Sargent, *CO_2 electroreduction to ethylene via hydroxide-mediated copper catalysis at an abrupt interface,* Science **360**, 783 (2018).

[11] F. P. G. de Arquer, C.-T. Dinh, A. Ozden, J. Wicks, C. McCallum, A. R. Kirmani, D.-H. Nam, C. Gabardo, A. Seifitokaldani, X. Wang, Y. C. Li, F. Li, J. Edwards, L. J. Richter, S. J. Thorpe, D. Sinton, and E. H. Sargent, *CO_2 electrolysis to multicarbon products at activities greater than 1 a cm-2,* Science **367**, 661 (2020).

[12] B. Endrődi, E. Kecsenovity, A. Samu, F. Darvas, R. V. Jones, V. Török, A. Danyi, and C. Janáky, *Multilayer electrolyzer stack converts carbon dioxide to gas products at high pressure with high efficiency,* ACS Energy Letters **4**, 1770 (2019).

[13] B. Endrődi, E. Kecsenovity, A. Samu, T. Halmágyi, S. Rojas-Carbonell, L. Wang, Y. Yan, and C. Janáky, *High carbonate ion conductance of a robust PiperION membrane allows industrial current density and conversion in a zero-gap carbon dioxide electrolyzer cell,* Energy & Environmental Science **13**, 4098 (2020).

[14] D. Higgins, C. Hahn, C. Xiang, T. F. Jaramillo, and A. Z. Weber, *Gas-diffusion electrodes for carbon dioxide reduction: A new paradigm,* ACS Energy Letters **4**, 317 (2018).

[15] T. Burdyny and W. A. Smith, *CO_2 reduction on gas-diffusion electrodes and why catalytic performance must be assessed at commercially-relevant conditions,* Energy & Environmental Science **12**, 1442 (2019).

[16] C. Long, X. Li, J. Guo, Y. Shi, S. Liu, and Z. Tang, *Electrochemical reduction of CO 2 over heterogeneous catalysts in aqueous solution: Recent progress and perspectives,* Small Methods , 1800369 (2018).

[17] H. Haspel and J. Gascon, *Is hydroxide just hydroxide? unidentical CO_2 hydration conditions during hydrogen evolution and carbon dioxide reduction in zero-gap gas diffusion electrode reactors,* ACS Applied Energy Materials **4**, 8506 (2021).

[18] J.-B. Vennekötter, T. Scheuermann, R. Sengpiel, and M. Wessling, *The electrolyte matters: Stable systems for high rate electrochemical CO_2 reduction,* Journal of CO_2 Utilization **32**, 202 (2019).

[19] C. J. Bondue, M. Graf, A. Goyal, and M. T. M. Koper, *Suppression of hydrogen evolution in acidic electrolytes by electrochemical CO_2 reduction,* Journal of the American Chemical Society **143**, 279 (2020).

[20] H. Ooka, M. C. Figueiredo, and M. T. M. Koper, *Competition between hydrogen evolution and carbon dioxide reduction on copper electrodes in mildly acidic media,* Langmuir **33**, 9307 (2017).

[21] M. C. O. Monteiro, F. Dattila, B. Hagedoorn, R. García-Muelas, N. López, and M. T. M. Koper, *Absence of CO_2 electroreduction on copper, gold and silver electrodes without metal cations in solution,* Nature Catalysis **4**, 654 (2021).

[22] H. Zhang, X. Chang, J. G. Chen, W. A. Goddard, B. Xu, M.-J. Cheng, and Q. Lu, *Computational and experimental demonstrations of one-pot tandem catalysis for electrochemical carbon dioxide reduction to methane,* Nature Communications **10** (2019), 10.1038/s41467-019-11292-9.

[23] M. Ma and W. A. Smith, *Nanostructured catalysts for the electrochemical reduction of CO_2,* in *Nanostructure Science and Technology* (Springer International Publishing, 2017) pp. 337–373.

[24] K. P. Kuhl, E. R. Cave, D. N. Abram, and T. F. Jaramillo, *New insights into the electrochemical reduction of carbon dioxide on metallic copper surfaces,* Energy & Environmental Science **5**, 7050 (2012).

[25] K. Yang, R. Kas, and W. A. Smith, *In situ infrared spectroscopy reveals persistent alkalinity near electrode surfaces during CO_2 electroreduction,* Journal of the American Chemical Society **141**, 15891 (2019).

[26] J.-B. Vennekoetter, R. Sengpiel, and M. Wessling, *Beyond the catalyst: How electrode and reactor design determine the product spectrum during electrochemical CO_2 reduction,* Chemical Engineering Journal **364**, 89 (2019).

[27] H.-R. Jhong, S. Ma, and P. J. Kenis, *Electrochemical conversion of CO_2 to useful chemicals: current status, remaining challenges, and future opportunities,* Current Opinion in Chemical Engineering **2**, 191 (2013).

[28] L. Fan, C. Xia, F. Yang, J. Wang, H. Wang, and Y. Lu, *Strategies in catalysts and electrolyzer design for electrochemical CO_2 reduction toward c2 products,* Science Advances **6**, eaay3111 (2020).

[29] S. Liang, N. Altaf, L. Huang, Y. Gao, and Q. Wang, *Electrolytic cell design for electrochemical CO_2 reduction,* Journal of CO_2 Utilization **35**, 90 (2020).

[30] N. Gupta, M. Gattrell, and B. MacDougall, *Calculation for the cathode surface concentrations in the electrochemical reduction of CO_2 in $KHCO_3$ solutions,* Journal of Applied Electrochemistry **36**, 161 (2005).

[31] L.-C. Weng, A. T. Bell, and A. Z. Weber, *Modeling gas-diffusion electrodes for CO_2 reduction,* Physical Chemistry Chemical Physics **20**, 16973 (2018).

[32] L.-C. Weng, A. T. Bell, and A. Z. Weber, *Towards membrane-electrode assembly systems for CO_2 reduction: a modeling study,* Energy & Environmental Science **12**, 1950 (2019).

[33] G. O. Larrazábal, P. Strøm-Hansen, J. P. Heli, K. Zeiter, K. T. Therkildsen, I. Chorkendorff, and B. Seger, *Analysis of mass flows and membrane cross-over in CO_2 reduction at high current densities in an MEA-type electrolyzer,* ACS Applied Materials & Interfaces **11**, 41281 (2019).

[34] M. Ma, E. L. Clark, K. T. Therkildsen, S. Dalsgaard, I. Chorkendorff, and B. Seger, *Insights into the carbon balance for CO_2 electroreduction on cu using gas diffusion electrode reactor designs,* Energy & Environmental Science **13**, 977 (2020).

[35] E. Jeng and F. Jiao, *Investigation of CO_2 single-pass conversion in a flow electrolyzer,* Reaction Chemistry & Engineering **5**, 1768 (2020).

[36] J. A. Rabinowitz and M. W. Kanan, *The future of low-temperature carbon dioxide electrolysis depends on solving one basic problem,* Nature Communications **11** (2020), 10.1038/s41467-020-19135-8.

[37] J. E. Huang, F. Li, A. Ozden, A. S. Rasouli, F. P. G. de Arquer, S. Liu, S. Zhang, M. Luo, X. Wang, Y. Lum, Y. Xu, K. Bertens, R. K. Miao, C.-T. Dinh, D. Sinton, and E. H. Sargent, *CO_2 electrolysis to multicarbon products in strong acid,* Science **372**, 1074 (2021).

[38] A. J. Welch, E. Dunn, J. S. DuChene, and H. A. Atwater, *Bicarbonate or carbonate processes for coupling carbon dioxide capture and electrochemical conversion,* ACS Energy Letters **5**, 940 (2020).

[39] S. Verma, B. Kim, H.-R. ". Jhong, S. Ma, and P. J. A. Kenis, *A gross-margin model for defining technoeconomic benchmarks in the electroreduction of CO_2,* ChemSusChem **9**, 1972 (2016).

[40] M. Jouny, W. Luc, and F. Jiao, *General techno-economic analysis of CO_2 electrolysis systems,* Industrial & Engineering Chemistry Research **57**, 2165 (2018).

[41] U. O. Nwabara, E. R. Cofell, S. Verma, E. Negro, and P. J. A. Kenis, *Durable cathodes and electrolyzers for the efficient aqueous electrochemical reduction of CO_2, journal = ChemSusChem,* **13**, 855 (2020).

[42] U. O. Nwabara, A. D. Hernandez, D. A. Henckel, X. Chen, E. R. Cofell, M. P. de Heer, S. Verma, A. A. Gewirth, and P. J. A. Kenis, *Binder-focused approaches to improve the stability of cathodes for CO_2 electroreduction,* ACS Applied Energy Materials **4**, 5175 (2021).

[43] Y. Xu, J. P. Edwards, S. Liu, R. K. Miao, J. E. Huang, C. M. Gabardo, C. P. O'Brien, J. Li, E. H. Sargent, and D. Sinton, *Self-cleaning CO2 reduction systems: Unsteady electrochemical forcing enables stability,* **6**, 809 (2021).

[44] M. Li, M. N. Idros, Y. Wu, T. Burdyny, S. Garg, X. S. Zhao, G. Wang, and T. E. Rufford, *The role of electrode wettability in electrochemical reduction of carbon dioxide,* Journal of Materials Chemistry A (2021), 10.1039/d1ta03636j.

[45] P. Jeanty, C. Scherer, E. Magori, K. Wiesner-Fleischer, O. Hinrichsen, and M. Fleischer, *Upscaling and continuous operation of electrochemical CO_2 to CO conversion in aqueous solutions on silver gas diffusion electrodes,* Journal of CO_2 Utilization **24**, 454 (2018).

[46] B. D. Mot, J. Hereijgers, M. Duarte, and T. Breugelmans, *Influence of flow and pressure distribution inside a gas diffusion electrode on the performance of a flow-by CO_2 electrolyzer,* Chemical Engineering Journal **378**, 122224 (2019).

[47] A. Löwe, C. Rieg, T. Hierlemann, N. Salas, D. Kopljar, N. Wagner, and E. Klemm, *Influence of temperature on the performance of gas diffusion electrodes in the CO_2 reduction reaction,* ChemElectroChem **6**, 4497 (2019).

[48] F. Bidault, D. Brett, P. Middleton, and N. Brandon, *Review of gas diffusion cathodes for alkaline fuel cells,* Journal of Power Sources **187**, 39 (2009).

[49] T. Burchardt, *An evaluation of electrocatalytic activity and stability for air electrodes,* Journal of Power Sources **135**, 192 (2004).

[50] K. Yang, R. Kas, W. A. Smith, and T. Burdyny, *Role of the carbon-based gas diffusion layer on flooding in a gas diffusion electrode cell for electrochemical CO_2 reduction,* ACS Energy Letters **6**, 33 (2020).

[51] C. M. Gabardo, C. P. O'Brien, J. P. Edwards, C. McCallum, Y. Xu, C.-T. Dinh, J. Li, E. H. Sargent, and D. Sinton, *Continuous carbon dioxide electroreduction to concentrated multi-carbon products using a membrane electrode assembly,* Joule **3**, 2777 (2019).

[52] D. Salvatore and C. P. Berlinguette, *Voltage matters when reducing CO_2 in an electrochemical flow cell,* ACS Energy Letters **5**, 215 (2019).

[53] Y. Chen, A. Vise, W. E. Klein, F. C. Cetinbas, D. J. Myers, W. A. Smith, T. G. Deutsch, and K. C. Neyerlin, *A robust, scalable platform for the electrochemical conversion of CO_2 to formate: Identifying pathways to higher energy efficiencies,* ACS Energy Letters **5**, 1825 (2020).

[54] R. Kas, A. G. Star, K. Yang, T. V. Cleve, K. C. Neyerlin, and W. A. Smith, *Along the channel gradients impact on the spatioactivity of gas diffusion electrodes at high conversions during CO_2 electroreduction,* ACS Sustainable Chemistry & Engineering **9**, 1286 (2021).

[55] C. P. O'Brien, R. K. Miao, S. Liu, Y. Xu, G. Lee, A. Robb, J. E. Huang, K. Xie, K. Bertens, C. M. Gabardo, J. P. Edwards, C.-T. Dinh, E. H. Sargent, and D. Sinton, *Single pass CO_2 conversion exceeding 85% in the electrosynthesis of multicarbon products via local CO_2 regeneration,* ACS Energy Letters **6**, 2952 (2021).

[56] Y. C. Li, G. Lee, T. Yuan, Y. Wang, D.-H. Nam, Z. Wang, F. P. G. de Arquer, Y. Lum, C.-T. Dinh, O. Voznyy, and E. H. Sargent, *CO_2 electroreduction from carbonate electrolyte,* ACS Energy Letters **4**, 1427 (2019).

[57] T. Li, E. W. Lees, M. Goldman, D. A. Salvatore, D. M. Weekes, and C. P. Berlinguette, *Electrolytic conversion of bicarbonate into CO in a flow cell,* Joule **3**, 1487 (2019).

[58] E. W. Lees, M. Goldman, A. G. Fink, D. J. Dvorak, D. A. Salvatore, Z. Zhang, N. W. X. Loo, and C. P. Berlinguette, *Electrodes designed for converting bicarbonate into CO,* ACS Energy Letters **5**, 2165 (2020).

[59] A. G. Fink, E. W. Lees, Z. Zhang, S. Ren, R. S. Delima, and C. P. Berlinguette, *Impact of alkali cation identity on the conversion of HCO_3 to CO in bicarbonate electrolyzers,* ChemElectroChem **8**, 2094 (2021).

[60] Z. Yin, H. Peng, X. Wei, H. Zhou, J. Gong, M. Huai, L. Xiao, G. Wang, J. Lu, and L. Zhuang, *An alkaline polymer electrolyte CO_2 electrolyzer operated with pure water,* Energy & Environmental Science **12**, 2455 (2019).

[61] B. Endrődi, A. Samu, E. Kecsenovity, T. Halmágyi, D. Sebők, and C. Janáky, *Operando cathode activation with alkali metal cations for high current density operation of water-fed zero-gap carbon dioxide electrolysers,* Nature Energy **6**, 439 (2021).

[62] Y. C. Li, D. Zhou, Z. Yan, R. H. Gonçalves, D. A. Salvatore, C. P. Berlinguette, and T. E. Mallouk, *Electrolysis of CO_2 to syngas in bipolar membrane-based electrochemical cells,* ACS Energy Letters **1**, 1149 (2016).

[63] D. A. Salvatore, D. M. Weekes, J. He, K. E. Dettelbach, Y. C. Li, T. E. Mallouk, and C. P. Berlinguette, *Electrolysis of gaseous CO_2 to CO in a flow cell with a bipolar membrane,* ACS Energy Letters **3**, 149 (2017).

[64] D. A. Vermaas, S. Wiegman, T. Nagaki, and W. A. Smith, *Ion transport mechanisms in bipolar membranes for (photo)electrochemical water splitting,* Sustainable Energy & Fuels **2**, 2006 (2018).

[65] J. C. Bui, I. Digdaya, C. Xiang, A. T. Bell, and A. Z. Weber, *Understanding multi-ion transport mechanisms in bipolar membranes,* ACS Applied Materials & Interfaces **12**, 52509 (2020).

[66] Z. Yan, J. L. Hitt, Z. Zeng, M. A. Hickner, and T. E. Mallouk, *Improving the efficiency of CO_2 electrolysis by using a bipolar membrane with a weak-acid cation exchange layer,* Nature Chemistry **13**, 33 (2020).

[67] M. A. Blommaert, D. Aili, R. A. Tufa, Q. Li, W. A. Smith, and D. A. Vermaas, *Insights and challenges for applying bipolar membranes in advanced electrochemical energy systems,* ACS Energy Letters **6**, 2539 (2021).

[68] R. I. Masel, Z. Liu, H. Yang, J. J. Kaczur, D. Carrillo, S. Ren, D. Salvatore, and C. P. Berlinguette, *An industrial perspective on catalysts for low-temperature CO_2 electrolysis,* Nature Nanotechnology **16**, 118 (2021).

3

Persistent high local pH during CO_2 electroreduction in an aqueous cell

Over the past decade, electrochemical carbon dioxide reduction has become a thriving area of research with the aim of converting electricity to renewable chemicals and fuels. Recent advances through catalyst development have significantly improved selectivity and activity. However, drawing potential dependent structure-activity relationships has been complicated, not only due to the ill-defined and intricate morphological and mesoscopic structure of electrocatalyts, but also by immense concentration gradients existing between the electrode surface and bulk solution. In this work, by using in-situ surface enhanced infrared absorption spectroscopy (SEIRAS) and computational modelling, we explicitly show that commonly used strong phosphate buffers cannot sustain the interfacial pH during CO_2 electroreduction on copper electrodes at relatively low current densities, < 10 mA/cm^2. The pH near the electrode surface was observed to be as much as 5 pH units higher compared to bulk solution in 0.2 M phosphate buffer at potentials relevant to the formation of hydrocarbons (– 1 V vs RHE), even on smooth polycrystalline copper electrodes. Drastically increasing the buffer capacity did not stand out as a viable solution for the problem as the concurrent production of hydrogen increased dramatically, which resulted in a breakdown of the buffer in a narrow potential range. These unforeseen results imply that most of the studies, if not all, on electrochemical CO_2 reduction to hydrocarbons in CO_2 saturated aqueous solutions were evaluated under mass transport limitations on copper electrodes. We underscore that the large concentration gradients on electrodes with high local current density (e.g. Nanostructured) have important implications on the selectivity, activity, and kinetic analysis, and any attempt to draw structure-activity relationships must rule out mass transport effects.

This chapter has been published in J. Am. Chem. Soc. **2019**, 141, 15891-15900.[1] K. Yang performed the electrochemical tests on Cu electrodes. Dr. R. Kas carried out the SEIRAS measurements and modelling work.

3.1. Introduction

Rising atmospheric CO_2 levels and associated climate change will put local and global economies under enormous pressure if immediate actions are not taken to escalate significant cuts in carbon emissions.[2] Due to the immense scale of the problem, the deployment of multiple technologies will be necessary to combat this problem depending on location, industry and other societal, economical, and political constraints. One of the most promising technologies to address these needs is the electrochemical reduction of CO_2 to CO, hydrocarbons and multi-carbon oxygenates.[3] This approach not only bypasses hydrogen production by supplying protons from solution, but also reduces energy transformation and separation costs when compared to thermo-catalytic processes.

Nanostructured metal electrodes have provided encouraging results in their ability to decrease the required overpotentials to form products such as HCOOH, CO and C_2H_4.[4–7] Regardless of the catalyst material and morphology, nanostructured and porous catalysts typically shift the onset potential of CO_2 reduction towards less negative potentials and/or provide better selectivity towards carbon-based products over H_2 evolution.[5, 8] Although the nanoscale effects and surface structure to the electrocatalytic activity cannot be overlooked on these electrodes,[9–12] the selectivity towards CO and C2 products over hydrogen at high currents can be very susceptible to mass transport effects.[13–16] One of the key reasons for this delicate interplay is the participation or absence of protons in the rate determining step of the formed product. The proton decoupled electron transfer during the formation of C2 products on copper surfaces has been well established independently by different research groups.[17–19]

Although less established, there is a noteworthy amount of evidence that the formation of CO on gold surfaces may also take place via a rate determining step where electron and proton transfer is decoupled.[20] Subsequently, there is a particular trend for the products that are formed via a pH independent (vs.NHE) pathway compared to the ones that are pH dependent, e.g. methane and hydrogen,[21, 22] as the (local) pH of the solution is increased.[23–25] The evaluation of different catalysts by minimizing the concentration difference between the bulk and surface is of key importance to not only compare the intrinsic activity and selectivity of a catalyst, but to also accurately test and provide meaningful input to computational calculations.[26]

During the electrochemical reduction of CO_2, the concentration of protons and CO_2 near the electrode surface is counterbalanced between consumption from the electrode, diffusion from the bulk solution, and homogeneous buffer reactions.[27] When the reactions are carried out at a high current density or in electrolytes that have poor buffer action and/or mass transport, the pH near the cathode surface is well known to increase compared to the bulk value.[28, 29] Although the impact of local conditions on the selectivity of metal electrodes is well recognized, simulated and reproduced,[19, 27, 28, 30, 31] it is still a common practice to test high surface area electrodes in very low buffer capacity solutions. While the surface structure of a catalyst is very important to determine its intrinsic selectivity and activity, the distinction between the effect of surface structure and mass transport effects on the electrocatalytic activity is not explicitly clear and needs to be urgently clarified in order to improve fundamental understanding of reaction mechanisms.[32] Recently, Dunwell et al. studied the concentration gradients near the electrode surface by using SEIRAS in bicarbonate solutions with special emphasis on the implications of the kinetic analysis.[30]

However, the activity and selectivity towards CO_2 reduction products has not been extensively described. Moreover, a comparison of simulation results with physical measurements is currently missing in the literature.[8, 24]

We studied the near-surface concentrations of reactants, e.g. protons and CO_2, during CO_2 electrolysis by using in-situ surface enhanced infrared absorption spectroscopy (SEIRAS) under densely buffered neutral pH concentrations in phosphate electrolytes. These electrolytes are commonly used as high buffer capacity solutions to evaluate and exclude local pH effects on the catalytic selectivity, and thus it is vital to understand their buffer capacity and mass transport to cathode during CO_2 electrolysis.[8, 33] In our work, we would not only like to test the buffer strengths of these solutions, but also attempt to find a suitable electrolyte which can minimize the difference between local and bulk environment for kinetic studies. The experimental results were supported by a computational model that takes into account bubble induced mass-transport and the concentration dependent solubility of CO_2 in order to mimic the conditions created during in-situ SEIRAS measurements. In addition, the activity and selectivity of a sputtered copper electrode and a very high surface area electrode composed of densely packed copper nanowires were tested with variable buffer concentrations, and the implications of these findings are thoroughly discussed. The experimental and computational data show that all concentrations of phosphate buffer breakdown quickly in a narrow potential window, with the lowest concentrations having the steepest pH gradient. These results suggested that most CO_2 electroreduction experiments on the formation of hydrocarbons and oxygenates have been done in mass transport limited configurations in CO_2 saturated aqueous solutions, which severely complicates the mechanistic insights that have been derived from them.

3.2. Experimental methods

Preparation of SEIRA active films 25 nm thick copper thin films were deposited onto a 60° bevelled germanium internal reflection element (IRE) by magnetron sputtering deposition. Although silicon is a better choice in terms of electrochemical stability, the transparency of silicon IRE does not allow measurements below 1000 cm^{-1}, which includes the crucial phosphate bands. Nevertheless, Ge IREs were suitable for this study due to the range of applied cathodic potentials that were used.[3] Before sputtering, Ge IRE was mirror polished by using 1.0 µm, 0.3 µm and 0.05 µm grain sized alumina paste, respectively, which was followed by thoroughly rinsing with iso-propyl alcohol and water. The IRE was transferred into the sputtering chamber in which a pressure of 1.8×10^{-7} mbar was maintained. Then it was placed to a suitable working distance and rotated at a velocity of 15°/s to enable a uniform deposition of copper. Following this, argon was allowed to flow through the sputtering system maintaining a pressure of 3 µbar, and copper was sputtered using a plasma power of 20 W, which resulted in a growth rate approximately 0.04 nm/s. The sputtering process was performed for 10 minutes to produce 25 nm thick copper films that resulted in a mirror finish similar to that of the germanium IRE. Side to side resistance of the films along the 2 cm wide IRE was measured after the sputtering and was found to be typically between 25-35 Ω.

Spectroelectrochemical measurements All spectroelectrochemical measurements were performed in a custom made modular cell schematically depicted in Figure 3.2(b). Copper

thin films sputtered on a Ge internal reflection element served as the cathode electrode. A Ag/AgCl (BASI) reference electrode in 3 M NaCl solution was used as the reference electrode, whilst the counter electrode was a graphite rod. Upon assembly, the cell was placed in a Bruker Vertex 70 spectrometer equipped with a liquid nitrogen cooled LN-MCT detector and a Veemax III ATR accessory. The spectrometer and sample compartment were purged with nitrogen (5.0 grade) for 30 min to remove atmospheric water vapor and CO_2. All electrochemical measurements were performed using a BioLogic SP-200 potentiostat. In order to obtain an appreciable signal, for all Cu thin films, an activation routine was applied consisting of three voltammetry cycles between 0.5 V and – 0.4 V vs. RHE in 0.1 M NaCl. After activation of the surface, the spectroelectrochemical cell was rinsed thoroughly with ultra-pure water and then a background spectrum was collected in electrolyte free water solutions. Voltammetry measurements were performed between 0 V and – 1.25 V vs RHE with a scan rate of 1 mV/s in various concentrations of CO_2 saturated phosphate buffers prepared from K_2HPO_4 and KH_2PO_4 salts (Sigma, ACS reagent grade). Simultaneously, IR spectra were collected in Kretschmann configuration at a resolution of 4 cm^{-1} and 32 co-added scans were recorded for each 10 mV. Solution resistance was measured by electrochemical impedance spectroscopy and extracted from a high frequency intercept of the Nyquist plot in the frequency range from 100 kHz to 10 Hz. All the potentials were corrected for IR losses after the experiments.

Preparation of Copper Electrodes Cu nanowires were synthesized on a Cu wire (99.9%, 1mm diameter, Sigma-Aldrich) and used as cathodes/working electrodes. The Cu wires were cleaned with acetone and ethanol in an ultrasonicator, each for 5 min separately, then rinsed with de-ionized water several times and dried with N_2. $Cu(OH)_2$ nanowires were first fabricated on the copper wire substrates using a wet chemical method. The cleaned copper substrates were immersed into a solution mixture containing 0.133 M $(NH_4)_2S_2O_8$ (98%, Sigma-Aldrich) and 2.667 M NaOH (99.99%, Alfa-Aesar) for 10 min. The color of wires changed from reddish brown to blue, indicating the formation of $Cu(OH)_2$ on the surface of Cu wire substrate. After 10 min, the Cu wires were taken out of the solution, thoroughly cleaned with de-ionized water and dried with nitrogen. Finally, Cu wires were placed into a tube oven at 180°C for 2h in air flow to form CuO nanowires. Smooth Cu electrodes were fabricated by magnetron sputtering deposition (AJA International Inc.)100 nm thick Cu on Ti substrate (99.5%, Alfa Aesar) with the rate of 0.14 nm/s using 50 watt DC power supply. The morphologies of catalysts before and after electrochemical CO_2 reduction were characterized using scanning electron microscope (Figure SI13) (SEM, JEOL, JSM-6010LA).

CO_2 electrolysis and analysis Electrochemical CO_2 reduction measurements were conducted in a custom made two-compartment H type of cell (Figure 3.1). The Cu electrodes were placed in the cathodic compartment (12 mL of electrolyte, 3 mL headspace) close to the Ag/AgCl reference electrode and served as the working electrode. A Pt mesh was used as the counter electrode and positioned in the anodic compartment, which was separated from the cathodic part by a Nafion-115 proton exchange membrane. Different concentrations of phosphate buffer (0.1 M, 0.25 M and 0.5 M, KH_2PO_4/K_2HPO_4 = 1:1) were used as the electrolytes. Electrolytes were saturated with CO_2 by purging CO_2 gas into the solutions for at least 4 h. During electrochemical CO_2 reduction tests, CO_2 was continuously purged into the catholyte and anolyte, both at a rate of 10-20 sccm through mass flow controllers (Bronkhorst High-Tech). A PARSTAT 4000A potentiostat was used for all electrolysis experiments. Before electrochemical measurements, a potential of – 0.8 V vs. Ag/AgCl

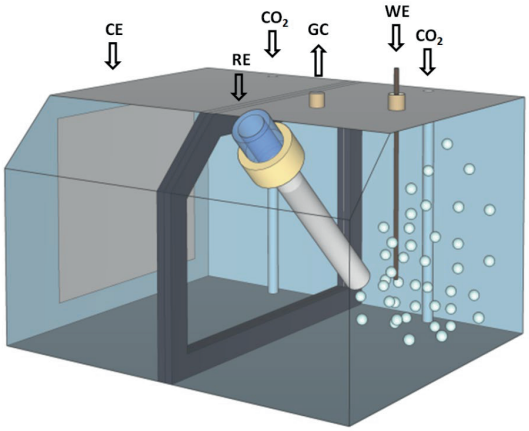

Figure 3.1: Illustration of the electrochemical cell used for CO_2 reduction.

was applied to reduce the CuO nanowires to Cu nanowires. All potentials reported in this work were IR corrected and converted to the reversible hydrogen electrode (RHE) for convenience. Each electrochemical measurement was conducted over a time span of 2200 s by applying a constant current under 1000 rpm stirring with a magnetic bar. During the experiments, gas products were collected and quantified by using online gas chromotography (GC) at 3 minute intervals (Compact GC 4.0, GAS). An average of six measurements were used unless any deactivation was observed, which was the case typically at high potentials. In such cases, the faradaic efficiency of H_2 increased gradually while the FE of C_2H_4 decreased as potential became less negative. After experiments, 5 mL liquid products were collected for nuclear magnetic resonance (NMR 400 MHz, Agilent) and high performance liquid chromatography (HPLC, Agilent 1260 Infinity) analysis. In a typical NMR measurement, 540 µL catholyte was mixed with 60 µL D_2O (99.9%, Sigma-Aldrich) containing 5 mM DMSO (99.7%, Sigma-Aldrich) as internal standard. 1H NMR spectrum was measured with 2 s presaturation delay, 2 s relaxation delay, 2 s acquisition time and water suppression. 50 µL liquid sample was injected to HPLC apparatus equipped with Hi-Plex H column with 0.02 M H_2SO_4 mobile phase. The surface roughness factor of the electrodes was determined by measuring the double layer capacitance of the Cu nanowires. Cyclic voltammograms with different scan rates between 0.05 V to 0.2 V (vs. RHE) were performed in a non-faradaic region in 0.1 M $NaClO_4$ solution (Figure SI5). The capacitance was obtained by plotting the geometric current density against the scan rate of the CVs. The surface roughness factor was calculated by comparing this capacitance value to that of a reported smooth polycrystalline Cu electrode.

3.3. Results and discussion

An Atomic Force Microscopy (AFM) image of a typical 25 nm thick Cu film sputtered on Ge is given in Figure 3.2(a). The film was composed of partially merged metal islands with an average diameter of 30 nm that were initially nucleated onto the Ge surface. Calibration and

experiments were conducted in a custom designed spectroelectrochemical cell in which the copper coated Ge internal reflection element (IRE) was mounted to the bottom of cell serving as the working electrode (Figure 3.2(b)). The SEIRA spectra of phosphate species on a 25 nm thick Cu film for different pH values were measured and the results are shown in Figure 3.2(c). The SEIRA spectrum taken at pH 4.34 exhibited three major peaks at 1152 cm^{-1}, 1076

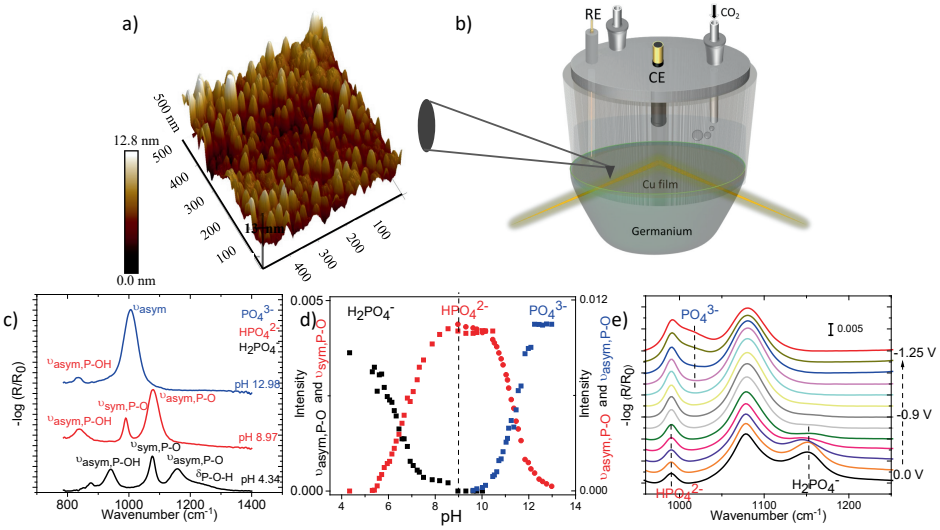

Figure 3.2: (a) AFM image of sputtered Cu film on to Ge. (b) Schematic representation of the spectroelectrochemical cell used for in-situ SEIRAS measurements. Reference electrode (RE) is Ag/AgCl and Counter electrode (CE) is a graphite rod. (c) pH dependent SEIRA spectra of phosphate solutions indicating the dominating species. (d) Equilibrium of phosphate species constructed by absorption in intensity in SEIRA spectrum. (e) Potential dependent changes in the concentrations of phosphate species near the electrode surface.

$cm^{-1}$and 941 cm^{-1}, which were assigned to asymmetrical ν_a(PO), symmetrical ν_s(PO) and asymmetrical ν_a(POH) vibrations of $H_2PO_4^-$, respectively.[34] After complete deprotonation of $H_2PO_4^-$ around pH 9, the spectra exhibited the same vibrational modes that slightly shifted to lower frequencies belonging to HPO_4^{2-}.[34] As the solution was changed to become more alkaline, the spectra became dominated by the asymmetrical stretching of the PO_4^{3-} molecule around 1005 cm^{-1}. To monitor the pH changes during electrolysis, calibration spectra were recorded between pH 5–12 by the addition of KOH to the parent $H_2PO_4^-$ solution and recording a spectrum every 0.2 ± 0.1 pH units (Figure SI1). The overlapping bands were deconvoluted to resolve the contributions from individual bands (Figure SI1), and peak heights were derived from ν_a(PO) of $H_2PO_4^-$ and ν_s(PO) of HPO_4^{2-} between pH 5–9 and ν_a(PO) of HPO_4^{2-} and PO_4^{3-} between pH 9–12. The deconvoluted peak contributions are plotted as a function of pH in Figure 3.2(d).

It is important to note that it is difficult to obtain SEIRAS active films with the same enhancement factors, and therefore the ratios of peaks are taken into account to determine the pH during electrochemical experiments. The changes in the spectra of phosphate species were recorded upon sweeping the potential in the cathodic direction with a scan rate of 1 mV/s for CO_2 purged phosphate solutions containing equimolar amounts of $H_2PO_4^-$ and

of HPO_4^{2-} (Figure 3.2(e)). The initial concentrations of $H_2PO_4^-$ and HPO_4^{2-} were slightly changed upon purging CO_2 due to the shift of the equilibrium towards $H_2PO_4^-$. As the potential was scanned towards more negative potentials, the shift of the equilibrium towards HPO_4^{2-} was apparent from the increase in the concentration of HPO_4^{2-} (ν_s(PO), 990 cm^{-1}) at the expense of $H_2PO_4^-$ (ν_a(PO),1152 cm^{-1}). Potentials more negative than – 1.0 V vs RHE gave rise to the ν_a(PO) mode of PO_4^{3-} as a shoulder around 1010 cm^{-1}indicating that the pH near the surface is above 9. The pH near the electrode surface was calculated for various potentials and curren densities by correlating the ratio of phosphate peaks in the sample spectra to the calibration spectra after assuming the resultant spectra are the linear combination of the phosphate species.[35]

Near surface concentrations of molecules during CO_2 electroreduction can be approximated computationally by the Nernst-Planck equation.[36, 37] However, recent in-situ SEIRAS measurements in bicarbonate solutions implied that physical measurements might be necessary to accurately quantify the local concentrations of molecules.[35] For SEIRA active smooth surfaces, the concentration of molecules within the boundary layer were calculated as a function of current density by including diffusion, bubble induced convective mixing and bulk reactions of buffer molecules in this study.[36, 38–40]

The electric field leading to the surface enhancement effect on SEIRA active thin metal electrodes decays in very short distances (5–10 nm) from the surface when compared to the thickness of the diffuse layer (30–300 µm), which allows the ability to monitor local concentrations of species as schematically depicted in Figure 3.3(a).[35, 41] Considering the high concentrations of the electrolytes, infrared absorption from the bulk electrolyte can be significant in addition to the SEIRA effect. However, the metal films further dampen infrared light, and for copper films the penetration depth of the evanescent wave was approximated to not extend longer than 50 nm.[42] The experimentally measured (Figure 3.3(b)) and simulated (Figure 3.3(c)) pH near the electrode surface is shown as a function of current density for different concentrations of phosphate buffers, 0.2, 0.5 and 1M, respectively. In spite of the discrepancies between the experimental data and the simulation results, the overall agreement is reasonable, considering the assumptions and simplifications made during the simulation which will be discussed in the next section. Three distinct regions for the local pH as a function of current density were observed, which was more apparent for high electrolyte concentrations, including two buffering regions, indicated by plateaus in local pH, and a breakdown of the parent buffer solution ($H_2PO_4^-$/HPO_4^{2-}). In the first region of low current density, the buffer solutions sustained the local pH with a reasonable difference (< 1.5) with respect to the bulk pH depending on the buffer capacity. Considering the fact that buffers are only effective in a certain range near the pKa, the steep increase in local pH between 8–10 can be seen as a result of the breakdown of the buffer. The current density where this was observed is particularly important because the steep increase in the pH in a very narrow window of current density will cause a huge overestimation of the kinetic overpotential. Strikingly, the current density where this happens was very low (< 10 mA/cm^2) for the commonly used 0.2 M phosphate buffer solution. In fact, the 0.2 M phosphate buffer barely showed a noticeable buffering region at all, and as the current density was increased the local pH also increased considerably fast.

Increasing the electrolyte concentration had a substantial effect on the buffering ability of the solution as anticipated. The buffer breakdown current density for 0.5 M and 1 M phos-

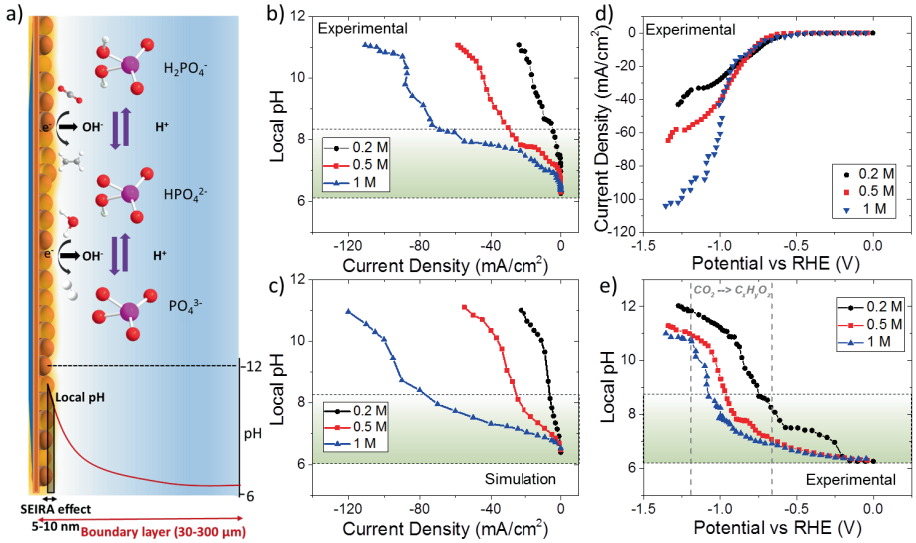

Figure 3.3: (a) Schematic representation of buffer reactions, pH gradient and probed area SEIRA. (b) Experimentally measured and (c) Simulated cathode surface pH as a function of phosphate buffer concentration and current density. (d) Current vs. Potential curve for different electrolyte concentrations. (e) Experimentally measured cathode surface pH as a function of potential. All solutions are composed of equimolar $H_2PO_4^-$ and HPO_4^{2-} mixtures. Shaded areas in b, c and d represent the buffering region that are relevant to local pH measurements.

phate was around – 30 mA/cm^2 and – 75 mA/cm^2, respectively which is reasonably high for an electrode tested in CO_2 saturated aqueous solution. However, the overall impact of the wider buffering region on the evaluation of the performance of electrocatalysts was remarkably dependent on the total current density at a specific potential. In Figure 3.3(d), the recorded current-potential curves during SEIRAS measurements are given for different electrolyte concentrations. All three electrolyte concentrations exhibited a similar current-potential profile until the current density was sufficient for breakdown of the particular buffer. The breakdown of each individual buffer leads to a plateau in the current-potential curves due to a sudden increase in the concentration overpotential. Please note that this region overlaps with the broad shoulder observed in phosphate buffers that was attributed to CO_2 reduction to formate and/or CO on copper electrodes.[43] More importantly, the rise in the current density at high potentials with increasing concentration of the buffer solution had a large impact on the buffering ability at a specific potential. This is more clearly reflected in Figure 3.3(e), where the local pH near the electrode surface is plotted as a function of the potential for different electrolyte concentrations. Remarkably, despite the large changes in the phosphate concentrations, the buffering ability at high potentials is limited due to the increase in the overall current density. The expansion of the buffer potential window with increasing electrolyte concentration was more evident between 0.2 M and 0.5 M, while doubling the concentration from 0.5 M to 1 M enlarged the potential window of the buffers only 50 mV. Nevertheless, high phosphate concentrations (> 0.5 M) exhibited an acceptable pH gradient at potentials between – 0.7 to – 1.0 V vs. RHE, which partially overlap with the formation of hydrocarbons. In addition, even though all the electrodes attained an

alkaline pH near the electrode surface at potentials more negative than – 1 V vs RHE, the high buffer capacity solutions still had a slightly lower local pH.

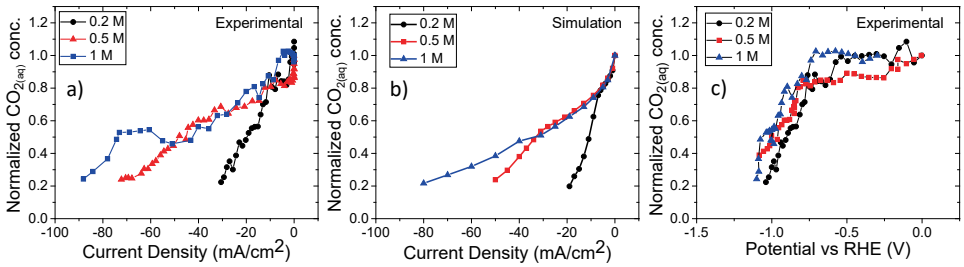

Figure 3.4: (a) Experimentally measured and (b) Simulated cathode surface concentrations of CO_2(aq) as a function of phosphate buffer concentration and current density) Experimentally measured changes in CO_2 concentration near the electrode surface as a function of potential. All solutions are composed of equimolar $H_2PO_4^-$ and HPO_4^{2-} mixtures. CO_2 concentrations are normalized to initial equilibrium concentrations.

CO_2 concentrations near the electrode surface were quantified by monitoring the change in the CO_2(aq) band intensity with respect to its initial intensity while sweeping the potential negatively (Figure SI2). The experimentally measured (Figures 3.4(a)) and simulated (Figure 3.4(b)) CO_2(aq) concentrations near the electrode surface were plotted as a function of current density for different concentrations of phosphate buffers, respectively. The initial decrease in the concentration of CO_2 with increasing current density was the result of electrochemical consumption on the electrode surface following similar rates at lower current density (< 5 mA/cm^2), which was more apparent in the simulation results.[27] More importantly, the consumption rate of CO_2 changed dramatically at particular current densities for different electrolyte concentrations. At this specific current density, nearly all $H_2PO_4^-$ was converted to HPO_4^{2-} (local pH around 9) for all electrolyte concentrations , and thus the increase in the consumption rate of CO_2 was result of the homogenous reaction of CO_2 with the cathodically produced hydroxide ions. This observation is also supported by the steady increase in (bi)carbonate concentrations near the electrode surface determined by the SEIRA spectra (Figure SI3). The change in the consumption rate was more evident in the simulation results, most likely due to the constant faradaic efficiency assumed at different current densities. Nevertheless, experimental and theoretical results for different electrolyte concentrations exhibited very similar patterns as a function of current density. However, the apparent beneficial role of high buffer capacity solutions is again not reflected in the potential curves. In Figure 3.4(c), a change in the CO_2(aq) concentration near the electrode surface is plotted against potential. The corresponding potential where CO_2 begins to be consumed appreciably and the formation of adsorbed CO were in good agreement with the onset potentials of hydrocarbons (– 0.75 V vs RHE) and CO (– 0.45 V vs RHE) on polycrystalline copper (Figure SI4). More importantly, similar to the local pH, the CO_2 concentration near the electrode surface exhibited only a slight dependence on the electrolyte concentration against the applied potential when compared to plots against current density. This observation challenges the common presumption that increasing the buffer capacity leads to a higher CO_2(aq) concentraion near the electrode surface at the same applied potential.

In order to link the aforementioned results to the performance of copper electrodes, the CO_2 reduction activity and selectivity of a sputtered flat copper electrode was evaluated. Additionally, a high surface area electrode composed of copper nanowires was tested to attempt to correlate the results obtained on flat copper surfaces to high surface electrodes. Scanning electron microscope (SEM) images of the sputtered and nanowire copper electrodes are shown in Figure 3.5(a) and 3.5(b), respectively. The roughness factors of the electrodes were found to be 2.4 and 55, respectively, by comparing to an electropolished copper surface (Figure SI5). Due to the extensive bubbling of hydrogen causing a disruption of electrochemical experiments at high electrolyte concentrations, and a relatively lower impact of doubling the concentration from 0.5 M to 1 M (see Figure 3.3(e)), lower electrolyte concentrations were used (0.1– 0.5 M) in our experiments, which cover the commonly used ranges in the literature.The partial current density of CO_2 electroreduction and H_2 evolution for smooth and nanowire copper electrodes are shown in Figure 3.5c and 3.5d. The incremental effect of the electrolyte concentration on the partial current density of HER was evident in a broad range of applied potentials for both smooth and nanowire electrodes, which is predominantly the result of a decrease in the concentration overpotential.

However, the partial current density for CO_2 reduction products exhibited a very small dependence on the electrolyte concentration and peaked between 10–12 mA/cm^2, and 50 and 60 mA/cm^2 on smooth and nanowire copper electrodes, respectively. This is most likely a result of mass transport limitations (Figure SI11) [24, 44] in which the lowest concentration of the electrolyte (0.1 M) showed a slightly lower mass transfer limited current density. Although the CO_2 solubility is lower at higher electrolyte concentrations, a slightly lower pH near the electrode surface and more extensive bubbling are considered to result in a slightly higher mass transfer limited current density for CO_2 reduction. It is important to note that the mass transport limited current density, normalized to the number electrons transferred for the formation of each product, is highly dependent on the cell design, distribution of the CO_2 gas and stirring efficiency.[45] Although the electrolysis experiments were conducted in the same cell for both electrodes, the nanowire electrodes showed an 4–5 fold increase in mass transport limited current density. This is a result of enhanced bubble induced mass transport found on the nanowire electrodes. For instance, Burdyny et al. recorded a 4 fold increase in mass transport limited current density for CO_2 electroreduction to CO when the morphology of gold electrodes was changed from nanoparticles to nanoneedles.[38] Therefore, we underscore that maintaining the consistency in hydrodynamics of the electrochemical cells may not necessarily lead to the same mass transfer limited current density depending on the morphology of the electrodes.

The potential dependent partial current density and FE of the all gas and liquid products for both electrodes were measured, and are presented in the supporting information. The partial current density versus potential plots are considered to be a better representation of the activity because a change in the selectivity of products can be influenced dramatically by the changes in the rates of HER. For instance, a higher selectivity towards CO_2 reduction products (72%) was obtained on the nanowire electrodes at low electrolyte concentrations when compared to the selectivity at high electrolyte concentrations (30%) at a potential of – 0.95 V vs RHE in (Figure SI6). Although this was found to be less prominent for sputtered copper electrodes, a change in selectivity towards CO_2 reduction products from 40% to 20% was also recorded by increasing the electrolyte concentration at a potential of – 1.05 V vs RHE (Figure SI7). However, the increased selectivity at low electrolyte concentrations was

largely a result of lower hydrogen production rather than an increase in the production rate of CO_2 reduction, as manifested from the partial current density plots.

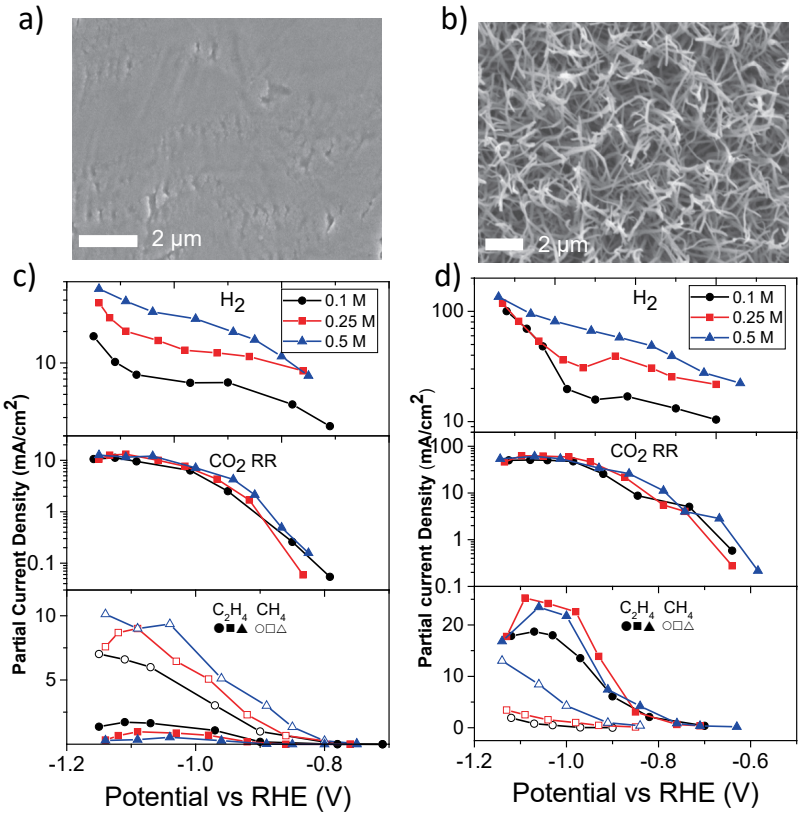

Figure 3.5: SEM image of the (a) Sputtered and (b) Nanowire copper electrodes. Partial current density of H_2, and CO_2 ethylene and methane as a function of potential and phosphate buffer concentration for (c) Sputtered and (d) Nanowire copper electrode.

Moreover, we would like to highlight the suppression of methane on the nanowire electrodes compared to the sputtered electrodes, which has led to a longstanding debate in the literature.[8, 24] The onset potential of methane on sputtered copper surfaces was around –0.85 V vs RHE while the onset potential was observed around – 1.1 V vs RHE at about at the same electrolyte concentration (0.1 M) on nanowire electrodes, as shown in Figure 3.5(c) and 3.5(d). A high concentration of phosphate buffer and very negative potentials (– 1.1 V) were necessary to produce appreciable amounts of methane with respect to ethylene on rough copper surfaces. Therefore, ethylene formation, along with other C2 and C3 products (Figure SI8), surpassed methane formation on rough copper surfaces at potentials between – 0.75 and – 1.0 V vs RHE in contrast to smooth copper electrodes where methane formation was dominant.

On the basis of the above experimental and computational results, in this section we discuss the correlation between these results and the insights that they provide in conjunction with previous studies for understanding, interpretation and implementing electrochemical CO_2 reduction. First, bicarbonate is by far the most commonly used electrolyte in aqueous electrochemical and is known to have lower buffer capacity than the phosphate buffers used in this study.[27, 33, 46] For instance, the local pH in 0.5 M NaHCO3 solution on a gold electrode was measured to be around 9 at 5 mA/cm^2,[30] while the same local pH was recorded around 40 mA/cm^2 for the 0.5 M phosphate buffer in this study. In spite of this fact, we explicitly showed that the pH near the electrode surface can be dramatically different from the bulk solution (> 5 pH units) in "well buffered" phosphate solutions (0.2 M) at potentials that are relevant to the formation of hydrocarbons (– 0.9 V) and at current densities < 20 mA/cm^2 which can be considered as very low for high surface area copper electrodes.[47] This clearly demonstrates that simply switching the buffer employed from bicarbonate to phosphate solutions to examine the effect of local pH at high potentials and/or high currents is not a straightforward method and most of the previous studies in aqueous electrochemical CO_2 reduction on copper electrodes in H-cells are taking place under mass transport limitations of protons. Increasing the buffer capacity of the electrolyte up to 1 M provided a great improvement on the buffer breakdown current density, however, the potential window that can be tested with a minimal pH gradient only slightly improved due to the increase in the rate of HER at the same applied potential. In other words, the increase in the buffer capacity of the solution promotes the development of a relatively lower local pH that correspondingly increases the rate of HER. Subsequently, higher current densities achieved in the same applied potential leads to only a minor improvement in the potential ranges that can be tested with a minimal concentration gradient.

Simulation results indicated that the higher local pH is predominantly governed by slow transport of buffer ions and a fast release of hydroxide ions from HER and CO_2 electroreduction. An exact match between the experimental and simulation was not obtained due to the potential dependent and broad distribution of CO_2 reduction products which complicates the bubble induced mass transport model. Any rigorous evaluation of the accuracy of electrochemical models should be performed in CO_2 free phosphate (or bicarbonate) buffer solutions by assuming near unity FE for hydrogen and avoiding bicarbonate formation due to CO_2 purging and breakdown of the buffer.

In our work, we focus on the product formation trends and their implications in CO_2 electroreduction. Nevertheless, the simulations performed remarkably well on predicting the trends and relative magnitudes of the local pH in different electrolyte concentrations, though there are small discrepancies between the experimental and simulation results especially after the breakdown of the parent phosphate buffer ($H_2PO_4^-/HPO_4^{2-}$). At concentrations of 0.2 M and 0.5 M of the phosphate buffer, the simulation slightly deviated from the measured local pH with an average of 0.57 and 0.43 pH units, respectively . One of the reasons might be the formation and accumulation of bicarbonate during the slow voltammetry scan which contributed to the buffer capacity of the solution at lower electrolyte concentrations, while during simulations galvanostatic steps were applied. Interestingly, when all the $H_2PO_4^-$ was converted to HPO_4^{2-}, OH^- ions reacted simultaneously with CO_2, bicarbonate and HPO_4^{2-}. Therefore, any buffer performing better than HPO_4^{2-}/PO_4^{3-} might reduce the concentration overpotential due to diminishing CO_2(aq) concentrations near the electrode surface. Using a 1 M concentration of phosphate buffer, the simulation results

mostly underestimated the local pH with an average of 0.47 pH units in contrast to lower concentrations. This is most likely a result of the assumptions made during the bubble induced mass transport model, i.e. constant bubble coverage and bubble departure diameter. It is important to note that this model drastically overestimates the local pH at high current densities, i.e. underestimates the buffer capacity, in the absence of bubble induced convection even after the addition of convective mass transport via stirring (Figure SI9). Therefore, it is highly important to take into account the bubble induced mass transport while performing simulations at high current densities. However, the mass transport models for bubble induced convection are highly dependent on the departure diameter and coverage of the bubbles.[39] Small changes in bubble departure diameter and coverages make a noticeable change in the simulated values, especially after the breakdown of the buffer (Figure SI10).

The production of SEIRA active films that are more analogous to the nanowire electrodes is restricted by the percolation limit of the metal films which allows only very thin films to be studied, typically below 100 nm.[48] While a direct quantitative comparison of the near surface concentrations of molecules between the sputtered Cu films and copper nanowire electrodes is not possible, a qualitative comparison of the two different electrodes revealed striking correlations. The alkaline pH near the electrode surface at potentials relevant to the formation of hydrocarbons was clearly observed by SEIRAS experiments on sputtered copper electrodes. Since the local current density on the nanowire electrodes is much higher due to their large electrochemically active surface area (ECSA), it is anticipated that the local pH is higher on the surface of these electrodes even in the presence of highly improved mass transport from the bubbles. This is indirectly evident from the dramatic increase in the partial current density of hydrogen with increasing electrolyte concentration (Figure 3.5(d)). Moreover, due to the 3 D structure of the nanowire electrodes, a gradient of CO_2 and pH likely exists along the catalyst layer,as depicted in Figure 3.6.[40] In this architecture, the reactants are required to be transported to the catalyst layer which extends along the diffusion layer, and mass transport inside the porous catalyst merely benefits from convective forces. Assuming that convective mass transport, e.g. vigorous stirring or a flowing electrolyte, in addition to bubble induced mass transport can sustain the bulk pH outside the nanowires in an ideal sceneario, the pH and concentration of CO_2 along the catalyst layer, where the former is dramatically different at the bottom of the nanowires. The reason for this difference is the higher diffusion coefficient of CO_2 molecules compared to phosphate ions. Subsequently, the production rate of CO_2 products likely to vary along the catalyst layer and normalizing the measured activity by ECSA is an average of catalytic activity containing partially exploited and non-exploited areas.

Moreover, depending on the porosity and thickness of the catalyst layer, the activation controlled region might be very narrow as charge transfer limited and mass transport limited regions are convoluted and hard to differentiate (Figure SI11 and SI12). These types of comparisons might be potentially misleading especially when the catalyst layer is too thick and/or CO_2 electroreduction takes place via pH dependent pathways. Similarly, using Tafel analysis to verify reaction mechanisms is only appropriate under activation controlled potentials where the impact of mass transfer limitations on the measured rates is minimized. Considering the concentration gradient along the catalyst layer and a relatively low current density for the breakdown of commonly used buffer solutions, this type of analysis must be done with great care. The implication of the poor mass transport on the kinetic analysis of

CO_2 electroreduction catalysts has been thoroughly discussed recently by Dunwell et al.[26]

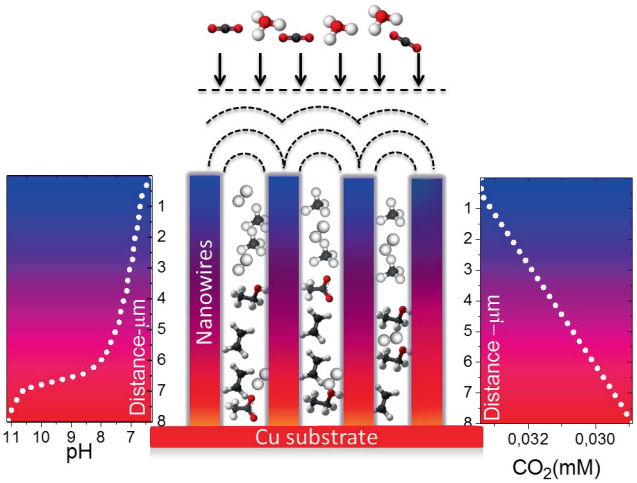

Figure 3.6: Schematic illustration and calculation of the reactant and product distribution along the catalyst layer.

The improved selectivity towards C2 and/or C3 products has been shown numerous times on roughened copper electrodes, regardless of the preparation method and resulting morphology.[24] Therefore, suppression of methane on these surfaces has led to some debate over whether there are undercoordinated active sites[49, 50] or as a result of a change in local conditions ,e.g. local pH, CO coverage and re-adsorption.[22, 51, 52] Although higher local pH itself is a result of poor mass transfer and/or buffer actions, for some products the electron and proton transfer is de-coupled during the rate determining step. For instance, the pH dependent and independent formation of methane and ethylene were recognized in the early studies of Hori.[18, 27] Therefore the rate of formation of ethylene is essentially blind to the pH changes near the electrode surface, unless the alkalinity leads to a concentration overpotential by the reaction between OH^- and CO_2(aq). Since this non-electrochemical reaction is typically slow, it can be minimized by having favourable mass transport to the electrode surface.[26] Moreover, CO coverage, and hence competition between *CO and *H has been identified recently as a potential parameter to sustain ethylene formation over a broad range of potentials, which still requires more independent studies.[51, 53] However, it is still not clear which factor plays the primary role in the suppression of methane and the formation of C2 compounds in a broad range of potentials. Nevertheless, we have shown that a high buffer capacity solution of 0.5 M phosphate was necessary to initiate an appreciable amount of methane formation on nanowire electrodes, while solutions with much lower buffer capacity were usually employed in the literature to test high surface area electrodes.[24] The onset potential of methane is sometimes shifted to more negative potentials and often not even observed (depending also on the tested potential region and hydrodynamics of the cell) when low buffer capacity solutions are used to test electrodes with high local current density.

3.4. Conclusion

Local concentration of molecules during CO_2 electroreduction was physically measured by SEIRAS and compared with the widely used mass transport simulations. The slightly extended mass transport model used in this study was quantitative enough to account for the relative magnitudes of what is recorded by SEIRAS, and prescriptive enough to predict new experiments when bubble induced mass transport effects were included. SEIRAS measurements provided crucial additional information as a function applied potential in contrast to simulations results which usually give information only as a function current density. Both experimental and calculation results strongly suggested that immense concentration gradients exist between the electrode surface and bulk in neutral solutions during CO_2 electroreduction to hydrocarbons on copper electrodes which is not able to contend with high buffer capacity solutions (1 M phosphate buffer). The resulting local pH on the surface of flat sputtered copper electrodes in densely buffered electrolytes were much higher than initially anticipated. Remarkably, even though increasing electrolyte concentration have a substantial effect on the buffering capacity of the solutions as a function of current density, a dramatic increase in HER resulted in only a slight improvement on the potential window that can be tested with minimal pH and CO_2(aq) gradients. It is important to reemphasize that although the morphology of the catalyst can provide significant changes in the activity and selectivity of the electrocatalysts, the distinct contributions of intrinsic activity and the local environment are currently far from being resolved. Considering that electrolysis in CO_2 saturated aqueous solutions cannot attain commercially viable rates of production at ambient pressure, evaluation of intrinsic activity and extraction of kinetic parameters in the absence of mass transport limitations should be the primary goal which can be potentially transferred to other type of electrochemical cell designs and practical applications.

References

[1] K. Yang, R. Kas, and W. A. Smith, *In situ infrared spectroscopy reveals persistent alkalinity near electrode surfaces during CO_2 electroreduction,* Journal of the American Chemical Society **141**, 15891 (2019).

[2] M. Robinson and T. Shine, *Achieving a climate justice pathway to 1.5 °c,* Nature Climate Change **8**, 564 (2018).

[3] E. V. Kondratenko, G. Mul, J. Baltrusaitis, G. O. Larrazábal, and J. Pérez-Ramírez, *Status and perspectives of CO_2 conversion into fuels and chemicals by catalytic, photocatalytic and electrocatalytic processes,* Energy & Environmental Science **6**, 3112 (2013).

[4] D. D. Zhu, J. L. Liu, and S. Z. Qiao, *Recent advances in inorganic heterogeneous electrocatalysts for reduction of carbon dioxide,* Advanced Materials **28**, 3423 (2016).

[5] L. Zhang, Z.-J. Zhao, and J. Gong, *Nanostructured materials for heterogeneous electrocatalytic CO_2reduction and their related reaction mechanisms,* Angewandte Chemie International Edition **56**, 11326 (2017).

[6] D. Higgins, C. Hahn, C. Xiang, T. F. Jaramillo, and A. Z. Weber, *Gas-diffusion electrodes for carbon dioxide reduction: A new paradigm,* ACS Energy Letters **4**, 317 (2018).

[7] T. Burdyny and W. A. Smith, *CO_2 reduction on gas-diffusion electrodes and why catalytic performance must be assessed at commercially-relevant conditions,* Energy & Environmental Science **12**, 1442 (2019).

[8] J. E. Pander, D. Ren, Y. Huang, N. W. X. Loo, S. H. L. Hong, and B. S. Yeo, *Understanding the heterogeneous electrocatalytic reduction of carbon dioxide on oxide-derived catalysts,* ChemElectroChem **5**, 219 (2017).

[9] Y. Li, F. Cui, M. B. Ross, D. Kim, Y. Sun, and P. Yang, *Structure-sensitive CO_2 electroreduction to hydrocarbons on ultrathin 5-fold twinned copper nanowires,* Nano Letters **17**, 1312 (2017).

[10] Y. Lum and J. W. Ager, *Evidence for product-specific active sites on oxide-derived cu catalysts for electrochemical CO_2 reduction,* Nature Catalysis **2**, 86 (2018).

[11] P. D. Luna, R. Quintero-Bermudez, C.-T. Dinh, M. B. Ross, O. S. Bushuyev, P. Todorović, T. Regier, S. O. Kelley, P. Yang, and E. H. Sargent, *Catalyst electro-redeposition controls morphology and oxidation state for selective carbon dioxide reduction,* Nature Catalysis **1**, 103 (2018).

[12] T. T. H. Hoang, S. Verma, S. Ma, T. T. Fister, J. Timoshenko, A. I. Frenkel, P. J. A. Kenis, and A. A. Gewirth, *Nanoporous copper–silver alloys by additive-controlled electrodeposition for the selective electroreduction of CO_2 to ethylene and ethanol,* Journal of the American Chemical Society **140**, 5791 (2018).

[13] Y. Pang, T. Burdyny, C.-T. Dinh, M. G. Kibria, J. Z. Fan, M. Liu, E. H. Sargent, and D. Sinton, *Joint tuning of nanostructured cu-oxide morphology and local electrolyte programs high-rate CO_2 reduction to C_2H_4,* Green Chemistry **19**, 4023 (2017).

[14] M. Ma, K. Djanashvili, and W. A. Smith, *Controllable hydrocarbon formation from the electrochemical reduction of CO_2 over cu nanowire arrays,* Angewandte Chemie International Edition **55**, 6680 (2016).

[15] X. Liu, P. Schlexer, J. Xiao, Y. Ji, L. Wang, R. B. Sandberg, M. Tang, K. S. Brown, H. Peng, S. Ringe, C. Hahn, T. F. Jaramillo, J. K. Nørskov, and K. Chan, *pH effects on the electrochemical reduction of CO_2 towards c2 products on stepped copper,* Nature Communications **10** (2019), 10.1038/s41467-018-07970-9.

[16] R. Kas, R. Kortlever, A. Milbrat, M. T. M. Koper, G. Mul, and J. Baltrusaitis, *Electrochemical CO_2 reduction on Cu_2O-derived copper nanoparticles: controlling the catalytic selectivity of hydrocarbons,* Phys. Chem. Chem. Phys. **16**, 12194 (2014).

[17] K. J. P. Schouten, Z. Qin, E. P. Gallent, and M. T. M. Koper, *Two pathways for the formation of ethylene in CO reduction on single-crystal copper electrodes,* Journal of the American Chemical Society **134**, 9864 (2012).

[18] Y. Hori, R. Takahashi, Y. Yoshinami, and A. Murata, *Electrochemical reduction of CO at a copper electrode,* The Journal of Physical Chemistry B **101**, 7075 (1997).

[19] A. S. Varela, M. Kroschel, T. Reier, and P. Strasser, *Controlling the selectivity of CO_2 electroreduction on copper: The effect of the electrolyte concentration and the importance of the local pH,* Catalysis Today **260**, 8 (2016).

[20] A. Wuttig, M. Yaguchi, K. Motobayashi, M. Osawa, and Y. Surendranath, *Inhibited proton transfer enhances au-catalyzed CO_2-to-fuels selectivity,* Proceedings of the National Academy of Sciences **113**, E4585 (2016).

[21] K. J. P. Schouten, E. P. Gallent, and M. T. Koper, *The influence of pH on the reduction of CO and CO_2 to hydrocarbons on copper electrodes,* Journal of Electroanalytical Chemistry **716**, 53 (2014).

[22] R. Kas, R. Kortlever, H. Yılmaz, M. T. M. Koper, and G. Mul, *Manipulating the hydrocarbon selectivity of copper nanoparticles in CO_2 electroreduction by process conditions,* ChemElectroChem **2**, 354 (2014).

[23] C.-T. Dinh, T. Burdyny, M. G. Kibria, A. Seifitokaldani, C. M. Gabardo, F. P. G. de Arquer, A. Kiani, J. P. Edwards, P. D. Luna, O. S. Bushuyev, C. Zou, R. Quintero-Bermudez, Y. Pang, D. Sinton, and E. H. Sargent, *CO_2 electroreduction to ethylene via hydroxide-mediated copper catalysis at an abrupt interface,* Science **360**, 783 (2018).

[24] S. Nitopi, E. Bertheussen, S. B. Scott, X. Liu, A. K. Engstfeld, S. Horch, B. Seger, I. E. L. Stephens, K. Chan, C. Hahn, J. K. Nørskov, T. F. Jaramillo, and I. Chorkendorff, *Progress and perspectives of electrochemical CO_2 reduction on copper in aqueous electrolyte,* Chemical Reviews **119**, 7610 (2019).

[25] S. Lee, J. D. Ocon, Y. il Son, and J. Lee, *Alkaline CO_2 electrolysis toward selective and continuous $HCOO^-$ production over SnO_2 nanocatalysts,* The Journal of Physical Chemistry C **119**, 4884 (2015).

[26] M. Dunwell, W. Luc, Y. Yan, F. Jiao, and B. Xu, *Understanding surface-mediated electrochemical reactions: CO_2 reduction and beyond,* ACS Catalysis **8**, 8121 (2018).

[27] Y. Hori, *Electrochemical CO_2 reduction on metal electrodes,* in *Modern Aspects of Electrochemistry* (Springer New York) pp. 89–189.

[28] M. Gattrell, N. Gupta, and A. Co, *A review of the aqueous electrochemical reduction of CO_2 to hydrocarbons at copper,* Journal of Electroanalytical Chemistry **594**, 1 (2006).

[29] J. Ryu, A. Wuttig, and Y. Surendranath, *Quantification of interfacial pH variation at molecular length scales using a concurrent non-faradaic reaction,* Angewandte Chemie International Edition **57**, 9300 (2018).

[30] M. Dunwell, X. Yang, B. P. Setzler, J. Anibal, Y. Yan, and B. Xu, *Examination of near-electrode concentration gradients and kinetic impacts on the electrochemical reduction of CO_2 using surface-enhanced infrared spectroscopy,* ACS Catalysis **8**, 3999 (2018).

[31] K. D. Yang, W. R. Ko, J. H. Lee, S. J. Kim, H. Lee, M. H. Lee, and K. T. Nam, *Morphology-directed selective production of ethylene or ethane from CO_2 on a Cu mesopore electrode,* Angewandte Chemie International Edition **56**, 796 (2016).

[32] A. D. Handoko, F. Wei, Jenndy, B. S. Yeo, and Z. W. Seh, *Understanding heterogeneous electrocatalytic carbon dioxide reduction through operando techniques,* Nature Catalysis **1**, 922 (2018).

[33] D. Ren, Y. Deng, A. D. Handoko, C. S. Chen, S. Malkhandi, and B. S. Yeo, *Selective electrochemical reduction of carbon dioxide to ethylene and ethanol on copper(i) oxide catalysts,* ACS Catalysis **5**, 2814 (2015).

[34] M. Klähn, G. Mathias, C. Kötting, M. Nonella, J. Schlitter, K. Gerwert, and P. Tavan, *IR spectra of phosphate ions in aqueous solution: predictions of a DFT/MM approach compared with observations,* The Journal of Physical Chemistry A **108**, 6186 (2004).

[35] O. Ayemoba and A. Cuesta, *Spectroscopic evidence of size-dependent buffering of interfacial pH by cation hydrolysis during CO_2 electroreduction,* ACS Applied Materials & Interfaces **9**, 27377 (2017).

[36] N. Gupta, M. Gattrell, and B. MacDougall, *Calculation for the cathode surface concentrations in the electrochemical reduction of CO_2 in $KHCO_3$ solutions,* Journal of Applied Electrochemistry **36**, 161 (2005).

[37] H. Hashiba, L.-C. Weng, Y. Chen, H. K. Sato, S. Yotsuhashi, C. Xiang, and A. Z. Weber, *Effects of electrolyte buffer capacity on surface reactant species and the reaction rate of CO_2 in electrochemical CO_2 reduction,* The Journal of Physical Chemistry C **122**, 3719 (2018).

[38] T. Burdyny, P. J. Graham, Y. Pang, C.-T. Dinh, M. Liu, E. H. Sargent, and D. Sinton, *Nanomorphology-enhanced gas-evolution intensifies CO_2 reduction electrochemistry,* ACS Sustainable Chemistry & Engineering **5**, 4031 (2017).

[39] H. Vogt and K. Stephan, *Local microprocesses at gas-evolving electrodes and their influence on mass transfer,* Electrochimica Acta **155**, 348 (2015).

[40] D. Raciti, M. Mao, and C. Wang, *Mass transport modelling for the electroreduction of CO_2 on Cu nanowires,* Nanotechnology **29**, 044001 (2017).

[41] M. Osawa, *Dynamic processes in electrochemical reactions studied by surface-enhanced infrared absorption spectroscopy (SEIRAS),* Bulletin of the Chemical Society of Japan **70**, 2861 (1997).

[42] P. Christensen and A. Hamnett, *Chapter 1 in-situ infrared studies of the electrode-electrolyte interface,* in *New Techniques for the Study of Electrodes and Their Reactions* (Elsevier, 1989) pp. 1–77.

[43] R. Kortlever, K. H. Tan, Y. Kwon, and M. T. M. Koper, *Electrochemical carbon dioxide and bicarbonate reduction on copper in weakly alkaline media,* Journal of Solid State Electrochemistry **17**, 1843 (2013).

[44] J. Resasco, L. D. Chen, E. Clark, C. Tsai, C. Hahn, T. F. Jaramillo, K. Chan, and A. T. Bell, *Promoter effects of alkali metal cations on the electrochemical reduction of carbon dioxide,* Journal of the American Chemical Society **139**, 11277 (2017).

[45] P. Lobaccaro, M. R. Singh, E. L. Clark, Y. Kwon, A. T. Bell, and J. W. Ager, *Effects of temperature and gas–liquid mass transfer on the operation of small electrochemical cells for the quantitative evaluation of CO_2 reduction electrocatalysts,* Physical Chemistry Chemical Physics **18**, 26777 (2016).

[46] J. Resasco, Y. Lum, E. Clark, J. Z. Zeledon, and A. T. Bell, *Effects of anion identity and concentration on electrochemical reduction of CO_2,* ChemElectroChem **5**, 1064 (2018).

[47] D. Ren, J. Fong, and B. S. Yeo, *The effects of currents and potentials on the selectivities of copper toward carbon dioxide electroreduction,* Nature Communications **9** (2018), 10.1038/s41467-018-03286-w.

[48] J.-T. Li, Z.-Y. Zhou, I. Broadwell, and S.-G. Sun, *In-situ infrared spectroscopic studies of electrochemical energy conversion and storage,* Accounts of Chemical Research **45**, 485 (2012).

[49] X. Feng, K. Jiang, S. Fan, and M. W. Kanan, *A direct grain-boundary-activity correlation for CO electroreduction on cu nanoparticles,* ACS Central Science **2**, 169 (2016).

[50] A. Verdaguer-Casadevall, C. W. Li, T. P. Johansson, S. B. Scott, J. T. McKeown, M. Kumar, I. E. L. Stephens, M. W. Kanan, and I. Chorkendorff, *Probing the active surface sites for CO reduction on oxide-derived copper electrocatalysts,* Journal of the American Chemical Society **137**, 9808 (2015).

[51] Y. Huang, A. D. Handoko, P. Hirunsit, and B. S. Yeo, *Electrochemical reduction of CO_2 using copper single-crystal surfaces: Effects of CO coverage on the selective formation of ethylene,* ACS Catalysis **7**, 1749 (2017).

[52] X. Wang, A. S. Varela, A. Bergmann, S. Kühl, and P. Strasser, *Catalyst particle density controls hydrocarbon product selectivity in CO_2 electroreduction on CuOx,* ChemSusChem **10**, 4642 (2017).

[53] M. Schreier, Y. Yoon, M. N. Jackson, and Y. Surendranath, *Competition between H and CO for active sites governs copper-mediated electrosynthesis of hydrocarbon fuels,* Angewandte Chemie International Edition **57**, 10221 (2018).

4

Role of the carbon-based gas diffusion layer on flooding in a GDE cell

The deployment of gas diffusion electrodes (GDEs) for the electrochemical CO_2 reduction (ECO2R) has enabled current densities an order of magnitude greater than aqueous H-cells. The gains in production, however, have come with stability challenges due to rapid flooding of GDEs, which frustrate both laboratory experiments and scale-up prospects. Here we investigate the role of carbon GDLs on the advent of flooding during ECO2R, finding that applied potential plays a central role in the observed instabilities. Electrochemical characterization of carbon GDLs with and without catalysts suggests that the high overpotential required during electrochemical ECO2R initiates hydrogen evolution on the carbon GDL support. These potentials impact the wetting characteristics of the hydrophobic GDL, resulting in flooding that is independent of ECO2R. Findings from this work can be extended to any electrochemical reduction reaction using carbon based GDEs (ECOR, EN2R) with cathodic overpotentials < – 0.65 V vs a reversible hydrogen electrode (RHE).

This chapter has been published in ACS Energy Lett. **2021**, 6, 33–40.[1]

4.1. Introduction

Carbon dioxide electrolysis is a technology with the potential to convert the most prevalent greenhouse gas into chemical feedstocks and fuels using renewable electricity.[2–4] As the field has advanced, it is clear that the reaction must occur at elevated reaction rates (e.g. high current densities), which has led to catalysts being positioned near a gas-liquid interface. This is typically achieved by using a gas diffusion electrode (GDE), where a catalyst is deposited on a gas diffusion layer (GDL).[5–7] Such application boosts the limiting CO_2 reduction current density over an order of magnitude higher when compared with electrodes in a conventional H-cell that are typically limited to current densities less than 60 mA/cm^2.[7–11]

A typical GDL consists of a porous matrix capable of allowing gas transport but limiting the transport of liquids.[12] GDLs have been employed for many systems and reactions such as fuel cells,[13] chlor-alkali electrolysis with oxygen depolarized cathodes,[14] and most recently CO_2 electrolysis. In CO_2 electrolysis various GDLs have been tested including carbon based,[15] metal-based,[16, 17] PTFE based,[18] and membrane based structures.[19] Among those, carbon based GDLs are the most prevalently reported in literature,[7, 8] with hydrophobicity imposed within a carbon matrix via PTFE coating. Unfortunately, the research community has shown that despite the excellent stability of carbon-based GDLs for other electrochemical reactions, in CO_2 reduction they suffer from extremely poor stability. In fact, flooding of the GDL will typically happen within several hours of operation, leading to a reduction in selectivity towards CO_2 reduction reaction products.[20–22] When flooding happens, a fraction of the pores within the originally hydrophobic GDL become filled by liquid. Water penetration into the GDL not only blocks CO_2 from reaching the active site on the catalyst surface by increasing the diffusion pathway, but it can also encourage salt precipitation which causes further failure by blocking the pore permanently. Thus, when flooding occurs, the performance becomes characterized by a switch in selectivity towards the hydrogen evolution reaction (HER), leading to an essential failure of the CO_2 electrolysis system.

Despite the recent increase in GDL usage for CO_2 electrolysis, instability of these structures, especially flooding is a well-studied phenomenon in fuel cell research.[23, 24] Several flooding mechanisms have been previously described including: electrowetting caused by a potential-driven change in the electrolyte-solid surface tension;[20, 25, 26] water pumping due to ion concentration gradients between reaction interface and bulk electrolyte;[25, 27, 28] salt precipitation due to ion build-up;[25, 27] and pressure differences between gas and liquid at the interface.[20, 21, 26–28] ECO2R-specific flooding mechanisms have also received attention. In a recent work Leonard et al. found that in a KOH electrolyte, flooding can be related to the total charge passed on electrodes, leading to salt precipitation after sufficient CO_2/OH- interactions.[22] Moreover, liquid products such as alcohols from ECO2R can further accelerate flooding as they tend to decrease the electrolyte-electrode surface tension of GDE, lowering the capillary pressure.[29] Lastly, Jouny et al. also observed flooding in a electrochemical CO reduction reaction (ECOR) system when using KOH as electrolyte, which they attributed to the condensation of water vapor.[30]

However, while different flooding mechanisms are possible over long-term electrochemical operation, there has not been a clear reason why flooding occurs almost immediately

during CO_2 electrolysis, typically within 1 hour.[22] In other words, can we understand why carbon-based GDEs used in so many other applications do not perform as advertised in the growing field of CO_2 electrolysis? Understanding such effects could help to provide a solution which impacts not only future commercialization potential of ECO2R technology, but also allows for greater ease to perform necessary long-term lab experiments on product selectivity and catalyst stability.[31]

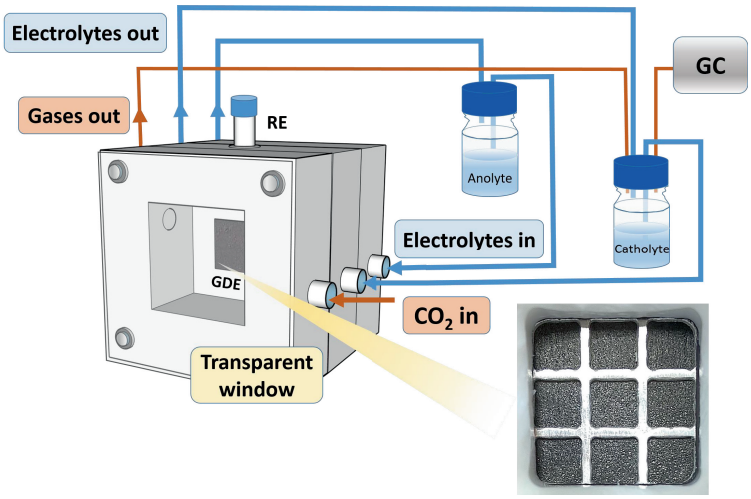

Figure 4.1: Illustration of the GDE cell for electrochemical CO_2 reduction.

In this work, we aim to elucidate the electrochemical factors leading to premature flooding of carbon-based gas diffusion layers during CO_2 electrolysis. We begin by investigating the electrochemical behavior of a bare carbon-based GDL, a silver catalyst on a carbon GDL, and a silver catalyst on a PTFE-based GDL under CO_2-free reaction environment to decouple the roles of HER and ECO2R. After noting a large activity difference for HER between carbon and silver coated GDL, we studied the electrochemical activity of a bare carbon GDL itself by comparing with other catalysts (Ag, Pt, Au, Cu) on the same support. With regards to premature flooding, the GDL stability (eg. resistivity to flooding) is subsequently found to be dependent on the potential applied and corresponding electrochemical activity of the carbon on the GDL. The primary conclusion of our work is that by reducing the catalyst onset potentials and operating in a suitable potential range, CO_2 electrolyzers can reach a longer lifetime before flooding occurs. Such stability would greatly improve both the usability of GDLs for testing CO_2 electrolysis catalysts and operation, as well as enabling stability for industrial application.

4.2. Experimental methods

Preparation of GDE. GDEs were made by magnetron sputtering (AJA International Inc.) different metal targets (Ag, Pt, Cu and Au, MaTeck Germany, 99,9 % purity) onto Freudenberg H14C19 GDL (Fuel Cell Store) to reach 25 nm nominal thickness. During sputtering power supply was kept at 50 W DC in a 20 sccm (standard cubic centimeters per minute) Ar atmosphere. The Ag/PTFE samples were made by sputtering 300 nm thick Ag on an PTFE membrane (Donaldson Company Inc.). Thicker catalyst layers were used as compared to the pure metal layers to increase the in-plane conductivity of the Ag/PTFE layer. During electrochemical operation the exposed geometric catalyst area was 1.5 cm^2.

Electrochemical tests. A flow cell with three compartments composed of gas, catholyte and anolyte chambers was used as reported from our group earlier. A slight modification was made in the PTFE containing the CO_2 gas channel where the cavity extended throughout the entire block. By blocking the gas channel with a transparent window, we were able to observe the flooding through the GDL during the experiments (Figure 4.1). For the electrochemical flooding experiments described in Figure 4.3, the dotted line data points represent the operating time when droplets were first observed from the gas side of GDE through the window. The solid line represents the operating time when droplets were evenly spread on the gas side of the GDEs, which we refer to as flooded. The shadowed region between the dotted and solid line then represents the time during which flooding happened (Figure SI3 and SI4).

For experiments performed in a CO_2 environment, CO_2 was fed through a mass controller (Bronkhorst High-Tech BV) at a flow rate of 15 sccm. For experiments performed in N_2 environment, N_2 was fed at a flow rate of 12 sccm to maintain the pressure between N_2 and catholyte same as when using 15 sccm CO_2. In all experiments the catholyte (80 mL) and anolyte (40 mL) were 1 M $KHCO_3$ (99.7 %, Sigma), supplied by a peristaltic pump at a rate of 5 mL/min. Nafion 115 proton exchange membrane was used to separate catholyte and anolyte. The electrochemically reacted gas and catholyte were sent into a gas-tight reservoir to balance the pressure at the gas and catholyte interface. Subsequently, gas was sent to GC for product analysis, while catholyte circulated back to catholyte chamber. Anolyte circulated through a different reservoir, which was open to atmosphere to allow anodic product O_2 to escape. The pH of electrolytes was measured before and after each test using a pH meter (HANNA, HI-98191). An illustration of the setup is shown in Figure 4.1.

Liner sweep voltammetry (LSV), chronopotentiometry and chronoamperometry curves of different GDEs were collected under both CO_2 and N_2 atmosphere using a potentiostat (PARSTAT 4000A). Ag/AgCl (saturated KCl) was used as reference electrode. Pt was used as anode. For LSV measurement, a potential window from – 0.6 V to – 2.5 V vs Ag/AgCl was swept with a scan rate of 10 mV/s, and 8 scans were recorded for each sample. For chronopotentiometry, different current densities (5 mA/cm^2 to 100 mA/cm^2) were applied until droplets were observed across the back of the GDEs. For chronoamperometry, different potentials (between – 0.5 V and – 0.85 V vs RHE) were applied on bare GDLs. All samples after electrochemistry were washed thoroughly with Milli-Q water and dried with N_2.

Electrochemical active surface area (ECSA) was determined by measuring the double layer capacitance (Cdbl) of the electrode. Cyclic voltammetry curves were collected in a non-faradaic region between 0.52 V to 0.62 V (vs RHE) by varying the scan rates from 30 mV/s to

110 mV/s in 0.1 M $NaClO_4$ solution (> 98.0%, Sigma). Geometric current density was then plotted against the scan rate to get the Cdbl values of our electrode. Roughness factor and ECSA were calculated by comparing Cdbl values obtained here with what was reported from literature on a smooth Ag electrode (Figure SI2).

Characterizations. Gas products were measured by an online GC (Compact GC 4.0, GAS) at 3.5 min intervals. Scanning electron microscopy (SEM, JEOL, JSM-6010LA) was used to characterize the surface morphology of the carbon GDL and different GDEs (Figure SI1, SI5 and SI6) before and after electrochemical tests, and no clear morphological change was observed on any GDEs after electrolysis. X-Ray photoelectron spectroscopy (XPS) was utilized with a Thermo Scientific K system with Al Kα X-Ray resource. Each measurement was sampled from a spot size of 400 µm, passing energy of 50 eV, energy step of 0.1 eV and a dwell time of 50 ms. 10 scans were taken for each C 1s, F 1s and O 1s in the vicinity of their binding energy. 10 steps of etching at 5s interval (around 0.2 nm/s) was performed on the same spot. C 1s, F 1s and O 1s spectra were measured again after each etching step. 3 spots were measured and analyzed for each sample. XPS spectra were corrected using the C 1s peak at 284.8 eV and U 2 Tougaard background in casaXPS.

4.3. Results and discussion

To investigate the effect of electrochemical reactions on premature GDL flooding, one approach is to decouple each part of the reaction process (i.e. GDL vs catalyst and HER vs ECO2R). Here, we used three different electrodes to decouple these effects: a bare carbon-based GDL (containing a carbon-PTFE microporous layer, Figure 4.2(a)), Ag deposited on this carbon-based GDL (Figure 4.2(b)), and Ag deposited on a PTFE-based GDL (a membrane made of PTFE, Figure 4.2(c)). Figure 4.2(d) shows the linear scan voltammetry (LSV) performed on a bare carbon GDL under a N_2 atmosphere in 1 M $KHCO_3$. In the 1st scan, the Faradaic onset potential is observed at – 0.7 V vs RHE (using 1 mA/cm^2 as the defining current density), with the corresponding electrochemical activity confirmed to be H_2 evolution. During the 2nd scan, the onset potential for HER is then observed to shift to more anodic potentials (– 0.65 V vs RHE). Upon repeated scans, the shape of the curve remains similar. The shift to anodic potentials indicates an increase in electrochemical activity. This may be due to the greater surface area of carbon in contact with the electrolyte, which is induced by the increased wetting of accessible carbon surfaces under an applied potential.[25] These results indicate that the bare carbon GDL is active for HER once it is in direct contact with the electrolyte and the applied potential is negative enough. Of note is that the applied potentials are within the commonly-reported potential range for CO_2 electrolysis.

Figure 4.2(e) shows LSV sweep of a Ag/GDL, where a thin layer of Ag was deposited via magnetron sputtering on the carbon GDL (Figure 4.2(b) and SI1). Notably, the Ag/GDL and bare GDL have similar onset potentials and activity for HER within the potential range of – 0.6 V to – 0.85 V vs RHE, indicating little difference in electrochemical activity between the two samples within this potential range. At more negative potentials (< – 0.85 V vs RHE), the activity of the Ag/GDL then becomes greater than that of the bare GDL.

To further investigate the role of Ag itself, we deposited Ag on a PTFE membrane, which has

been used as gas diffusion substrate for CO_2 electrolysis.[11, 18, 32] LSVs in Figure 4.2(e) show that Ag has a higher overpotential and lower activity in the scanned potential window (– 0.2 V to – 1.1 V vs RHE), compared with the bare carbon GDL under neutral pH conditions (1 M $KHCO_3$). Furthermore, the difference in HER activity between the bare GDL and the Ag/GDL can be explained by the activity of the Ag/PTFE sample, where the activity of carbon is removed. To rule out the influence of different surface roughness of the carbon-based and PTFE-based GDLs(Figure SI1), we normalized the current densities in Figure 4.2(e) to the electrochemical surface area (ECSA) current densities (Figure SI2). After

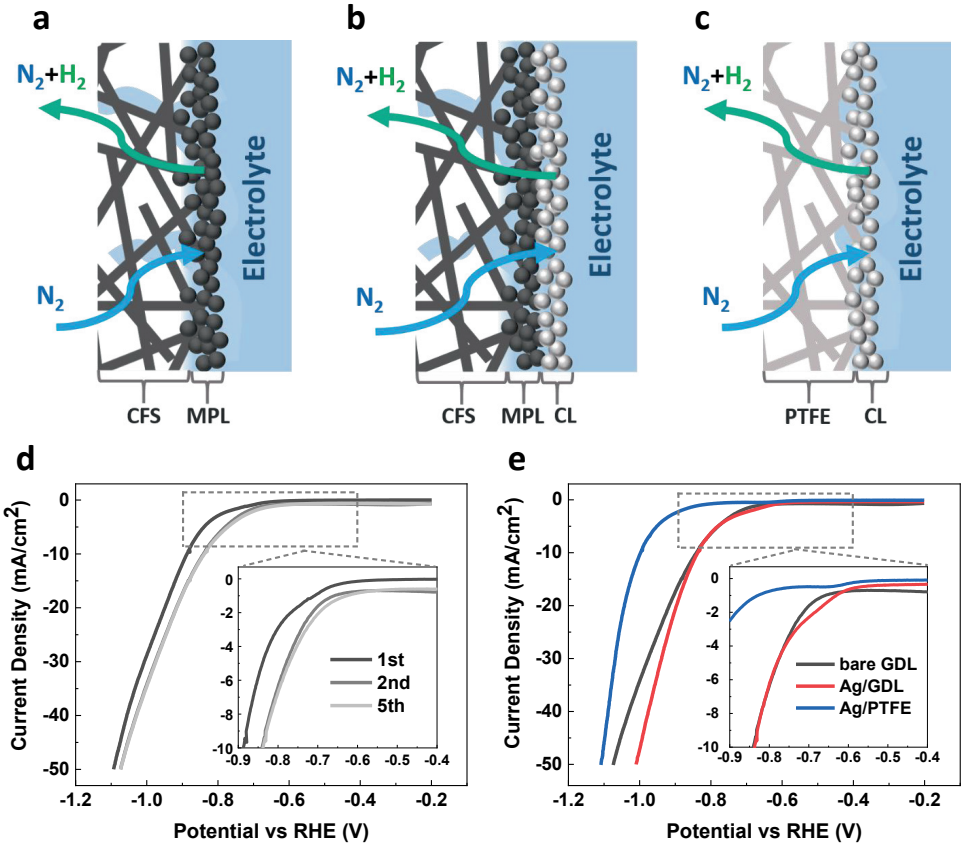

Figure 4.2: Illustration of the (a) bare GDL, (b) Ag/GDL and (c) Ag/PTFE. (d) Multiple scans of linear scan voltammetry (LSV) of a bare carbon GDL performed under N_2 conditions. (e) Comparison of the 2nd LSV scans for the GDL configurations shown in (a)-(c). The insert figures in (d) and (e) show the enlarged rectangle regions. CFS represents carbon fiber paper; MPL represents microporous layer (which contains a mixture of carbon nanoparticles and PTFE) and CL represents catalyst layer respectively. All LSV scans used a scan rate of 10 mV/s in 1M $KHCO_3$.

normalizing, pure Ag on a PTFE substrate still gives the lowest performance for HER among the bare GDL, Ag/GDL and Ag/PTFE electrodes. The results in Figure 4.2 conclude that during electrochemistry in a N_2 environment, carbon is a more active catalyst than Ag for HER (in the tested potential windows), and a substantial fraction of the Faradaic reactions could

be electrochemically driven by the carbon GDL instead of Ag.

When changing the atmosphere from N_2 to CO_2, the LSV scans (Figure 4.3(a)) show that the Ag/GDL sample has a smaller overpotential and higher activity when compared to the same catalyst in a N_2 environment or to the bare GDL. Conversely, the activity of the bare GDL is reduced under CO_2 atmosphere compared to when it was under N_2 at lower current densities. Such observations could be explained by Zhang et al. showing that co-adsorbed CO from ECO2R will weaken the binding energy between adsorbed H and the catalyst surface, which suppresses hydrogen formation.[33]

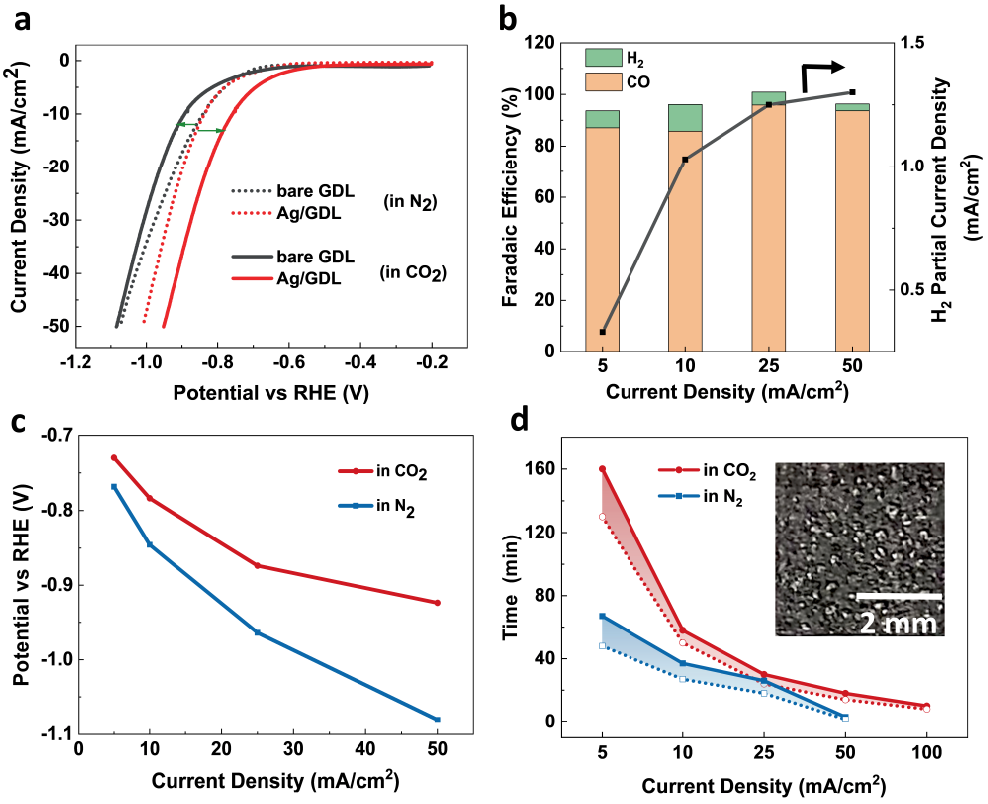

Figure 4.3: (a) Comparison of 2nd LSVs on bare GDL and Ag/GDL in N_2 and CO_2 atmosphere. (b) FE (left) and partial current density to H_2 on Ag/GDL during ECO2R at different current densities. (c) Potentials needed during in CO_2 and N_2 conditions at different current densities. (d) Time when flooding happened (open dots represent time when liquid droplets started to be observed. Solid dots represent time when GDE was totally flooded. Insert picture shows the image of a totally flooded sample.)

When performing chronopotentiometry of the Ag/GDL sample in a CO_2 environment at various current densities, we observe that hydrogen is always measured (Figure 4.3(b)). Further, the partial current density towards H_2 (right y-axis) increases as the total current/potential increases. Pairing the applied potentials (Figure 4.3(c)) with the LSV curves of the bare GDL (Figure 4.3(a)), we hypothesize that a portion of the H_2 production observed on the

Ag/GDL sample (Figure 4.3(b)) could originate from the carbon substrate. The carbon GDL, which is meant to play a passive electrochemical role, is then active towards the competing electrochemical reaction. Figure 4.3(c) shows the potentials corresponding to the different current densities in CO_2 and N_2 conditions during chronopotentiometry. At the same current density, the measured potential in a CO_2 atmosphere is less negative than under N_2 conditions due to the better kinetics for ECO2R than HER on Ag/GDL (shown in Figure 4.3(a)). Under CO_2 conditions, however, the potentials are still great enough that carbon can be active for HER (< – 0.65 V vs RHE).

During the chronopotentiometry measurements, we also observed the time taken for initial and full flooding of the GDL in both N_2 and CO_2 environments using a Ag/GDL (Figure 4.3(d)). There are two takeaways from these experiments: 1) at all current densities, flooding was observed to happen faster in a N_2 environment than in a CO_2 environment, and 2) in both the CO_2 and N_2 environments the time to flooding decreased as current densities were increased. At 50 mA/cm^2, for example, liquid droplets were observed across the back of the entire GDL after only 3 minutes in a N_2 environment, and approximately 20 minutes in a CO_2 environment (Figure SI7). As carbon is expected to be the primary active catalyst for HER in a N_2 environment from the LSV curves in Figure 4.2, the faster flooding times indicate that activation of the carbon surface is contributing to the premature flooding mechanism of the carbon GDL. The eventual flooding of the samples in a CO_2 environment may then also be attributable to carbon activation, even if the Ag catalyst layer contributes to much of the Faradaic current density (Figure 4.3(a)). In short, the results in Figure 4.3 indicate that premature flooding is due to the potential-driven reduction in the capillary pressure between the electrolyte and GDL substrate. Consequently, the electrolyte wets the microporous layer (MPL) of the GDL and gradually fills in its pores while carbon in the GDL becomes active for HER.

To investigate further and indicate possible solutions to flooding, we repeated the analysis with metal catalysts which are more active than Ag for HER in attempt to limit the reactions which occur on the carbon support. First, we performed LSVs in a N_2 environment on a variety of metal-GDL combinations (Pt, Au and Cu). Platinum is a well-known catalyst for HER, which shows excellent activity (Figure 4.4(a)). Although the LSVs indicate the Cu/GDL and Au/GDL electrodes are not as active as the Pt/GDL, they still exhibit lower onset potentials than the bare GDL and Ag/GDL.[34]

Chronoamperometry was performed on these electrodes similar to the Ag/GDL samples. For the Pt/GDL electrode (Figure 4.4(b)), no droplets were observed on the back of the GDL after 3 hours of operation at 10 mA/cm^2 or 50 mA/cm^2. In contrast, the Ag/GDL in a N_2 environment flooded after 40 minutes of operation at 10 mA/cm^2, and only 3 minutes at 50 mA/cm^2. These results are explained by observing the corresponding potentials for Pt/GDL (– 0.1 V and – 0.45 V vs RHE at 10 and 50 mA/cm^2, respectively), which are smaller than the observed onset potential for carbon to conduct HER (– 0.65 V vs RHE, shown in Figure 4.2(e) and Figure 4.4(b)). For the Cu/GDL sample, which shows lower HER onset potentials than the Ag/GDL but worse than the Pt/GDL, flooding occurred after 160 minutes of operation at 10 mA/cm^2. The Cu sample then showed greater resistance to flooding at an identical current density to Ag/GDL. As the potential increases during operation, the applied potential becomes similar to the Ag/GDL, at which point flooding is observed to occur.

In a CO_2 atmosphere, the Cu/GDL and Au/GDL both have a lower onset potential than

the Ag/GDL,[35, 36] and bare GDL (Figure 4.4(c)), similar to what is reported in literature. [37, 38] Chronopotentiometry in Figure 4.4(d) shows that to reach the same current density at 10 mA/cm^2, the potential needed on the Cu/GDL is less negative than on the Ag/GDL. The system was able to run for more than 3 hours without flooding on the Cu/GDL, whereas on the Ag/GDL, flooding occurred after 1 hour. Both in N_2 and CO_2 environment, the potential drifted to more negative potentials on the Cu/GDL, possibly resulting from physical degradation or restructuring of the copper catalyst. Nevertheless, we cannot draw such conclusions based on the SEM results, as there was no obvious morphological change after electrolysis on all GDLs (Figure SI5 and SI6). In brief, the results from Figure 4.4 confirm our hypothesis that catalysts with a lower onset potential than carbon will be more resistant to flooding of the gas diffusion layer during electrochemical operation.

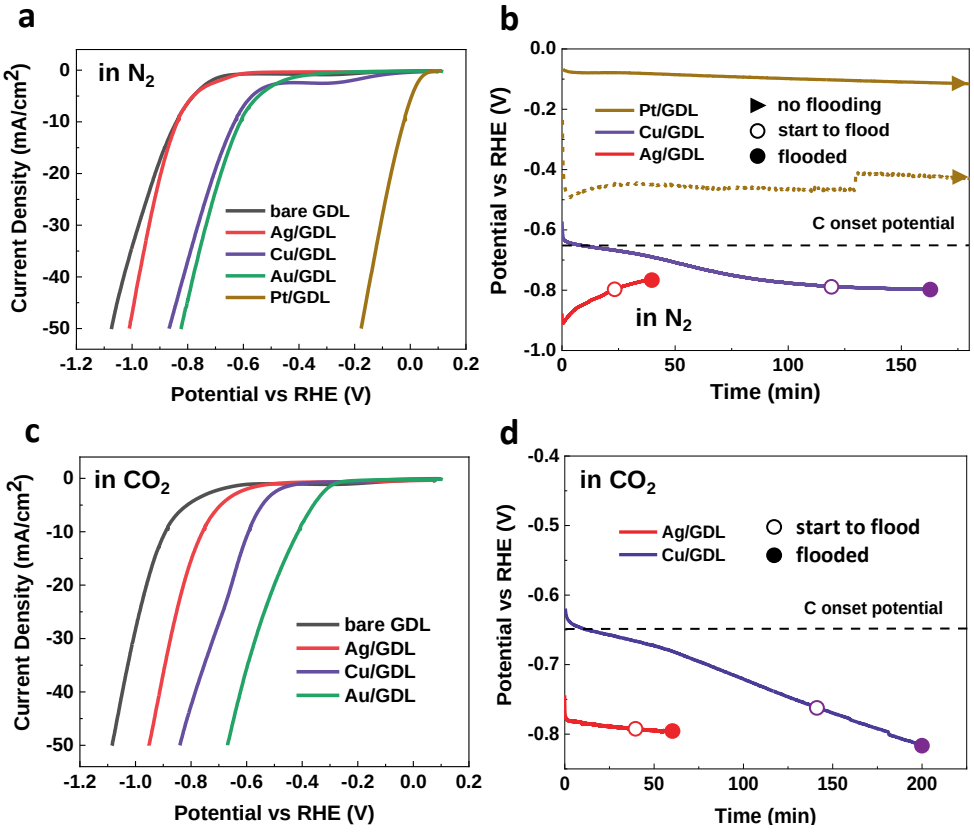

Figure 4.4: LSVs on different catalysts deposited onto carbon GDL in 1 M $KHCO_3$ and a N_2 reaction environment (a) and a CO_2 reaction environment (c). (b) Potentials and time when flooding happened on Ag/GDL, Cu/GDL and Pt/GDL samples at 10 mA/cm^2 in a N_2 environment (dotted line shows 50mA/cm^2 on Pt). (d) Potentials and time when flooding happened on Ag/GDL and Cu/GDL samples at 10 mA/cm^2 in a CO_2 environment. Open circles indicate droplet observation on the back of the GDL. Closed circles indicate droplets across the entire back of the GDL. The dashed line shows the onset potential of carbon defined at 1 mA/cm^2 taken from the LSV curves.

To further understand the role of potential and current density on flooding, we performed chronoamperometry at different fixed potentials on a bare GDL under a N_2 atmosphere in 1 M $KHCO_3$. Figure 4.5a shows that at applied potentials of – 0.51 V and – 0.6 V vs RHE, no flooding was observed after 4 hours of operation. The corresponding current densities for these potentials are less than 1 mA/cm^2. When increasing the potential to – 0.68 V vs RHE, initial flooding was observed after 70 minutes, followed by fully dispersed flooding after 160 minutes. At – 0.83 V vs RHE, flooding occurred at a faster rate, reaching a fully flooded state after only 50 minutes. Over the course of operation, the current densities are also seen to steadily increase. We anticipate the activity increase occurs due to a larger wetted surface area of carbon that is accessible for the reaction as flooding occurs (see Figure 4.2(a)). Such behavior indicates that flooding of the carbon microporous layer may be steadily occurring at the beginning of the reaction before it can be detected visually, rather than occurring suddenly. From these results we conclude that the premature flooding mechanism requires the carbon surface to be active for HER, and that higher potentials/current densities on the

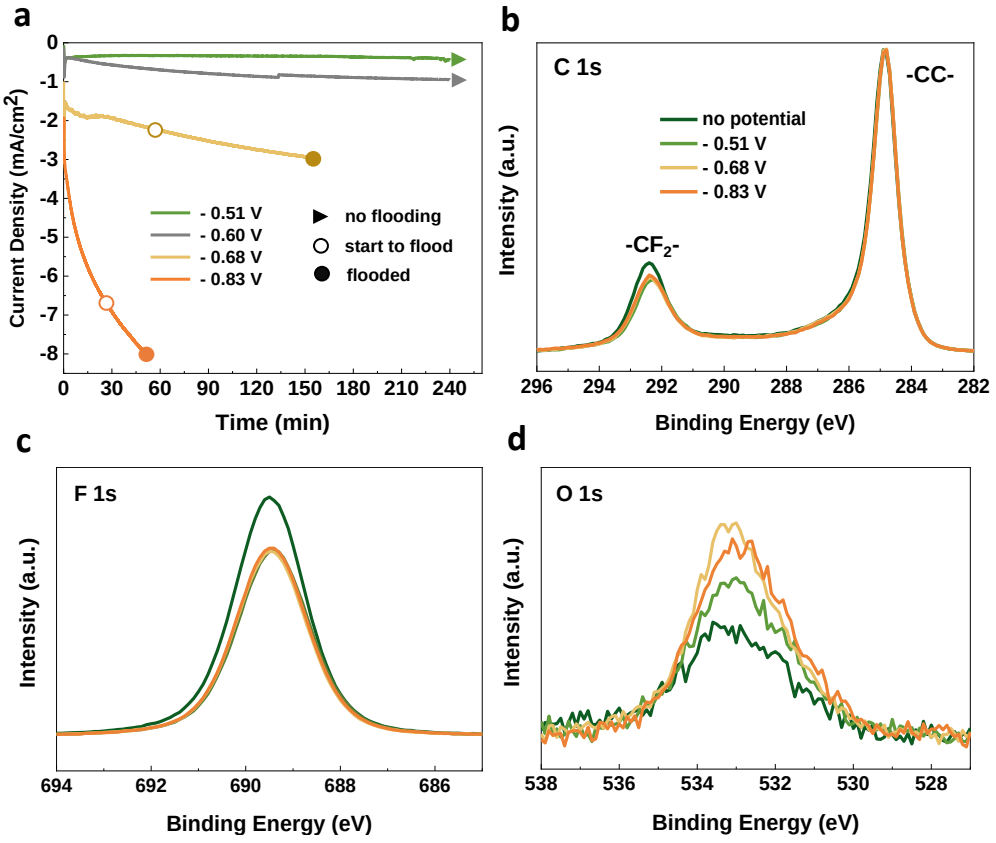

Figure 4.5: (a) current densities and time when flooding happened on bare GDL at different potentials under N_2 condition. Open circles indicate droplet observation on the back of the GDL. Closed circles indicate droplets across the entire back of the GDL. XPS spectra of C 1s (b), F 1s (c) and O 1s (d) of different GDL samples.

carbon surface increase the rate of flooding.

To investigate potential chemical change on the surface of the GDL which may cause flooding as a result of the applied potential, we performed XPS measurement on the above carbon GDLs (Figure 4.5(a)) after chronoamperometry. The blank sample was a bare GDL, which was put in a flow cell in the same manner as other GDLs for 4 hours, but without any potential applied. No flooding was observed on the blank sample. Figure 4.5(b)-(d) shows the C 1s, F 1s and O 1s spectra of different GDL surfaces after normalization against C 1s (-CC- at 284.8 eV).

As a semi-quantitative method, the XPS peak area represents the relative ratio of elements and thus their concentrations. Figure 4.5(b) and 4.5(c) shows a decrease of C 1s (-CF2-) and F 1s signals, while an increase of O 1s peak on GDLs applied with potentials, compared with the blank bare GDL. Table S1 also shows a decreased surface atomic ratio of C 1s (-CF2-) and F 1s. F 1s ratio decreases by 12.5 %, which is more obvious than C 1s due to its larger relative sensitivity factor (RSF). Such a decrease suggests that some amount of PTFE may decompose under negative potentials as reported previously (at – 2 V vs SCE).[39, 40] Although the potentials in our work are less negative than this, the decomposition of PTFE on the GDE can be faster than its foil/membrane form and potentially occur at more anodic potentials.[41] Once the PTFE degrades, the C-F bonds will break, and C can combine with C to form C=C bonds. Carbon can also combine with O in the electrolyte to form C-O (or C=O etc.). A minor increase in the oxygen signals and atomic ratios were observed when potentials were applied. (Figure 4.5(d) and Table SI1).

It is worth mentioning that no K^+ was detected by XPS on all samples (Figure SI8). Thus, we can rule out the influence of unwashed $KHCO_3$ salt on C 1s and O 1s XPS spectra. Furthermore, after etching the surface for 5 seconds and 45 seconds respectively, we still see the decreased C 1s (-CF2-) and F 1s peaks and increase in the O 1s peak (Figure SI9 and SI10). This result indicates that potential induced GDL changes also happen in sublayers under the surface. Nevertheless, little difference is observed when comparing the C 1s and F 1s signals between – 0.51 V, – 0.68 V and – 0.83 V vs RHE, suggesting overall similar chemical conditions of the MPL's surface under applied potentials (a mixture of carbon and PTFE surfaces). Together with the electrochemical data, we hypothesize that water penetration may in fact be due to electrowetting effects of the exposed carbon particles, rather than a change in the structure of the MPL. Electrowetting reduces the solid-liquid interfacial tension between the carbon-electrolyte, and would result in a reduced contact angle as the applied potentials become more cathodic. Via the Young-Laplace equation, the resulting capillary pressure on the carbon surface may then supersede the opposing capillary pressure of the PTFE surfaces which contain a larger contact angle ($\theta_{PTFE} > 90°$). Under this scenario, the pores of the MPL would become flooded in the presence of an applied potential (see SI for a further description).

We observed flooding of a carbon GDL under both N_2 and CO_2 environments, meaning that the flooding mechanism described here is independent of CO_2 electrolysis conditions. In fact, under ECO2R conditions, the GDL took longer to flood than in N_2. Our proposed flooding mechanism then differs from the recent work by Leonard et al. which showed that the primary reason for GDL flooding was driven through salt precipitation during CO_2 electrolysis.[22] The differences between our work and that of Leonard et al. is the use of $KHCO_3$ instead of KOH. We hypothesize that we observed different flooding mechanisms

because ECO2R under alkaline conditions requires lower electrode potentials as has been shown extensively in literature.[18, 42] For example, in KOH Dinh et al.[18] reached current densities > 300 mA/cm^2 on a carbon GDL before the cathode potential reached – 0.6 V vs RHE. We then expect the carbon surface to be unable to perform HER, and the potential would be low enough to avoid the flooding mechanism discussed here which occurred between – 0.6 V to – 0.83 V vs RHE. Combined with the results from Leonard et al., we can then infer that the "first flooding mechanism" that is observed during CO_2 electrolysis is a function of the chosen electrolyte and the activity of the catalyst. In a KOH electrolyte, salt precipitation due to the total charge passed could then reasonably expected to occur before the flooding mechanism described here. It is also worth mentioning that even during electrochemical CO reduction reported by Jouny et al.[30], where no salt formation occurs between KOH and CO, flooding was noted to be an issue when current densities were increased to 500 mA/cm^2 (the corresponding potential was approximately – 0.65 V vs RHE).

To reach long-term stable operation of GDLs for CO_2 electrolysis, one way of mitigating flooding is through the continued development of catalysts with lower onset potentials, high activity and surface area. As demonstrated with the Pt/GDL, a sufficiently active catalyst can avoid this problem. A secondary approach can be modifying the surface of the carbon in the MPL with an additional material that is inactive for ECO2R, but changes the wetting and electrochemical properties. This would have the added benefit of preventing small amounts of HER production from the GDL which can slightly increase overall ECO2R selectivity. Lastly, continued development of non-carbon GDLs is also encouraged, particularly ones which decouple the traditional requirements for a GDL (conductivity, hydrophobicity and porosity) but remain functional over larger areas. For example, Tiwari et al. reported a Gortex-based GDE, where metallic mesh was used as the current collector to provide conductivity, while a Gortex membrane was used to provide hydrophobicity and porosity.[14] It is worth noting that our work and most others reported in literature used commercial GDLs without any pretreatment. Further work modifying or pretreating GDLs may prove useful in understanding or preventing flooding mechanisms.

4.4. Conclusion

In this work, we investigated the role of carbon-based GDL and applied potential on flooding during electrochemical ECO2R. Electrochemical characterization of bare carbon and electrodes coated with various metals suggests that high negative potentials needed to drive ECO2R result in changes in the wetting characteristics of carbon based GDL. The potential-induced flooding strongly suggest that the HER taking place on the carbon GDL accelerates the wetting of initially hydrophobic GDL. We propose that by improving catalyst activity and operating CO_2 electrolysis in a suitable (i.e. low) potential range, as well as further modifying GDL configurations, CO_2 electrolyzers would reach longer stability. Results in this work not only help to improve stability studies at the lab scale for electrochemical CO_2 reduction, but also its possibility for future applications in industry. The findings are also expected to apply to other reduction reactions (ECOR, EN2R) using carbon GDEs where sufficiently high cathodic overpotentials are required.

References

[1] K. Yang, R. Kas, W. A. Smith, and T. Burdyny, *Role of the carbon-based gas diffusion layer on flooding in a gas diffusion electrode cell for electrochemical CO_2 reduction,* ACS Energy Letters **6**, 33 (2020).

[2] Y. Hori, *Electrochemical CO_2 reduction on metal electrodes,* in *Modern Aspects of Electrochemistry* (Springer New York, 2008) pp. 89–189.

[3] W. A. Smith, T. Burdyny, D. A. Vermaas, and H. Geerlings, *Pathways to industrial-scale fuel out of thin air from CO_2 electrolysis,* Joule **3**, 1822 (2019).

[4] M. Fleischer, P. Jeanty, K. Wiesner-Fleischer, and O. Hinrichsen, *Industrial approach for direct electrochemical CO_2 reduction in aqueous electrolytes,* in *Zukünftige Kraftstoffe* (Springer Berlin Heidelberg, 2019) pp. 224–250.

[5] S. Verma, B. Kim, H.-R. ". Jhong, S. Ma, and P. J. A. Kenis, *A gross-margin model for defining technoeconomic benchmarks in the electroreduction of CO_2,* ChemSusChem **9**, 1972 (2016).

[6] T. Burdyny and W. A. Smith, *CO_2 reduction on gas-diffusion electrodes and why catalytic performance must be assessed at commercially-relevant conditions,* Energy & Environmental Science **12**, 1442 (2019).

[7] B. Endrődi, G. Bencsik, F. Darvas, R. Jones, K. Rajeshwar, and C. Janáky, *Continuous-flow electroreduction of carbon dioxide,* Progress in Energy and Combustion Science **62**, 133 (2017).

[8] S. Hernandez-Aldave and E. Andreoli, *Fundamentals of gas diffusion electrodes and electrolysers for carbon dioxide utilisation: Challenges and opportunities,* Catalysts **10**, 713 (2020).

[9] K. Yang, R. Kas, and W. A. Smith, *In situ infrared spectroscopy reveals persistent alkalinity near electrode surfaces during CO_2 electroreduction,* Journal of the American Chemical Society **141**, 15891 (2019).

[10] L.-C. Weng, A. T. Bell, and A. Z. Weber, *Modeling gas-diffusion electrodes for CO_2 reduction,* Physical Chemistry Chemical Physics **20**, 16973 (2018).

[11] F. P. G. de Arquer, C.-T. Dinh, A. Ozden, J. Wicks, C. McCallum, A. R. Kirmani, D.-H. Nam, C. Gabardo, A. Seifitokaldani, X. Wang, Y. C. Li, F. Li, J. Edwards, L. J. Richter, S. J. Thorpe, D. Sinton, and E. H. Sargent, *CO_2 electrolysis to multicarbon products at activities greater than 1 a cm-2,* Science **367**, 661 (2020).

[12] A. Forner-Cuenca, J. Biesdorf, L. Gubler, P. M. Kristiansen, T. J. Schmidt, and P. Boillat, *Engineered water highways in fuel cells: Radiation grafting of gas diffusion layers,* Advanced Materials **27**, 6317 (2015).

[13] D. P. Wilkinson, J. Zhang, R. Hui, J. Fergus, and X. Li, eds., *Proton Exchange Membrane Fuel Cells* (CRC Press, 2009).

[14] P. Tiwari, G. Tsekouras, G. F. Swiegers, and G. G. Wallace, *Gortex-based gas diffusion electrodes with unprecedented resistance to flooding and leaking,* ACS Applied Materials & Interfaces **10**, 28176 (2018).

[15] G. L. D. Gregorio, T. Burdyny, A. Loiudice, P. Iyengar, W. A. Smith, and R. Buonsanti, *Facet-dependent selectivity of cu catalysts in electrochemical CO_2 reduction at commercially viable current densities,* ACS Catalysis **10**, 4854 (2020).

[16] J. Zhang, W. Luo, and A. Züttel, *Self-supported copper-based gas diffusion electrodes for CO_2 electrochemical reduction,* Journal of Materials Chemistry A **7**, 26285 (2019).

[17] W. Luo, J. Zhang, M. Li, and A. Züttel, *Boosting CO production in electrocatalytic CO_2 reduction on highly porous zn catalysts,* ACS Catalysis **9**, 3783 (2019).

[18] C.-T. Dinh, T. Burdyny, M. G. Kibria, A. Seifitokaldani, C. M. Gabardo, F. P. G. de Arquer, A. Kiani, J. P. Edwards, P. D. Luna, O. S. Bushuyev, C. Zou, R. Quintero-Bermudez, Y. Pang, D. Sinton, and E. H. Sargent, *CO_2 electroreduction to ethylene via hydroxide-mediated copper catalysis at an abrupt interface,* Science **360**, 783 (2018).

[19] G. O. Larrazábal, P. Strøm-Hansen, J. P. Heli, K. Zeiter, K. T. Therkildsen, I. Chorkendorff, and B. Seger, *Analysis of mass flows and membrane cross-over in CO_2 reduction at high current densities in an MEA-type electrolyzer,* ACS Applied Materials & Interfaces **11**, 41281 (2019).

[20] P. Jeanty, C. Scherer, E. Magori, K. Wiesner-Fleischer, O. Hinrichsen, and M. Fleischer, *Upscaling and continuous operation of electrochemical CO_2 to CO conversion in aqueous solutions on silver gas diffusion electrodes,* Journal of CO_2 Utilization **24**, 454 (2018).

[21] B. D. Mot, J. Hereijgers, M. Duarte, and T. Breugelmans, *Influence of flow and pressure distribution inside a gas diffusion electrode on the performance of a flow-by CO_2 electrolyzer,* Chemical Engineering Journal **378**, 122224 (2019).

[22] M. E. Leonard, L. E. Clarke, A. Forner-Cuenca, S. M. Brown, and F. R. Brushett, *Investigating electrode flooding in a flowing electrolyte, gas-fed carbon dioxide electrolyzer,* ChemSusChem **13**, 400 (2019).

[23] P. K. Das, A. Grippin, A. Kwong, and A. Z. Weber, *Liquid-water-droplet adhesion-force measurements on fresh and aged fuel-cell gas-diffusion layers,* Journal of The Electrochemical Society **159**, B489 (2012).

[24] R. L. Borup, J. R. Davey, F. H. Garzon, D. L. Wood, and M. A. Inbody, *PEM fuel cell electrocatalyst durability measurements,* Journal of Power Sources **163**, 76 (2006).

[25] T. Burchardt, *An evaluation of electrocatalytic activity and stability for air electrodes,* Journal of Power Sources **135**, 192 (2004).

[26] A. Löwe, C. Rieg, T. Hierlemann, N. Salas, D. Kopljar, N. Wagner, and E. Klemm, *Influence of temperature on the performance of gas diffusion electrodes in the CO_2 reduction reaction,* ChemElectroChem **6**, 4497 (2019).

[27] F. Bidault, D. Brett, P. Middleton, and N. Brandon, *Review of gas diffusion cathodes for alkaline fuel cells,* Journal of Power Sources **187**, 39 (2009).

[28] N. A. Hampson and A. J. S. McNeil, *The electrochemistry of porous electrodes: Flow-through and three-phase electrodes,* in *Electrochemistry* (Royal Society of Chemistry) pp. 1–65.

[29] M. E. Leonard, M. J. Orella, N. Aiello, Y. Román-Leshkov, A. Forner-Cuenca, and F. R. Brushett, *Editors' choice—flooded by success: On the role of electrode wettability in CO_2 electrolyzers that generate liquid products,* Journal of The Electrochemical Society **167**, 124521 (2020).

[30] M. Jouny, W. Luc, and F. Jiao, *High-rate electroreduction of carbon monoxide to multi-carbon products,* Nature Catalysis **1**, 748 (2018).

[31] U. O. Nwabara, E. R. Cofell, S. Verma, E. Negro, and P. J. A. Kenis, *Durable cathodes and electrolyzers for the efficient aqueous electrochemical reduction of CO 2,* ChemSusChem **13**, 855 (2020).

[32] C. M. Gabardo, C. P. O'Brien, J. P. Edwards, C. McCallum, Y. Xu, C.-T. Dinh, J. Li, E. H. Sargent, and D. Sinton, *Continuous carbon dioxide electroreduction to concentrated multi-carbon products using a membrane electrode assembly,* Joule **3**, 2777 (2019).

[33] Y.-J. Zhang, V. Sethuraman, R. Michalsky, and A. A. Peterson, *Competition between CO_2 reduction and CH_2 evolution on transition-metal electrocatalysts,* ACS Catalysis **4**, 3742 (2014).

[34] S. Trasatti, *Work function, electronegativity, and electrochemical behaviour of metals,* Journal of Electroanalytical Chemistry and Interfacial Electrochemistry **39**, 163 (1972).

[35] J.-B. Vennekoetter, R. Sengpiel, and M. Wessling, *Beyond the catalyst: How electrode and reactor design determine the product spectrum during electrochemical CO_2 reduction,* Chemical Engineering Journal **364**, 89 (2019).

[36] B. Endrődi, E. Kecsenovity, A. Samu, F. Darvas, R. V. Jones, V. Török, A. Danyi, and C. Janáky, *Multilayer electrolyzer stack converts carbon dioxide to gas products at high pressure with high efficiency,* ACS Energy Letters **4**, 1770 (2019).

[37] Y. Chen, C. W. Li, and M. W. Kanan, *Aqueous CO_2 reduction at very low overpotential on oxide-derived au nanoparticles,* Journal of the American Chemical Society **134**, 19969 (2012).

[38] Z.-C. Huang-fu, Q.-T. Song, Y.-H. He, J.-J. Wang, J.-Y. Ye, Z.-Y. Zhou, S.-G. Sun, and Z.-H. Wang, *Electrochemical CO_2 reduction on cu and au electrodes studied using in situ sum frequency generation spectroscopy,* Physical Chemistry Chemical Physics **21**, 25047 (2019).

[39] D. Barker, D. Brewin, R. Dahm, and L. Hoy, *The electrochemical reduction of polytetrafluoroethylene,* Electrochimica Acta **23**, 1107 (1978).

[40] G. S. Shapoval, A. P. Tomilov, A. A. Pud, and V. A. Vonsyatskii, *Electrochemical reductive destruction of polytetrafluoroethylene,* Theoretical and Experimental Chemistry **20**, 234 (1984).

[41] M. Schulze, K. Bolwin, E. Glzow, and W. Schnurnberger, *XPS analysis of PTFE decomposition due to ionizing radiation,* Fresenius' Journal of Analytical Chemistry **353**, 778 (1995).

[42] B. Kim, S. Ma, H.-R. M. Jhong, and P. J. Kenis, *Influence of dilute feed and pH on electrochemical reduction of CO_2 to CO on ag in a continuous flow electrolyzer,* Electrochimica Acta **166**, 271 (2015).

5

Cation-driven increases of CO_2 utilization in a BPMEA for CO_2 electrolysis

Advancing reaction rates for electrochemical CO_2 reduction (ECO2R) in membrane electrode assemblies (MEAs) have boosted the promise of the technology, while exposing new shortcomings. Among these is the maximum utilization of CO_2, which is capped at 50% (CO as targeted product) due to unwanted homogeneous reactions. Using bipolar membranes in an MEA (BPMEA) has the capability to prevent parasitic CO_2 losses, but their promise is dampened by poor CO_2 activity and selectivity. In this work, we enable a 3-fold increase in the CO_2 reduction selectivity of a BPMEA system by promoting alkali cation (K^+) concentrations on the catalyst's surface, achieving a CO Faradaic efficiency of 68%. When compared to an anion exchange membrane, the cation-infused BPM system shows a 5-fold reduction in CO_2 loss at similar current densities, while breaking the 50% CO_2 utilization mark. The work provides a combined cation and BPM strategy for overcoming CO_2 utilization issues in CO_2 electrolyzers.

This chapter has been published in ACS Energy Lett. **2021**, 6, 4291-4298.[1]

5.1. Introduction

The field of electrochemical CO_2 reduction (ECO2R) has advanced substantially in the past decade. Activity, selectivity and stability have been improved due to the deployment of gas diffusion electrodes as a catalytic support in flowing catholyte cells and membrane electrode assemblies (MEAs).[2–5] Despite improvements, the intrinsic homogeneous reactions which occur alongside the desired ECO2R make the process less favourable, with over half of all reacted CO_2 lost to carbonate instead of value-added products.[6–9]

The loss of CO_2 occurs when the required protons for ECO2R are provided by water-splitting, which results in OH^- being produced in equal proportion to the electrons transferred. In the presence of OH^-, CO_2 reacts chemically to form HCO_3^- and CO_3^{2-} ions (eq S1-S5). These reactions not only decrease utilization of the inputted CO_2, but also lower system conductivity and result in salt precipitation in the CO_2 gas channel in the presence of alkali cations.[10, 11] Unless this issue can be resolved, CO_2 utilization efficiency (Eq.1) will inevitably plateau at a maximum of 50% for for CO production in neutral and alkaline media.[12–14] Here CO_2 utilization efficiency is defined as the ratio of the reacted CO_2 that is converted to the target product carbon monoxide, to that of the total CO_2 reacted in the system (CO_2 -> CO, $HCOO^-$, HCO_3^-, CO_3^{2-}). The CO_2 utilization efficiency is considered independent of flow rate and is not to be confused with the total single-pass conversion of CO_2 within the system, for which the reader is referred elsewhere[9, 13].

CO_2 utilization efficiency= [CO_2 (to CO)]/[CO_2 (consumed)] (1)

In order to reduce CO_2 consumption by OH^-, a promising approach is to introduce excess H^+ near the cathode's surface. Protons can be provided either directly from an acidic catholyte, or via the membrane. Both approaches allow for the neutralization of OH^- and regeneration of CO_2 which has already been converted to (bi)carbonates. For example recently, Huang et al. reported ECO2R on Cu in an acid environment, which increased single-pass CO_2 utilization to 77% in a GDE flow cell.[15] Here the protons required for CO_2 electrolysis are still envisioned to come from water-splitting, resulting in OH^- formation similar to neutral and alkaline electrolytes. However the excess protons in the surrounding electrolyte both neutralize excess OH^- and reclaim CO_2 that was lost to (bi)carbonate. While high CO_2 utilizations are reached in this case, the dominant reaction remains H_2 at around 40% Faradaic efficiency because of the excess number of protons. Importantly, the excess protons provided in this system are not linked to the current density applied, implying that different optimal input acidities and flow rates are required for different current densities. A more recent work was able to reach higher FEs of 90% for CO_2 to CO on Au in acidic media,[16] but the maximum utilizations achievable and homogeneous reactions were not discussed. It is then unclear if these demonstrated high FEs can be simultaneously achieved with high utilizations.

Alternatively to using acidic catholytes, protons can be internally-generated proportionally to the applied current density through ion exchange membranes. Using a cation exchange membrane (CEM) coupled with an anolyte that is acidic solution or pure water[17–19] would permit protons to be efficiently transferred to the cathode only in the amount required to offset the formed OH^-. With proper interface engineering of the catalyst, elec-

trolyte and membrane, these protons could be used to regenerate CO_2 rather than undergoing direct proton reduction to H_2. For instance, recent work from O'Brien et al. demonstrated a CO_2 single pass conversion of 85% using pure water and an IrO_2 catalyst on the anode side with a CEM for proton shuttling.[19]

A final approach to provide protons to the cathode is to use a bipolar membrane (BPM) operating in reversed bias, which results in water dissociation at the sandwiched cation and anion membrane interfaces.[20–22] Under such operating, a proton is sent to the cathode and hydroxide to the anode. In addition to providing a proton source to the cathode, a BPM further allows for the use of an alkaline anolyte and Ni anode, at the penalty of higher membrane voltages. Previous efforts to employ BPMs in an MEA configuration (BPMEA), however, have been unable to limit excess H_2 production, giving poor CO_2 reduction selectivities and subsequently low CO_2 utilizations. Researchers have attributed excess H_2 to both low hydration of the membrane[23] and too high concentrations of H^+ at the cathode/membrane interface[24].

In all of the above scenarios, however, researchers have separately determined the importance of having alkali cations present at the electrode-electrolyte interface when performing ECO2R. Unlike alkaline conditions where high ECO2R Faradaic efficiencies can be achieved over a range of cation concentrations, recent work in acidic or neutral-pH cathode conditions highlights that special consideration of cation concentrations are required to achieve high CO_2 reduction selectivities.[25–29] Combining these observations with previous BPMEA demonstrations that have traditionally suffered from poor CO_2 reduction selectivities, we hypothesized that the low selectivity in a BPMEA system could be overcome by increasing cation concentrations at the cathode.[18, 19, 28] Thus if the low parasitic CO_2 loss of BPM's can be achieved simultaneously with improved CO_2 reduction performance, high CO_2 utilization efficiencies would be possible as a result.

In this work, we first took advantage of the traditionally undesired ion crossover in BPMs to increase the concentrations of cations at the cathode in a BPMEA configuration. The large concentration gradient of cations from the anolyte to the cathode provided a diffusion of K^+ ions to the cathode's surface, resulting an ECO2R selectivity improvement of 3-fold as a result of increased anolyte concentrations. Then, we compared the CO_2 converted to CO and CO_2 lost to electrolyte in both BPMEA and an anion exchange membrane (AEM) employed system (AEMEA). Results show that the CO_2 lost in a BPMEA cell is around 5 times lower than in an AEMEA cell in high alkaline environment. As a consequence, with increased Faradaic efficiencies, the resulting CO_2 utilization efficiency is 2 times higher in a BPMEA system.

5.2. Experimental methods

All experiments were performed in a 5 cm^2 CO_2 MEA electrolyzer (Dioxide Materials). Ag GDE was used as cathode with an active surface area of 6.25 cm^2 (2.5 cm x 2.5 cm). The Ag GDEs were made by magnetron sputtering (AJA International Inc.) 100 nm Ag on Sigracet® 39BC gas diffusion layer (Ion Power GmbH) with 50 W DC power supply. Nickel foam (3 cm * 3 cm, Recemat BV) was used as anode. Between cathode and anode, a 4 cm x 4 cm bipolar membrane (Fumasep® FBM) or Sustainion® anion exchange membrane (X37-50 Grade RT,

Dioxide Materials) was inserted to conduct ions. The cell was assembled and compressed using a torque wrench which was tightened to 4 Nm. Concentration of 0.2 M, 1 M and 3 M KOH (Sigma-Aldrich, 99.99%) solutions were used as anolyte. Humidified CO_2 was fed into the cell with 50 sccm flowrate through a mass controller (Bronkhorst High-Tech BV). The outlet flowrate was measured by a MFM (mass flow meter, Bronkhorst High-Tech BV). KOH anolyte was sent to the cell with a 20 mL/min flowrate via a peristaltic pump (MasterFlex®).

Chronopotentiometry at current density of 50, 100, 150, and 200 mA/cm^2 was applied using a potentiostat (PARSTAT). In BPM experiments, each current density was held for 20 minutes. While during AEM experiments, the time was shortened to 15 minutes due to serious salt formation problem, which could cause the cell to fail quickly. Gas products were analyzed by an online gas chromatography (compact GC 4.0, GAS). Injections were taken every 5 minutes and gas concentration already stabilized during the 2nd injection. Faradic efficiency was calculated based the average product concentration of 4 injections (BPM) or 3 injections (AEM). Anolyte samples were collected and analyzed by high-performance liquid chromatography (HPLC, Agilent Technologies).

In determining the CO_2 utilization efficiency towards CO, only two values must be determined. The amount of CO_2 converted to CO, and the total amount of the pure inputted CO_2 which is consumed on the cathode part. In our system the CO_2 conversion to CO was calculated using the outlet flow rate as measured by a mass flow metre and data from the GC which provided the CO concentration in the outlet stream:

$$V_{CO_2\ to\ CO} = C_{CO} * V_{outlet}\ (\text{mL/min})$$

where C_{CO} denotes CO concentration measured by GC. V_{outlet} was measured by MFM. Note that one mole of CO_2 gas can be converted to one mole of CO gas, meaning the CO_2 consumption rate to produce CO is the same to the CO production rate. Therefore, we could estimate the CO_2 loss by using the equation:

$$V_{CO_2\ lost} = V_{inlet} - (V_{outlet} - V_{H_2}), \text{where } V_{H_2} = C_{H_2} * V_{outlet}\ (\text{mL/min})$$

V_{inlet} was measured by MFC. Here we considered the impact of V_{H_2} when calculating the CO_2 consumption rates because in the BPMEA cell case there is a large amount of H_2 gas in the outlet stream. In the AEMEA case, in contrast, H_2 volumetric flow rate was not considered due to its negligible H_2 production. The CO_2 loss should arise from : 1) the formation of (bi)carbonate then crossover to anode and release as CO_2; 2) salt precipitation, and 3) formate product cross-over to the anode. We counted CO_2 to $HCOO^-$ as loss since the liquid product in the MEA cells cannot be easily collected. All the CO_2 consumed in the cell is:

$$V_{CO_2\ consumed} = V_{CO_2\ to\ CO} + V_{CO_2\ lost}$$

5.3. Results and discussion

Within a BPM operating under reversed bias (Figure 5.1 and 5.2(a)), the current transported across the membrane is not unidirectional as is the case for a CEM or AEM, but is rather bidirectional due to the production of both H^+ and OH^- to transport charge equivalent to the system current density. While H^+/OH^- transport is the desired operational effect, researchers have noted ion crossover as an important property of BPMs, and generally described this as an unwanted effect especially at low current densities.[20, 21, 30] Here we sought to use concentration dependent ion crossover as a beneficial effect to provide varying concentrations of K^+ to the cathode/membrane interface of a BPMEA.

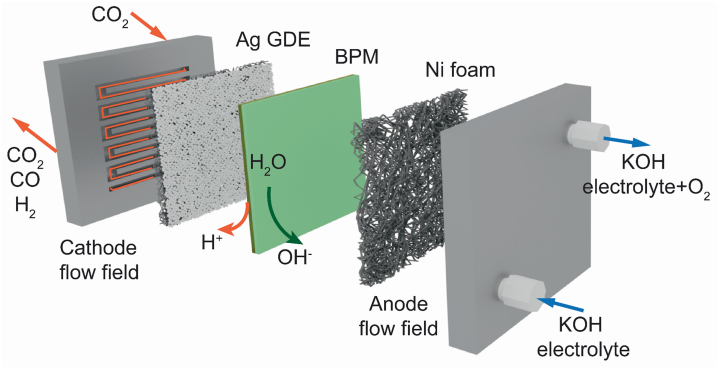

Figure 5.1: Illustration of BPM under reversed bias in a MEA cell.

In the BPMEA configuration shown in Figure 5.2(a), ion crossover of K^+ from the anode to the cathode will occur as a result diffusion and migration, both of which are concentration dependent.[31, 32] In order to promote further cation flux to the cathode in a BPMEA cell for ECO2R, we varied the concentration of the KOH anolyte from 0.2 M to 3 M and subsequently performed electrochemical CO_2 reduction at various current densities. In the low cation concentration case (0.2 M KOH) shown in Figure 5.2(b), CO Faradaic efficiencies remain low and decrease from 23% at 50 mA/cm^2, to 16% at 200 mA/cm^2. As ample CO_2 is available because of the gaseous CO_2 phase in close proximity to the catalyst layer, the decreasing trend in CO is due to favourable hydrogen evolution kinetics rather than limited CO_2. Without the presence of a catholyte buffer, this is likely due to excess H^+ flux providing a high proton concentration at elevated current densities. Upon increasing the anolyte concentration, the CO selectivity steadily rises however, becoming on par with H_2 at 200 mA/cm^2 for the 3 M KOH case (Figure 5.2(d)). At even lower current densities of 50 mA/cm^2, a CO selectivity of 68% is reached. The upward trend in ECO2R selectivity then tracks that of increased K^+ concentrations (see Figure SI1).The activity obtained in 3 M KOH here is very similar to what was reported by Lees et al for direct 3 M $KHCO_3$ reduction in a MEA cell equipped with a BPM.[33]

To investigate whether the observed selectivity changes are instead a function of increased OH^- concentration or system conductivity, we utilized a 0.2 M KOH + 0.4 M K_2CO_3 anolyte mixture to decouple K^+ and OH^- effects (chronopotentiometry in Figure SI2). The anolyte

solution then has the same pH of 13.5 as 0.2 M KOH (Table S1), but a K^+ concentration of 1 M. Figure SI3 shows that the CO Faradaic efficiency in this mixture solution (53%) is similar to the 1 M KOH case at 50 mA/cm^2, and much higher than the 0.2 M KOH case (24%). As current densities are increased further to 200 mA/cm^2, the 0.2 M KOH + 0.4 M K_2CO_3 case actually achieves the highest performance at a CO FE of 42%. The hypothesis for this increase of performance is that the crossover of K^+ is probably higher in the mixture than in 1M KOH. Although the K^+ concentration is the same in both solutions, measurements investigating the crossover in BPMs have shown dependence on property of ions (cations and anions) existed in the solutions, which leads to different K^+ crossover rate as a result.[30] The combined results in Figure 5.2 and SI3 then show that ECO2R can be improved in a BPMEA system via increased K^+ flux to the cathode, instead of the higher local pH provided by higher concentration of OH^-.In all cases the flux of potassium in the system is expected to reach a steady-state between the anode and cathode compartments which equilibrates within the first few minutes of an experiment as indicated by the stable CO selectivity after the first GC injection (Figure SI4).

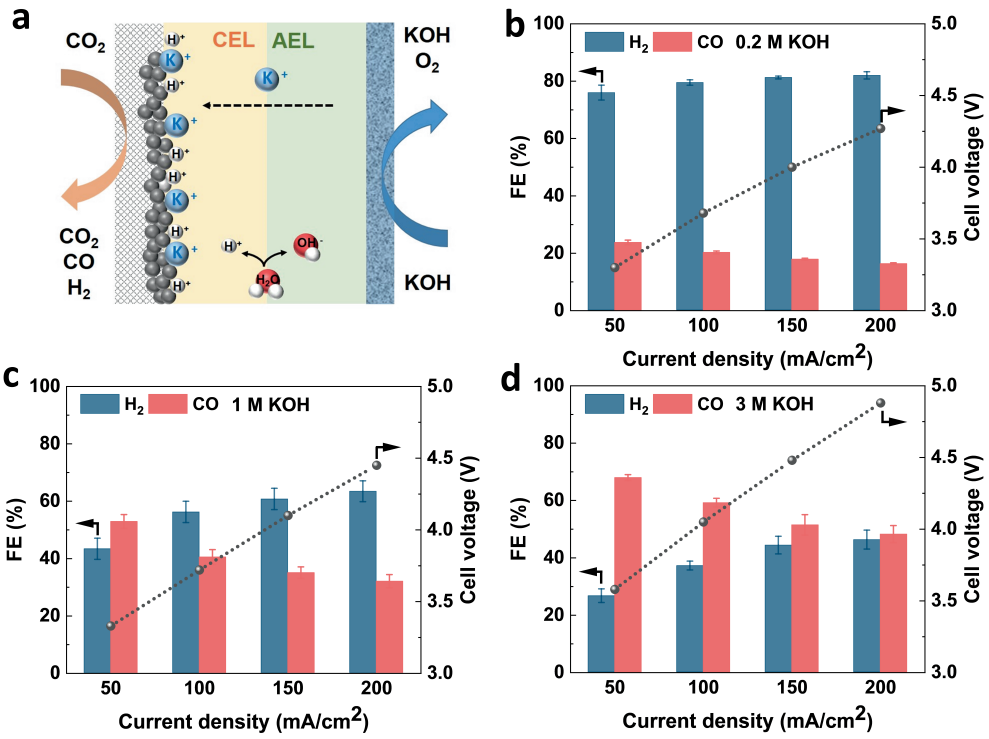

Figure 5.2: Illustration of BPMEA system (a) and Faradaic efficiency and cell voltage as function of current density in different concentrations of KOH solution in a BPMEA (b-d).

It should be noted that the cell voltage is also increasing as the anolyte concentration increases (right y-axis in Figure 5.2 and SI5). To account for the large ohmic resistance of the FumaTech® BPM used in these experiments (130 -160 µm), we subtracted the voltage which is induced by the ohmic resistance (Table S2). After correcting, the voltages show

similar values at same current densities in all electrolytes (Figure SI6). However, the high voltage is not the cause for a higher ECO2R performance. At the same voltage around 4 V, CO partial current density is still the highest in 3 M KOH solution (Figure SI7). Furthermore, ECO2R was also conducted using pure water as an anolyte in the BPMEA system. All CO Faradaic efficiencies show less than 10% (Figure SI8), which is significantly lower than the performance in 0.2 M KOH solution. It is worth mentioning that during the whole course of the experiment, the pH of the anolyte remained the same in the BPMEA system (Table S1). Such high stability by maintaining the pH of electrolyte is another advantage of a BPM, and indicates that CO_2 crossover is relatively low compared to an AEM.[34] The stable pH also suggests that water dissociation occurred during ECO2R, and OH^- produced by BPM could supplement OH^- lost during the oxygen evolution reaction (OER).

In order to compare the CO_2 utilization efficiency of the BPMEA case, we also need a point of comparison for a high CO selectivity configuration. For this we reproduced experiments for a Ag-sputtered catalyst in an MEA configuration with an AEM (Figure 5.3(a)). We performed AEM experiments over a similar range of anolyte concentrations for comparison purposes, and to observe any effects from increased cation concentrations. As shown in Figure 5.3(c-d), ECO2R activity is overall higher when using an AEM than using a BPM, which is consistent with what is reported in literature.[35] Over the range of tested current densities, CO always remains the dominant product, ranging from 70-90% in selectivity. No strong

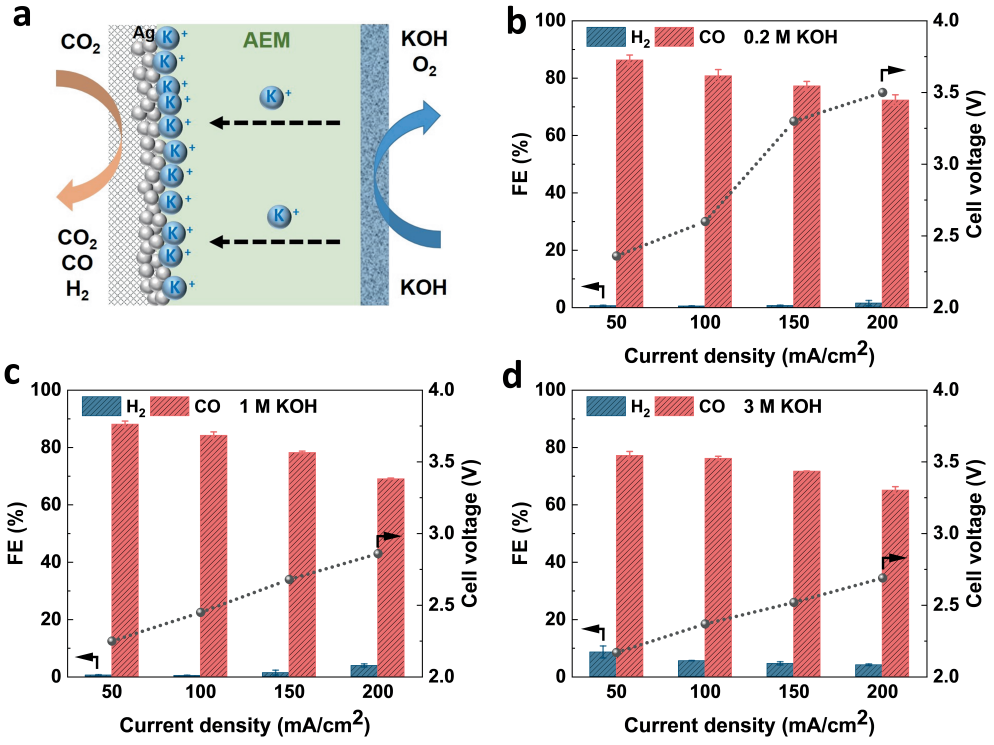

Figure 5.3: Illustration of an AEMEA system (a) and Faradaic efficiency and cell voltage as function of current density in different concentrations of KOH solution in an AEMEA (b-d).

dependence on the anolyte concentration is noted over the 0.2 M to 3 M range tested. The results show that in neutral or alkaline media such as in an AEMEA system, high ECO2R activity still can be achieved even when cation concentrations are low. Dioxide Materials® even reported high CO Faradaic efficiency using 10 mM $KHCO_3$ as anolyte in the same AEMEA cell.[35] The improved selectivity has been explained by the better kinetics of ECO2R than HER in such environment, where the proton donor in both cases is from water and cations play a lesser role in selectivity as compared to acidic media.[15, 36]

It is worth briefly discussing the decrease in CO Faradaic efficiency observed in the AEM case as a function of current density and KOH concentration. Upon increasing both the drop in CO selectivity is replaced by a higher Faradaic efficiency of $HCOO^-$, which we observed in the anolyte stream through high-pressure liquid chromatograph (HPLC) tests.[7] The higher $HCOO^-$ FE at these conditions has been observed elsewhere and linked to increases in local reaction pH.[37]

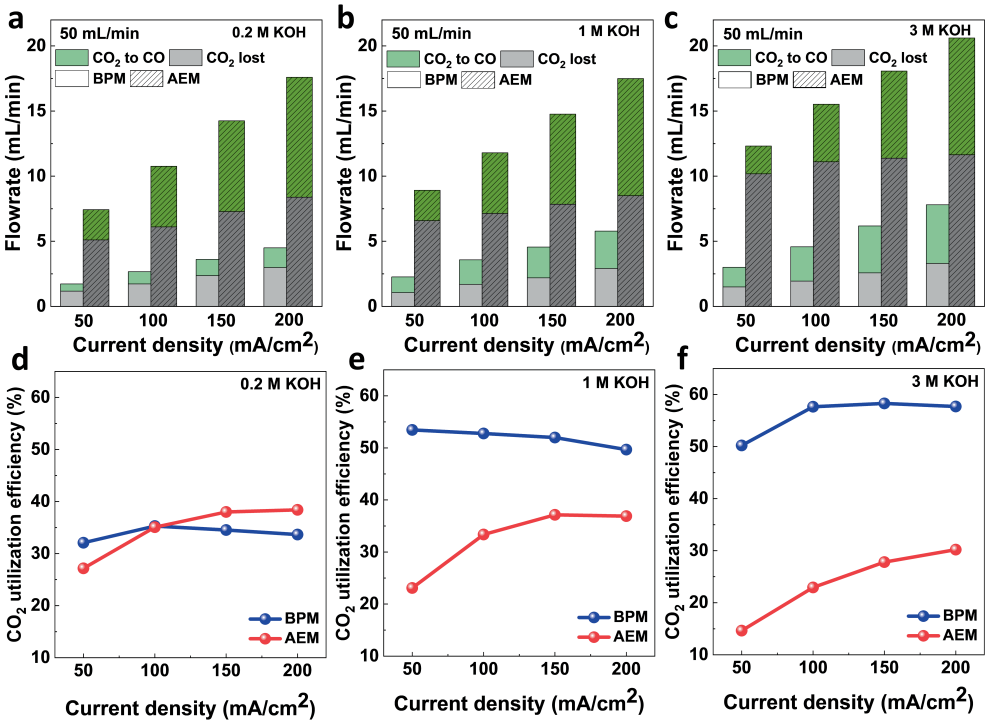

Figure 5.4: CO_2 converted to CO and lost CO_2 in flowrate (a-c) and CO_2 utilization efficiency (d-f) as function of current density in both BPMEA and AEMEA systems. CO_2 inflow is 50 mL/min.

With both the BPMEA and AEM selectivity results acquired, we compared the overall CO_2 utilization efficiency (Eq. 1) towards CO of the two systems, now taking into account the amount of CO_2 that is lost to unwanted (bi)carbonate reaction. Here Figure 5.4(a-c) shows the conversion of CO_2 to CO, as well as the overall CO_2 lost in absolute terms of flow rate, while the CO_2 utilization efficiency is presented in Figures 5.4(d-f). The results in Figure

5.4 (a-c) are useful to highlight the differences between the BPMEA and AEM systems. In particular by observing the grey areas of these images, we can see that in an AEM configuration the amount of CO_2 consumed by OH^- and formate production increases with current density and KOH concentration. Meanwhile, the green areas for the AEM remain similar with anion concentration, collectively leading to CO_2 utilization efficiencies below 40% in all cases (Figure 5.4(d-f)). Conversely, observing the behaviour of the BPMEA system, CO_2 lost does not vary significantly with varying anolyte concentrations. For all concentrations studied, the unwanted loss of CO_2 is roughly 1 mL/min at 50 mA/cm^2 and 3 mL/min at 200 mA/cm^2. When paired with the improved Faradaic efficiencies with increasing K^+ concentrations, the overall CO_2 utilization efficiency increases for the BPMEA system, leading to a high of 60% in 3 M KOH (Figure 5.4(f)), with unwanted CO_2 lost 4-5 times lower than the AEM case. We note that the experimental results show that CO_2 is still consumed in a BPMEA cell, albeit to a much lesser extent. This indicates that the amount of H^+ flux from BPM is not large enough to neutralize all the OH^- produced or regenerate all CO_2 converted to (bi)carbonate during electrolysis. As for conversion of CO_2 to CO (green area in Figure 5.4(a-c)), AEMEA outperforms BPMEA in all KOH concentrations due to its higher FE for ECO2R.The CO2 single pass conversion efficiency in the BPMEA cell is also calculated accordingly (Figure SI9).

Combined the results show the simultaneously benefit of using a BPMEA with increased cation flux to the cathode. We maintain low parasitic reactions by providing a proton flux from the BPM to the cathode, while increasing Faradaic efficiency by also providing higher K^+ concentrations to the cathode. The dependency can viewed clearly in Figure 5.5(a) where the lost CO_2 remains flat due to the BPM, while increased cations improve CO_2 selected towards CO, even in a likely acidic reaction environment.

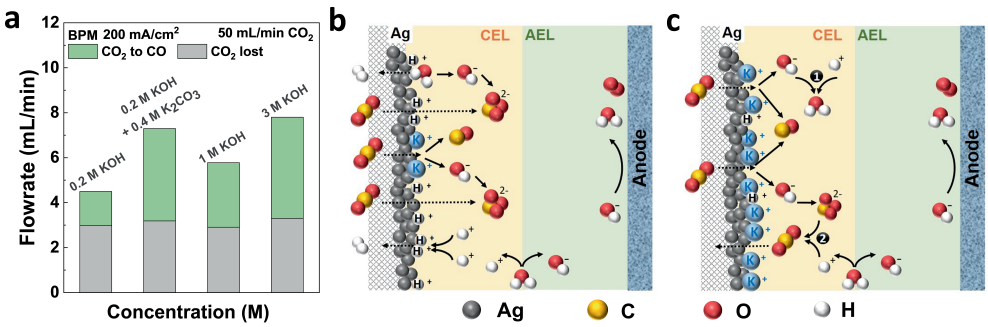

Figure 5.5: (a) CO_2 converted to CO and CO_2 lost in electrolyte in all concentrations at 200 mA/cm^2 in a BPMEA system. CO_2 inflow is 50 mL/min. (b) Carbon balance in a BPMEA cell with lower CO_2 utilization and (c) increased CO_2 utilization by H^+ neutralizing OH^- (1) or H+ regenerating CO_2 through reacting with (bi)carbonates(2).

It is worth mentioning that the utilization efficiency is lowest in 0.2 M KOH in the BPMEA system, which can be explained by the low performance of ECO2R when cations are less available on the catalyst's surface (CO FE < 20%). This is explained by the hydrogen evolution reaction (HER) maintaining favourable kinetics over ECO2R under cation-limited acidic conditions.[16, 28] In the absence of cations and ECO2R, the H^+ from the BPM is as-

sumed to be directly reduced to H_2 on the catalyst's surface instead of neutralizing all OH^- generated from water and CO_2 reduction. [28, 36] Thus, CO_2 utilization efficiencies have been shown to be even lower than the theoretical amount of 50% as shown in Figure 5.5(b). With an increased availability of cations in the 1 M and 3 M KOH cases, ECO2R kinetics which requires protons to come from water-splitting are however more favoured than HER. The H^+ from the BPM is then hypothesized to partially neutralize the OH^- and regenerate CO_2 from (bi)carbonates (Figure 5.5(c)) instead of directly being reduced to H_2. Thus CO_2 utilization efficiencies are improved. For deeper understanding of the mechanisms, localized concentrations and pathways of H^+ in such a system, a detailed modelling is required in future which accounts for both the acid and base versions of homogeneous and heterogeneous reactions.

From the presented results, a number of operational comparisons can also be made about the BPMEA and AEMEA cases independent of CO_2 utilization. We would like to point out that the cell voltages needed are smaller in an AEMEA than a BPMEA system. After correcting the voltages for cell resistance (Figure SI6, SI10), the voltages in the BPMEA are around 0.9 V – 1 V higher than in the AEMEA cell. This extra voltage for the BPMEA is explained by the minimum voltage needed for the water dissociation inside a BPM, which is around 0.83 V, as well as additional driving force at the given current density.[20] Nevertheless BPMs have the potential of reaching higher CO_2 utilization as demonstrated in this work, which under a proper technoeconomic analysis could be evaluated to determine if it offsets the added required voltage. In addition, BPMs can maintain stable anolyte pH without electrolyte replenishment. Usage of non-noble catalysts as anodes is then a possible option, which can add extra merit to a BPMEA system.

In a further assessment we note a substantial reduction in salt precipitation for the BPMEA case, which supports the reduced consumption of CO_2 by the electrolyte. A major cause for the failure of CO_2 electrolyzer when using an AEM is salt precipitation and blockage of the gas flow field. That happens typically in around 1 hour (Figure SI11). In an AEMEA cell, salt accumulation partially blocked the gas flow field in 1 M KOH, and fully blocked the gas channel in the 3 M KOH case after 80 minutes of operational time. However, in a BPMEA system, no salt was observed after the same duration in 1 M KOH, and there was little salt formed in 3 M KOH. Further running the BPMEA cell with 1 M KOH anolyte at 100 mA/cm^2 showed stable cell voltage, CO Faradaic efficiency and anolyte pH during 5.5 hours without any salt formation on the gas channel as shown in Figure SI12. These results imply that the potassium and carbonate concentration reaches a steady-state value below the salt precipitation limit at this current density and anolyte concentration. Thus once a certain potassium concentration is reached on the cathode-side, potassium is not expected to accumulate indefinitely and will instead form a balance. Similarly the formed carbonate in the BPMEA case will also not continuously build-up, and is expected to physically crossover the CEM of the BPMEA. Less salt formation also indicates that less CO_2 is consumed to (bi)carbonate, which is consistent with results shown in Figure 5.4. It is noted that the morphology of the Ag catalyst after the ECO2R test in both the BPMEA and AEMEA cells did not change (Figure SI13), suggesting a good stability of Ag in both cells during the CO_2 reduction process.

We hypothesize that with future modification of the BPMEA system, the catalyst could further favour CO_2 reduction over HER. Under such circumstances, excessive H^+ from BPM

could otherwise effectively neutralize OH^- produced, instead of resulting in HER as shown in Figure 5.5(b), or quickly react with the (bi)carbonate ions and regenerate CO_2 (Figure 5.5(c)). For instance, to improve the cation concentration at the catalyst surface in a MEA cell with a pure water anolyte, Endrődi et al mixed CO_2 gas feed with alkali-cation containing solutions.[18] With this treatment, ECO2R to CO reached several times higher activity than without any treatment, although it required repeat implementation. Other solutions could be coating catalyst layer with an ionomer that has suitable cation groups in favour of ECO2R.[19] Using catalysts that have better kinetics for ECO2R than Ag, could also favour ECO2R over HER.[38] Further developments may also allow for a reduction in cell voltages. As demonstrated by Oener et al.[39] incorporating catalysts within the BPM architecture can decrease the overpotential needed for water dissociation and thus minimize the overall BPMEA cell voltages for high-rate CO_2 electrolysis. Further reductions in are also foreseen by optimizing the full contact between the cathode, membrane and anode to ensure that all electrochemical surfaces are fully functional. A challenge in such a system is to ensure that the proton flux from the BPM can function optimally with a potentially thicker cathode layer. With beneficial local environment and better catalysts in a BPMEA cell, however, there is upward potential for CO_2 utilization efficiency and energy efficiency with the given approach.

5.4. Conclusion

In this work, we reported an increased ECO2R performance in a MEA system coupled with a BPM under reversed bias. This was achieved by allowing higher cation concentration to be transported to the catalyst surface. Our results showed that CO Faradaic efficiency improved from less than 20%, as reported in literature, by 3-fold to 68%. With the current-dependent H^+ produced from the BPM, lost CO_2 was also reduced by 5-fold in BPMEA cell. Thus a CO_2 utilization efficiency was achieved, which was 2 times higher than in an AEMEA cell. Furthermore, BPMEA cell also showed better stability than AEMEA by maintaining a stable pH of anolyte and preventing rapid salt precipitation at cathode. With further advancement in the commercial BPM, we anticipate the BPMEA could be a promising option for higher CO_2 utilization efficiencies. In addition, this work addresses the importance of cation embedment while using a MEA configuration, which guides to an advanced design for next generation CO_2 electrolyzers.

References

[1] K. Yang, M. Li, S. Subramanian, M. A. Blommaert, W. A. Smith, and T. Burdyny, *Cation-driven increases of CO_2 utilization in a bipolar membrane electrode assembly for CO_2 electrolysis,* , 4291 (2021).

[2] C.-T. Dinh, T. Burdyny, M. G. Kibria, A. Seifitokaldani, C. M. Gabardo, F. P. G. de Arquer, A. Kiani, J. P. Edwards, P. D. Luna, O. S. Bushuyev, C. Zou, R. Quintero-Bermudez, Y. Pang, D. Sinton, and E. H. Sargent, *CO_2 electroreduction to ethylene via hydroxide-mediated copper catalysis at an abrupt interface,* Science **360**, 783 (2018).

[3] T. Burdyny and W. A. Smith, *CO_2 reduction on gas-diffusion electrodes and why catalytic performance must be assessed at commercially-relevant conditions,* Energy & Environmental Science **12**, 1442 (2019).

[4] D. Higgins, C. Hahn, C. Xiang, T. F. Jaramillo, and A. Z. Weber, *Gas-diffusion electrodes for carbon dioxide reduction: A new paradigm,* ACS Energy Letters **4**, 317 (2018).

[5] B. Endrődi, E. Kecsenovity, A. Samu, T. Halmágyi, S. Rojas-Carbonell, L. Wang, Y. Yan, and C. Janáky, *High carbonate ion conductance of a robust PiperION membrane allows industrial current density and conversion in a zero-gap carbon dioxide electrolyzer cell,* Energy & Environmental Science **13**, 4098 (2020).

[6] J. A. Rabinowitz and M. W. Kanan, *The future of low-temperature carbon dioxide electrolysis depends on solving one basic problem,* Nature Communications **11** (2020), 10.1038/s41467-020-19135-8.

[7] G. O. Larrazábal, P. Strøm-Hansen, J. P. Heli, K. Zeiter, K. T. Therkildsen, I. Chorkendorff, and B. Seger, *Analysis of mass flows and membrane cross-over in CO_2 reduction at high current densities in an MEA-type electrolyzer,* ACS Applied Materials & Interfaces **11**, 41281 (2019).

[8] M. Ma, E. L. Clark, K. T. Therkildsen, S. Dalsgaard, I. Chorkendorff, and B. Seger, *Insights into the carbon balance for CO_2 electroreduction on cu using gas diffusion electrode reactor designs,* Energy & Environmental Science **13**, 977 (2020).

[9] C.-T. Dinh, Y. C. Li, and E. H. Sargent, *Boosting the single-pass conversion for renewable chemical electrosynthesis,* Joule **3**, 13 (2019).

[10] B. Endrődi, E. Kecsenovity, A. Samu, F. Darvas, R. V. Jones, V. Török, A. Danyi, and C. Janáky, *Multilayer electrolyzer stack converts carbon dioxide to gas products at high pressure with high efficiency,* ACS Energy Letters **4**, 1770 (2019).

[11] D. S. Ripatti, T. R. Veltman, and M. W. Kanan, *Carbon monoxide gas diffusion electrolysis that produces concentrated c2 products with high single-pass conversion,* Joule **3**, 240 (2019).

[12] L.-C. Weng, A. T. Bell, and A. Z. Weber, *Towards membrane-electrode assembly systems for CO_2 reduction: a modeling study,* Energy & Environmental Science **12**, 1950 (2019).

[13] E. Jeng and F. Jiao, *Investigation of CO_2 single-pass conversion in a flow electrolyzer,* Reaction Chemistry & Engineering **5**, 1768 (2020).

[14] R. Kas, A. G. Star, K. Yang, T. V. Cleve, K. C. Neyerlin, and W. A. Smith, *Along the channel gradients impact on the spatioactivity of gas diffusion electrodes at high conversions during CO_2 electroreduction,* ACS Sustainable Chemistry & Engineering **9**, 1286 (2021).

[15] J. E. Huang, F. Li, A. Ozden, A. S. Rasouli, F. P. G. de Arquer, S. Liu, S. Zhang, M. Luo, X. Wang, Y. Lum, Y. Xu, K. Bertens, R. K. Miao, C.-T. Dinh, D. Sinton, and E. H. Sargent, *CO_2 electrolysis to multicarbon products in strong acid,* Science **372**, 1074 (2021).

[16] M. C. O. Monteiro, M. F. Philips, K. J. P. Schouten, and M. T. M. Koper, *Efficiency and selectivity of CO_2 reduction to CO on gold gas diffusion electrodes in acidic media,* Nature Communications **12** (2021), 10.1038/s41467-021-24936-6.

[17] Z. Yin, H. Peng, X. Wei, H. Zhou, J. Gong, M. Huai, L. Xiao, G. Wang, J. Lu, and L. Zhuang, *An alkaline polymer electrolyte CO_2 electrolyzer operated with pure water,* Energy & Environmental Science **12**, 2455 (2019).

[18] B. Endrődi, A. Samu, E. Kecsenovity, T. Halmágyi, D. Sebők, and C. Janáky, *Operando cathode activation with alkali metal cations for high current density operation of water-fed zero-gap carbon dioxide electrolysers,* Nature Energy **6**, 439 (2021).

[19] C. P. O'Brien, R. K. Miao, S. Liu, Y. Xu, G. Lee, A. Robb, J. E. Huang, K. Xie, K. Bertens, C. M. Gabardo, J. P. Edwards, C.-T. Dinh, E. H. Sargent, and D. Sinton, *Single pass CO_2 conversion exceeding 85% in the electrosynthesis of multicarbon products via local CO_2 regeneration,* ACS Energy Letters **6**, 2952 (2021).

[20] D. A. Vermaas, S. Wiegman, T. Nagaki, and W. A. Smith, *Ion transport mechanisms in bipolar membranes for (photo)electrochemical water splitting,* Sustainable Energy & Fuels **2**, 2006 (2018).

[21] J. C. Bui, I. Digdaya, C. Xiang, A. T. Bell, and A. Z. Weber, *Understanding multi-ion transport mechanisms in bipolar membranes,* ACS Applied Materials & Interfaces **12**, 52509 (2020).

[22] M. A. Blommaert, D. Aili, R. A. Tufa, Q. Li, W. A. Smith, and D. A. Vermaas, *Insights and challenges for applying bipolar membranes in advanced electrochemical energy systems,* ACS Energy Letters **6**, 2539 (2021).

[23] D. A. Salvatore, D. M. Weekes, J. He, K. E. Dettelbach, Y. C. Li, T. E. Mallouk, and C. P. Berlinguette, *Electrolysis of gaseous CO_2 to CO in a flow cell with a bipolar membrane,* ACS Energy Letters **3**, 149 (2017).

[24] Y. Chen, A. Vise, W. E. Klein, F. C. Cetinbas, D. J. Myers, W. A. Smith, T. G. Deutsch, and K. C. Neyerlin, *A robust, scalable platform for the electrochemical conversion of CO_2 to formate: Identifying pathways to higher energy efficiencies,* ACS Energy Letters **5**, 1825 (2020).

[25] J. Resasco, L. D. Chen, E. Clark, C. Tsai, C. Hahn, T. F. Jaramillo, K. Chan, and A. T. Bell, *Promoter effects of alkali metal cations on the electrochemical reduction of carbon dioxide,* Journal of the American Chemical Society **139**, 11277 (2017).

[26] S. Ringe, E. L. Clark, J. Resasco, A. Walton, B. Seger, A. T. Bell, and K. Chan, *Understanding cation effects in electrochemical CO_2 reduction,* Energy & Environmental Science **12**, 3001 (2019).

[27] A. G. Fink, E. W. Lees, Z. Zhang, S. Ren, R. S. Delima, and C. P. Berlinguette, *Impact of alkali cation identity on the conversion of HCO_3^- to CO in bicarbonate electrolyzers,* ChemElectroChem **8**, 2094 (2021).

[28] M. C. O. Monteiro, F. Dattila, B. Hagedoorn, R. García-Muelas, N. López, and M. T. M. Koper, *Absence of CO_2 electroreduction on copper, gold and silver electrodes without metal cations in solution,* Nature Catalysis **4**, 654 (2021).

[29] L. D. Chen, M. Urushihara, K. Chan, and J. K. Nørskov, *Electric field effects in electrochemical CO_2 reduction,* ACS Catalysis **6**, 7133 (2016).

[30] M. A. Blommaert, J. A. H. Verdonk, H. C. Blommaert, W. A. Smith, and D. A. Vermaas, *Reduced ion crossover in bipolar membrane electrolysis via increased current density, molecular size, and valence,* ACS Applied Energy Materials **3**, 5804 (2020).

[31] L. Tang, *Concentration dependence of diffusion and migration of chloride ions,* Cement and Concrete Research **29**, 1463 (1999).

[32] L. Tang, *Concentration dependence of diffusion and migration of chloride ions,* Cement and Concrete Research **29**, 1469 (1999).

[33] E. W. Lees, M. Goldman, A. G. Fink, D. J. Dvorak, D. A. Salvatore, Z. Zhang, N. W. X. Loo, and C. P. Berlinguette, *Electrodes designed for converting bicarbonate into CO,* **5**, 2165 (2020).

[34] M. Ma, S. Kim, I. Chorkendorff, and B. Seger, *Role of ion-selective membranes in the carbon balance for CO_2 electroreduction via gas diffusion electrode reactor designs,* Chemical Science **11**, 8854 (2020).

[35] Z. Liu, H. Yang, R. Kutz, and R. I. Masel, *CO_2 electrolysis to CO and O_2 at high selectivity, stability and efficiency using sustainion membranes,* Journal of The Electrochemical Society **165**, J3371 (2018).

[36] C. J. Bondue, M. Graf, A. Goyal, and M. T. M. Koper, *Suppression of hydrogen evolution in acidic electrolytes by electrochemical CO_2 reduction,* Journal of the American Chemical Society **143**, 279 (2020).

[37] A. Seifitokaldani, C. M. Gabardo, T. Burdyny, C.-T. Dinh, J. P. Edwards, M. G. Kibria, O. S. Bushuyev, S. O. Kelley, D. Sinton, and E. H. Sargent, *Hydronium-induced switching between CO_2 electroreduction pathways,* Journal of the American Chemical Society **140**, 3833 (2018).

[38] K. Yang, R. Kas, W. A. Smith, and T. Burdyny, *Role of the carbon-based gas diffusion layer on flooding in a gas diffusion electrode cell for electrochemical CO_2 reduction,* ACS Energy Letters **6**, 33 (2020).

[39] S. Z. Oener, M. J. Foster, and S. W. Boettcher, *Accelerating water dissociation in bipolar membranes and for electrocatalysis,* **369**, 1099 (2020).

A

Persistent high local pH during CO_2 electroreduction in an aqueous cell

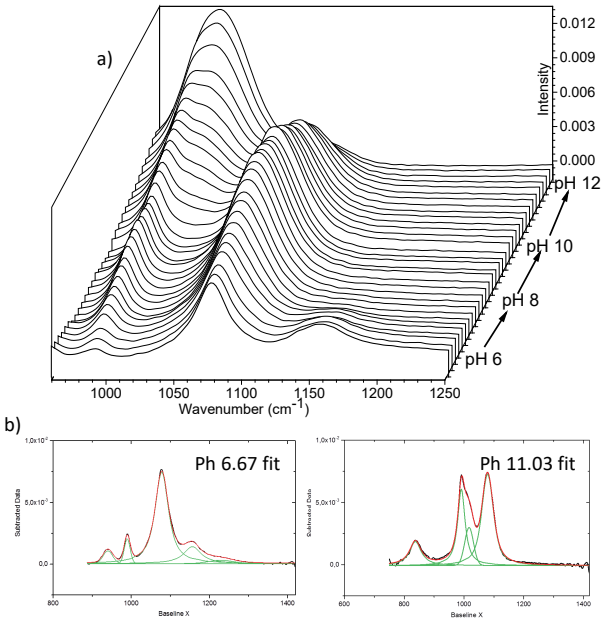

Figure A.1: (a) SEIRA spectra of phosphate species for different pH values between 6 and 12 under an applied potential of + 0.1 V vs RHE. The spectra were obtained by addition of KOH to parent KH_2PO_4 solution. (b) Individual peaks for each phosphate species were deconvoluted by using OriginPro.

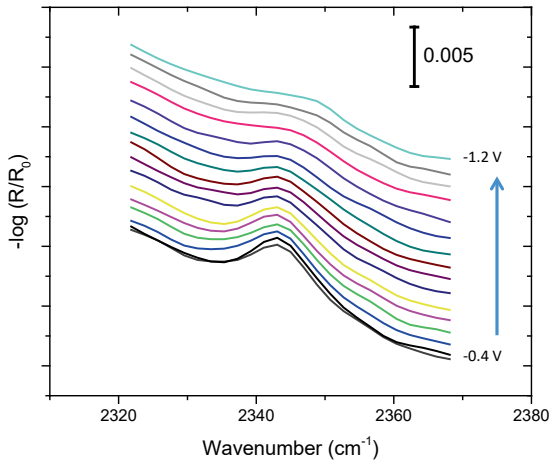

Figure A.2: Potential dependent changes in the asymmetrical stretching of CO_2(aq).

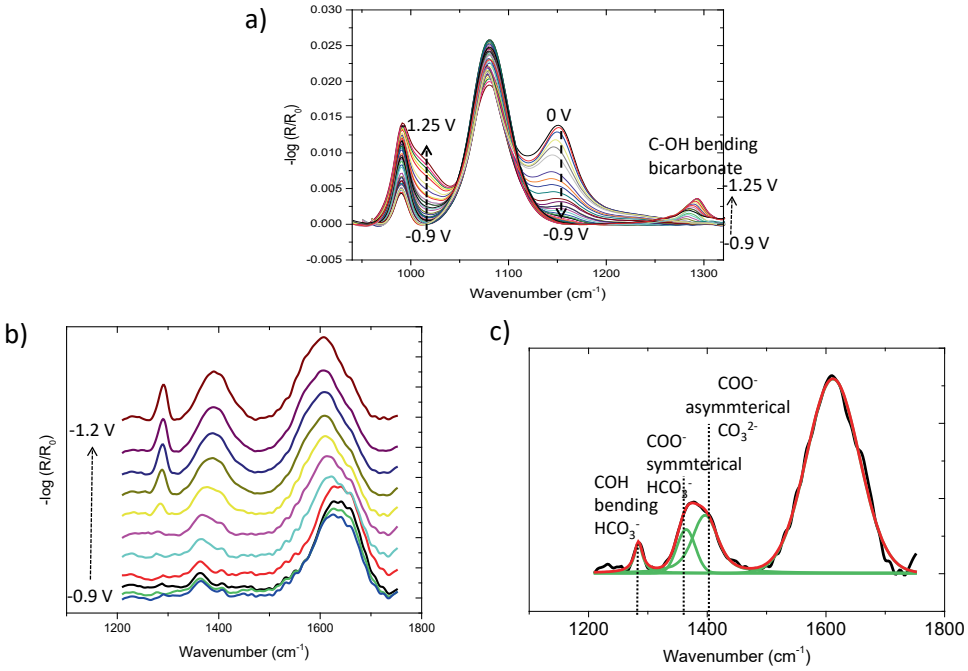

Figure A.3: (a) Detection of bicarbonate coincides with alkaline pH (> 9) near the electrode surface. (b) Change in (bi)carbonate and water bands at high potential region. (c) Individual peaks for (bi)carbonate species were deconvoluted by using OriginPro. Note that bicarbonate has another mode overlapping with water and usually hard to deconvolute.

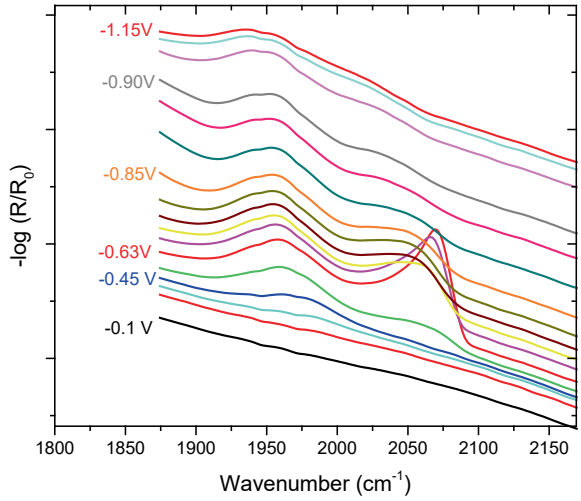

Figure A.4: Adsorption of CO as a function of potential given for 0.5 M phosphate buffer.

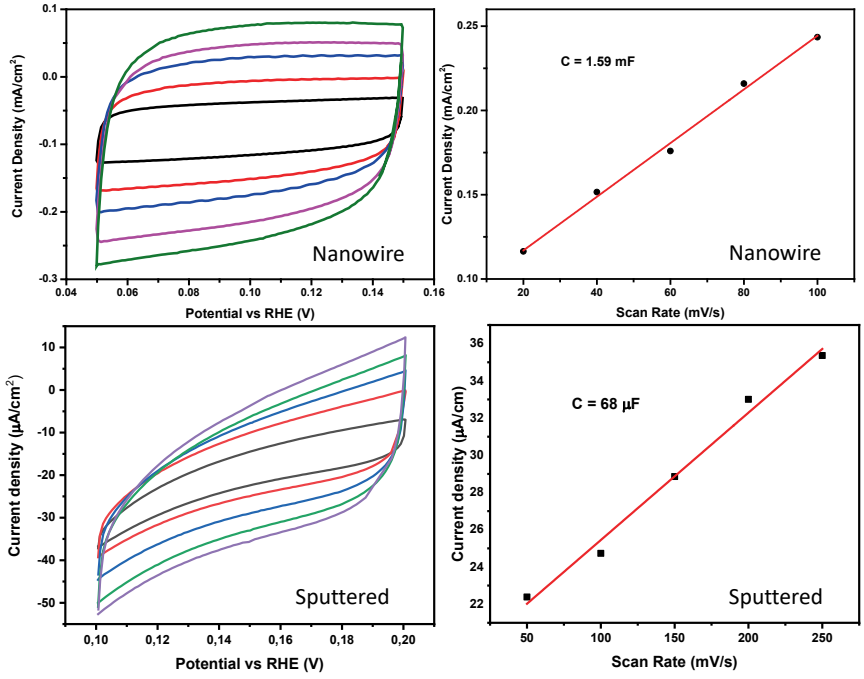

Figure A.5: Determination of double layer capacitance and roughness factor in 0.1 M $NaClO_4$ for Nanowire and sputtered copper electrodes.

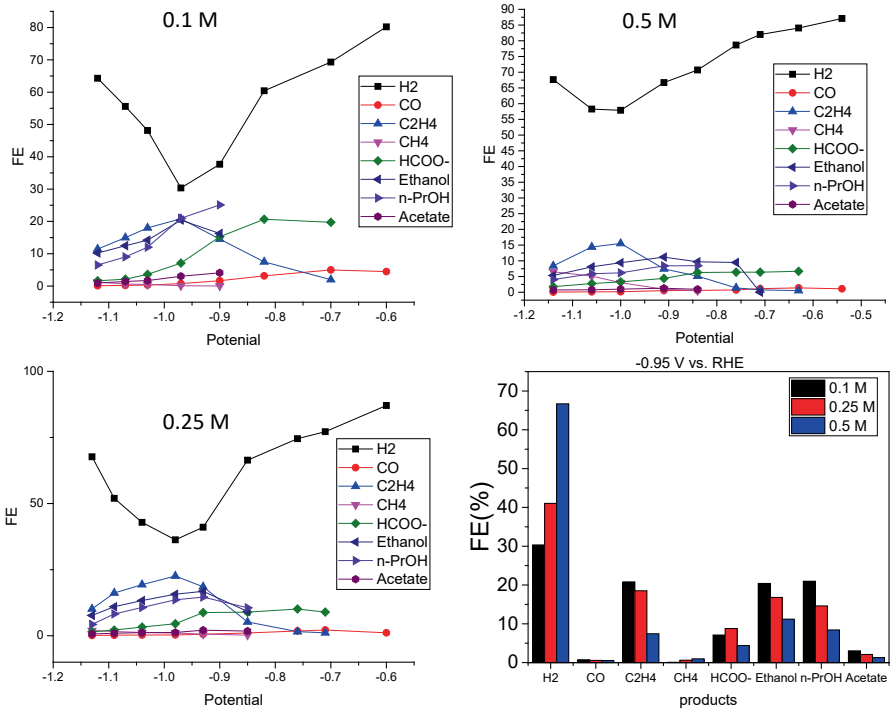

Figure A.6: Faradaic efficiency of gaseous and liquid products as a function of electrolyte concentration for nanowire copper electrodes.. The electrolytes are composed of equimolar amounts of $H_2PO_4^-$ and HPO_4^{2-}. FE of hydrogen increased notably at higher electrolyte concentrations and the selectivity towards C2 and C3 products decreased at potentials between - 0.7 V vs RHE to - 1 V vs RHE as a function of electrolyte concentration. The decrease in the selectivity of CO_2 reduction products are mostly result of increase in the hydrogen production (see main text).

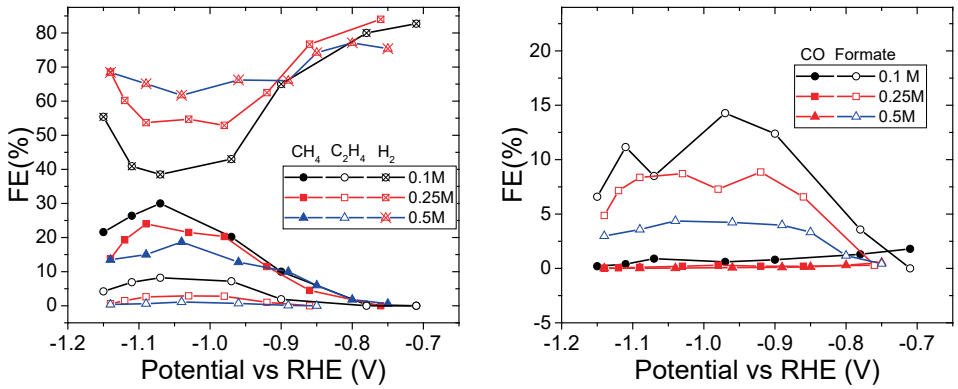

Figure A.7: Faradaic efficiency of gaseous and liquid products as a function of electrolyte concentration for sputtered copper electrodes.. The electrolytes are composed of equimolar amounts of $H_2PO_4^-$ and HPO_4^{2-}. FE of hydrogen increased notably at higher electrolyte concentrations and the selectivity towards C1 and C2 products decreased at potentials between - 0.8 V vs RHE to - 1.1 V vs RHE as a function of electrolyte concentration. The decrease in the selectivity of CO_2 reduction products are mostly result of increase in the hydrogen production (see main text).

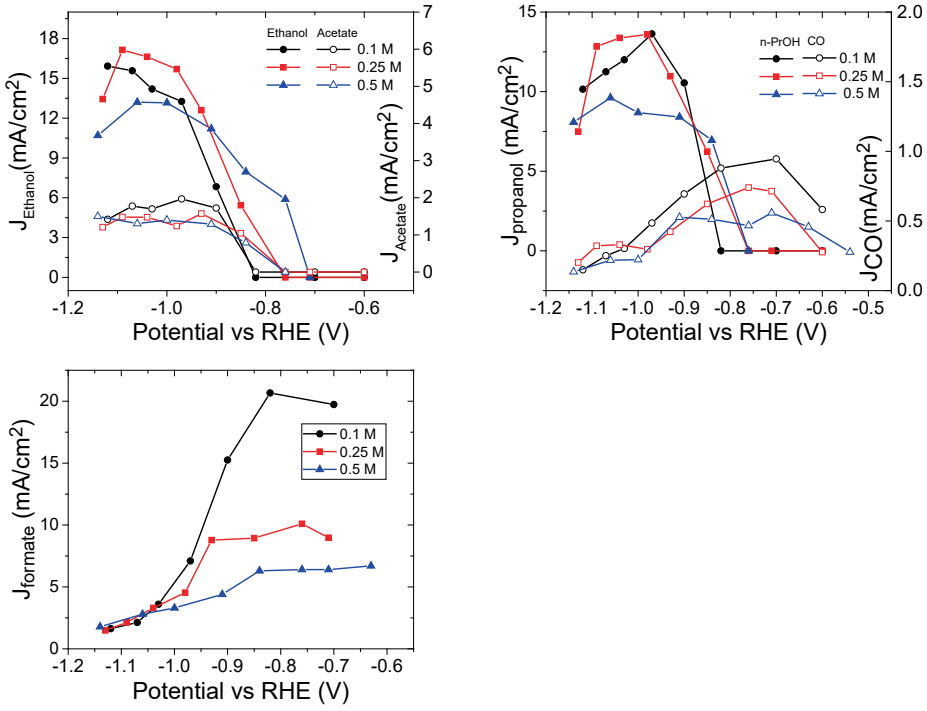

Figure A.8: Partial current density of of gaseous and liquid products as a function of electrolyte concentration for nanowire electrodes. Partial current density of Methane, Ethylene and Hydrogen are given in main text.

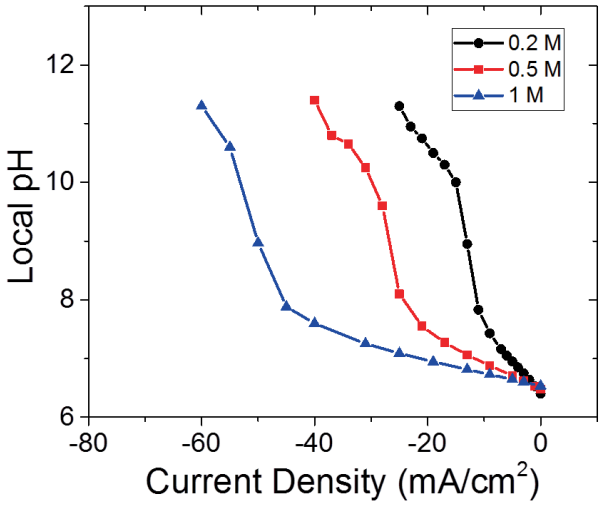

Figure A.9: Local pH as a function of current density calculated by including diffusion and convection via stirring (without bubble induced convection). Double layer thickness is taken as 100 µm which is a typical thickness that can be achieved with extensive magnetic stirring. This value is used commonly for calculating near surface concentration of molecules during CO_2 electroreduction.This graph indicates the model dramatically underestimates the buffer capacity without bubble induced mass transport term at high currents (> 20 mA/cm^2).

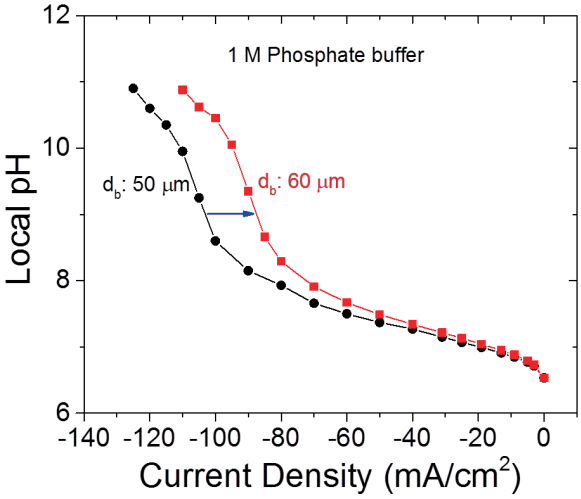

Figure A.10: Local pH as a function of current density calculated by bubble induced mass transport model for two different bubble departure diameters (d_b). The difference after breakdown of the buffer is notably high compared to buffered region.

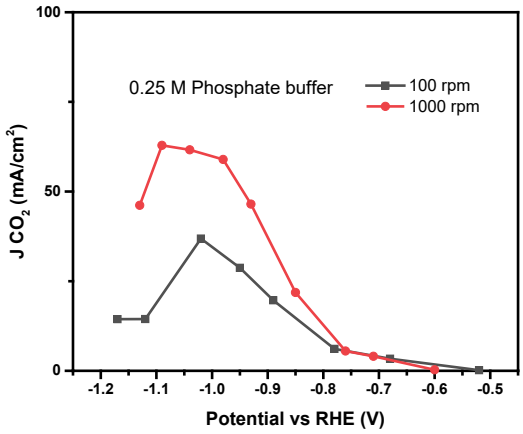

Figure A.11: Effect of stirring on the partial current density of CO_2 reduction.

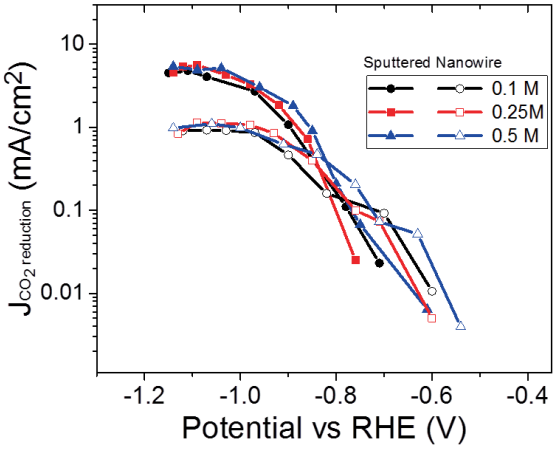

Figure A.12: Electrochemically active surface area normalized partial current density for CO_2 reduction.

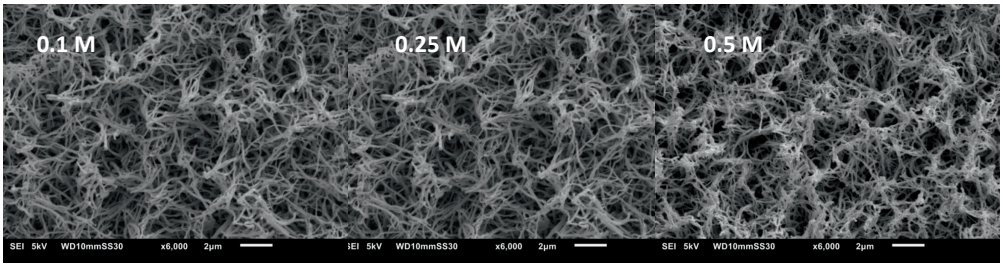

Figure A.13: SEM images of the copper nanowires after electrolysis in different phosphate buffer concentrations.

B

Role of the carbon-based gas diffusion layer on flooding in a GDE cell

Discussion regarding the onset of flooding due to Electrowetting

The microporous layer (MPL) of a GDL is composed of an inhomogeneous mixture of carbon nanoparticles and PTFE. The solid surfaces exposed to the electrolyte (present through the MPL) are then combinations of pure PTFE and exposed carbon which each have a different surface tension between their surface and the electrolyte. Under an applied potential, materials can exhibit electrowetting due to the applied electric field, which effectively lowers the free energy between the solid and liquid. The solid-liquid surface tension (γ_{SL}) then decreases, which manifests as a decrease in the macroscopic contact angle (θ) as a result of Young's Equation, while the other two surface tensions remain fixed (γ_{SG} and γ_{LG}):

$$\cos\theta = \frac{\gamma_{SG} - \gamma_{SL}}{\gamma_{LG}} \tag{B.1}$$

As the exposed carbon nanoparticles experience a drop in θ_{carbon} with applied potential, a capillary force (P_C) will arise that tries to drive electrolyte into the pores of the MPL, as long as $\theta < 90°$ as per the Young-Laplace equation below. For pores with small radii, r, these capillary forces can result in a substantial driving force.

$$P_C = P_L - P_V = \frac{2\gamma\cos\theta}{r} \tag{B.2}$$

In an MPL, however, the PTFE surfaces are intentionally engineered to provide the opposite capillary forces because of a higher contact angle for PTFE, $\theta > 90°$. Thus, an individual pore in an MPL will be expected to flood when the overall capillary pressure of the combined carbon/PTFE surfaces within a given pore is a positive value. We hypothesize that electrowetting of the carbon surface is sufficient to cause such a scenario. Higher potentials will decrease θ_{carbon} values, which result in greater overall capillary pressures causing

faster flooding of the MPL.

We note that the pores of an MPL are quite inhomogeneous, and will sometimes have more exposed carbon than PTFE, and vice versa. Whether individual pore throats result in a positive or negative capillary pressure can then vary with the applied potential, with an increasing number of flooding pores as the applied potential increases.

Table B.1: surface atomic ratio of C, F and O on different GDLs

	Surface Atomic Ratio (%)			
Peak	no potential	- 0.51 V	- 0.68 V	- 0.83 V
C 1s (-CC-)	48.99	53.83	53.86	52.71
C 1s (-CF2-)	13.97	13.43	13.31	13.88
F 1s	36.10	31.52	31.13	31.78
O 1s	0.94	1.22	1.7	1.63

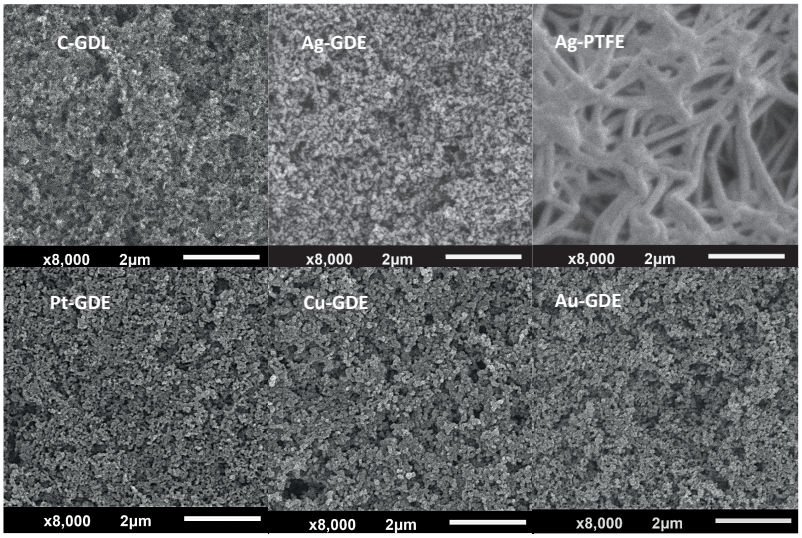

Figure B.1: SEM images of different catalyst deposited GDLs before electrochemical tests.

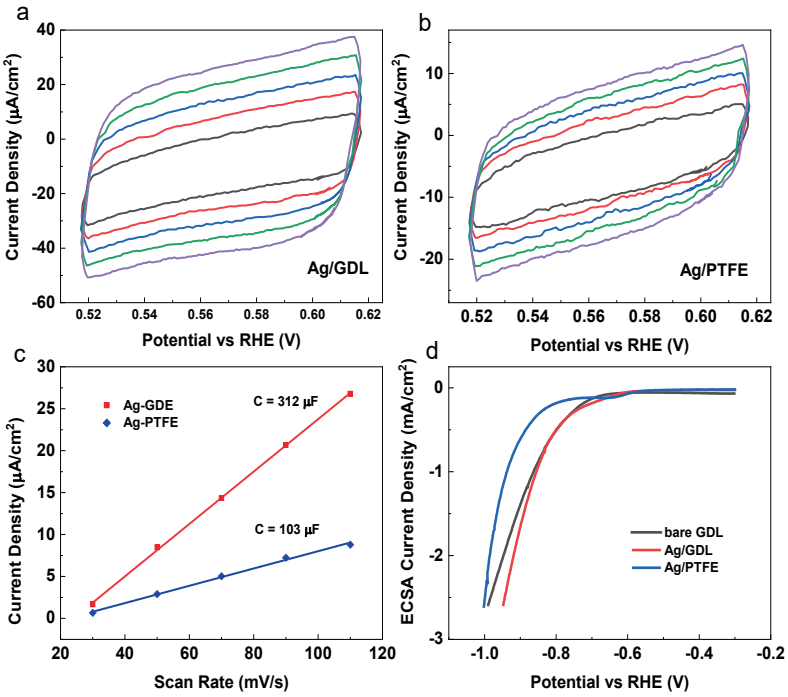

Figure B.2: Surface roughness factor of Ag/GDL and Ag/PTFE and their ECSA normalized LSV scans.

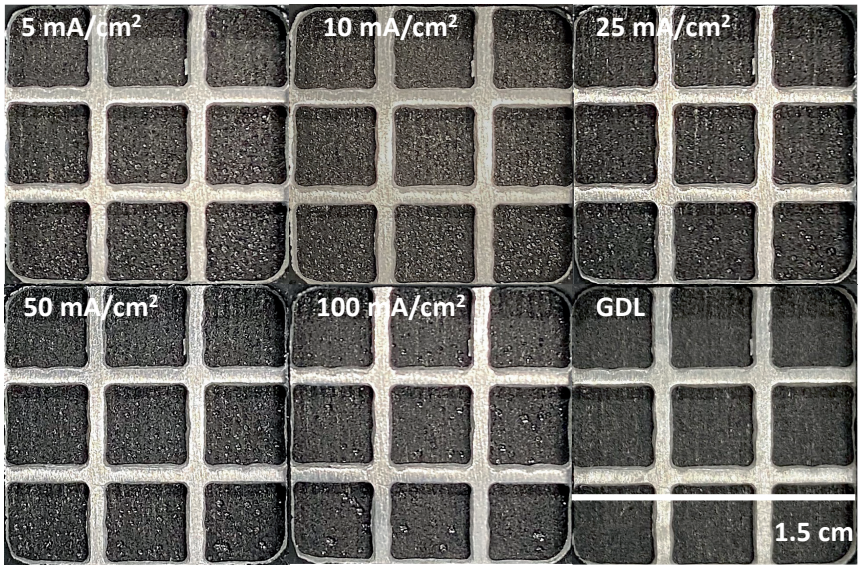

Figure B.3: Pictures of flooded GDEs after CO_2 reduction at different current densities.

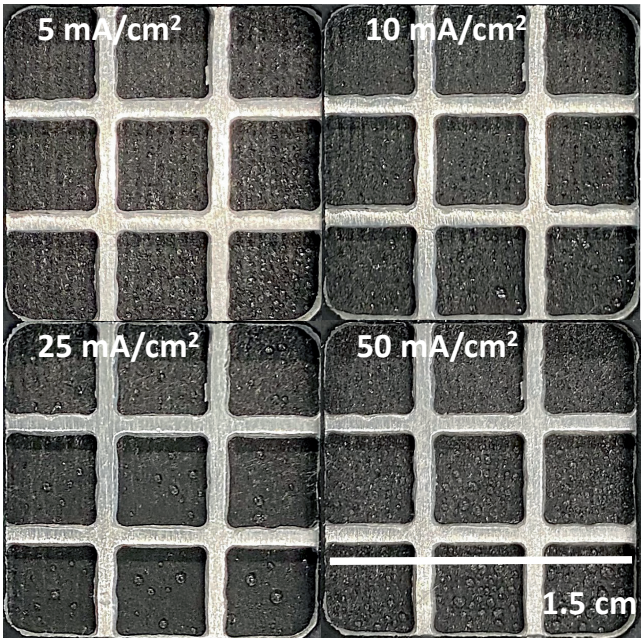

Figure B.4: Pictures of flooded GDEs after H_2 evolution reactions at different current densities.

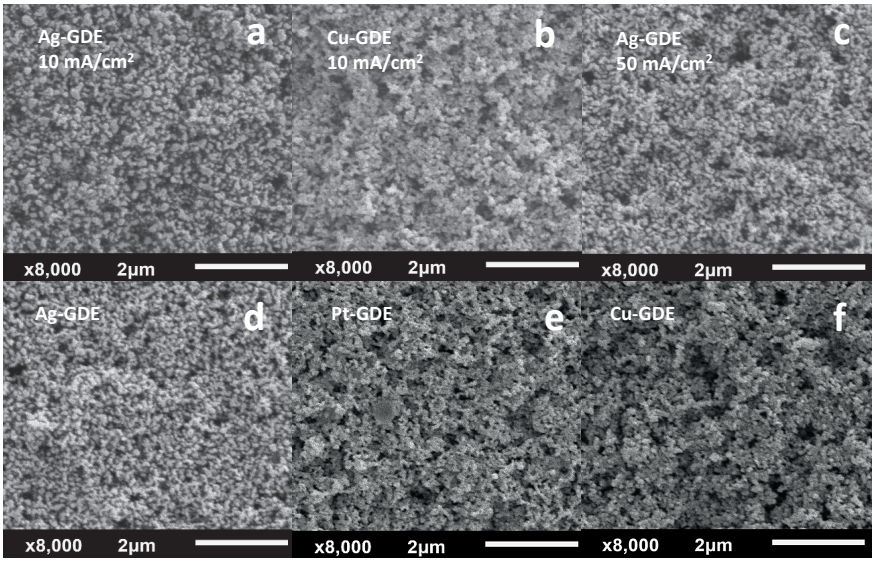

Figure B.5: (a-c)SEM images of different catalyst deposited GDLs after ECO2R;(d-f)SEM images of different catalyst deposited GDLs after HER at 10 mA/cm^2.

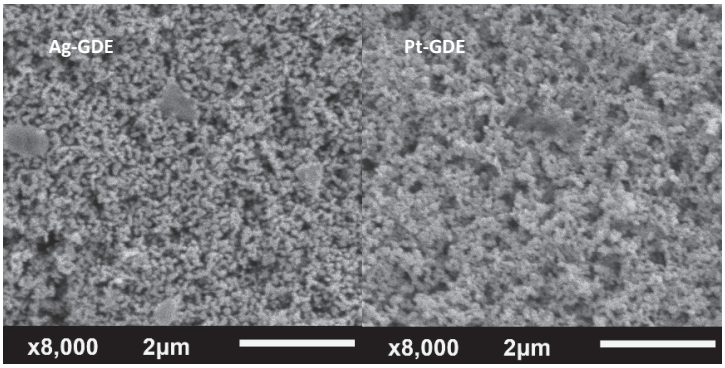

Figure B.6: SEM images of different catalyst deposited GDLs after HER at 50 mA/cm^2.

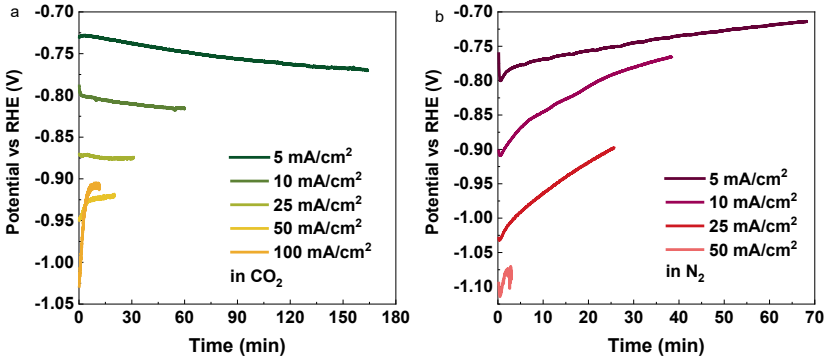

Figure B.7: Potentials and time when flooding happened for ECO2R (a) and HER (b) at different current densities (mA/cm^2).

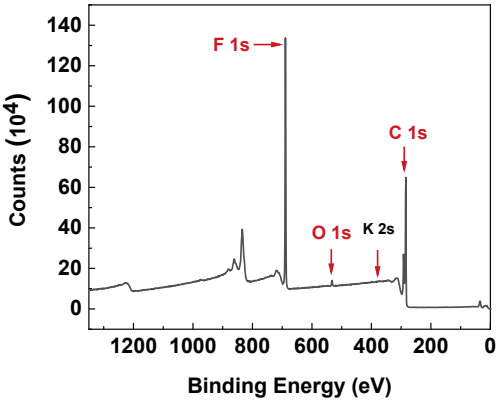

Figure B.8: XPS surface survey scan of the GDL sample after chronoamperometry under – 0.68 V vs RHE.

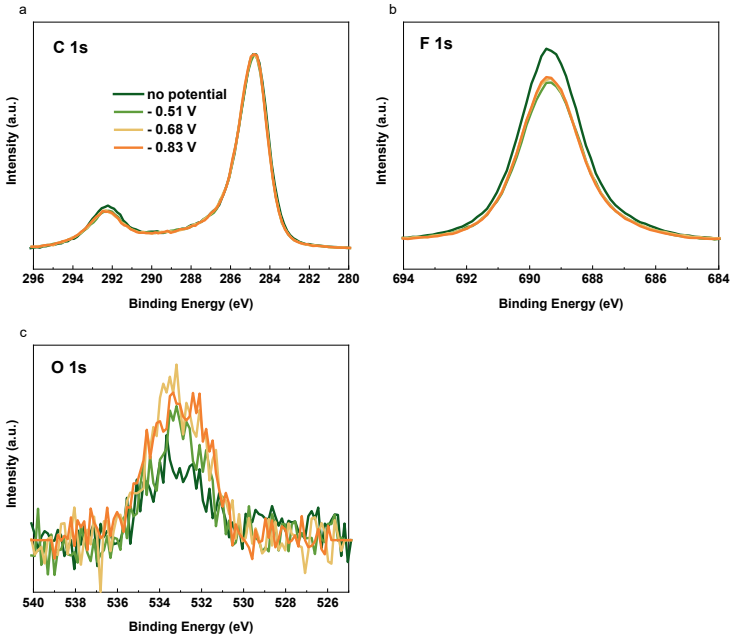

Figure B.9: C 1s (a), F 1s (b) and O 1s (c) XPS spectra of different GDLs after etching the surface for 5 seconds.

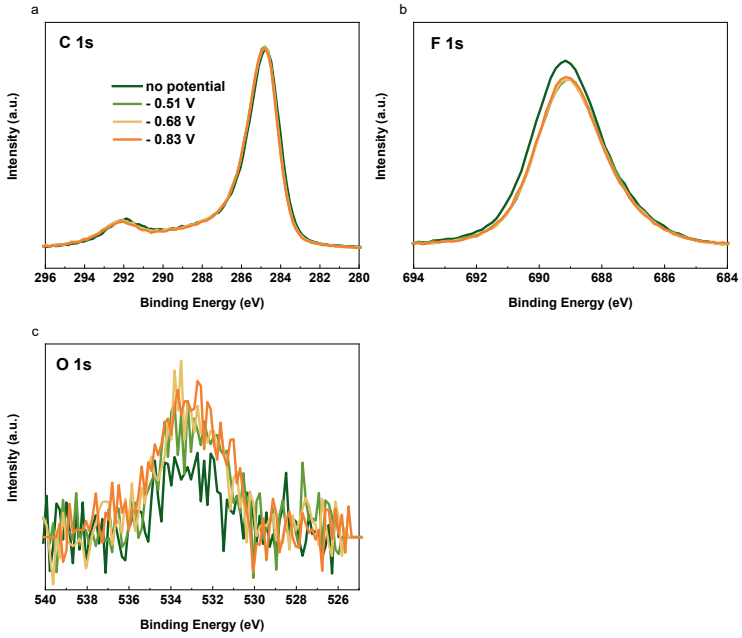

Figure B.10: C 1s (a), F 1s (b) and O 1s (c) XPS spectra of different GDLs after etching the surface for 45 seconds.

C

Cation-driven increases of CO_2 utilization in a BPMEA for CO_2 electrolysis

Equations:

$$CO_2 + H_2O + 2e^- \Rightarrow CO + 2OH^- (-0.11 \text{ V vs RHE}) \quad (1)$$

$$2H_2O + 2e^- \Rightarrow H_2 + 2OH^- \quad (0 \text{ V vs RHE}) \quad (2)$$

$$CO_2 + OH^- \Leftrightarrow HCO_3^- \quad (3)$$

$$HCO_3^- + OH^- \Leftrightarrow CO_3^{2-} + H_2O \quad (4)$$

$$CO_2 + 2OH^- \Leftrightarrow CO_3^{2-} + H_2O \quad (5)$$

Table C.1: pH of anolyte before and after CO_2 reduction in both BPMEA and AEMEA cells

	BPM		AEM	
solution	before	after	before	after
0.2 M KOH	13.5	13.48	13.5	7.46
1 M KOH	14	14.08	14	13.55
3 M KOH	14.6	14.6	14.6	14.5
0.2 M KOH + 0.4 M K_2CO_3	13.54	13.52		

Table C.2: Cell resistance of BPMEA and AEMEA cells in different solutions

Cell resistance (ohms)	BPM	AEM
0.2 M KOH	0.6	0.17
1 M KOH	0.75	0.18
3 M KOH	1.1	0.13
0.2 M KOH + 0.4 M K_2CO_3	1	

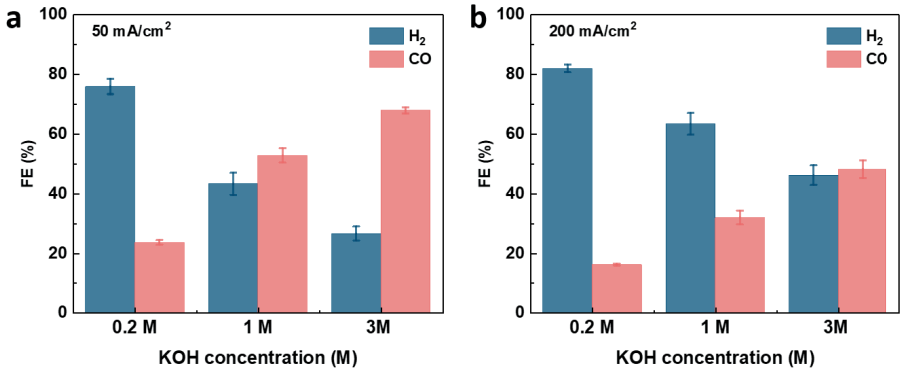

Figure C.1: Faradaic efficiency of H_2 and CO as function of KOH anolyte concentrations at 50 and 200 mA/cm^2 in BPMEA cell.

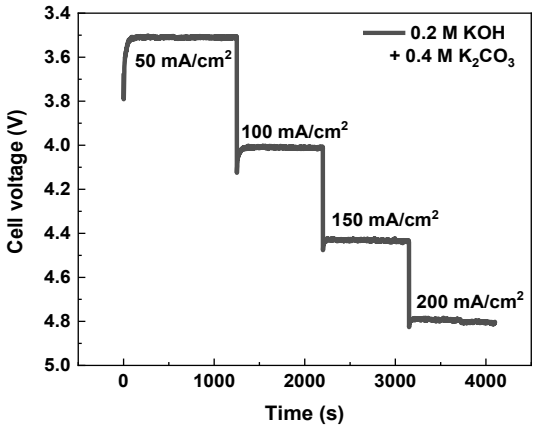

Figure C.2: Cell voltage at different current densities in a BPMEA cell in 0.2 M KOH + 0.4 M K_2CO_3 electrolytes.

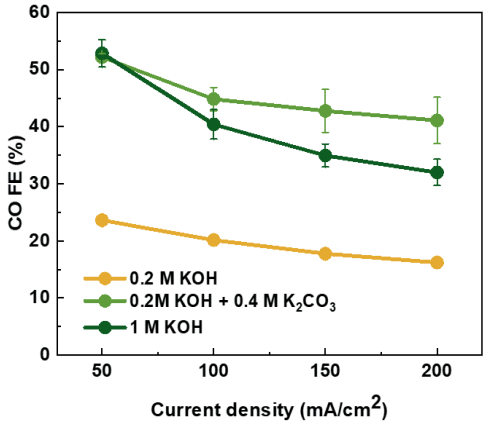

Figure C.3: CO Faradic efficiency in different concentrations of electrolyte.

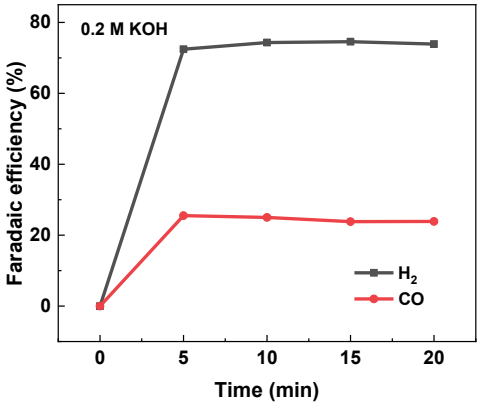

Figure C.4: Faradaic efficiency as function of time in a BPMEA cell using 0.2 M KOH anolyte.

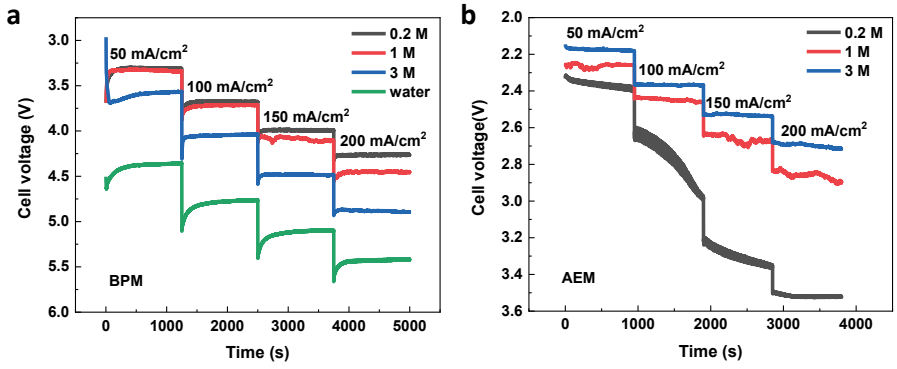

Figure C.5: Cell voltage at different current densities in a BPMEA and a AEMEA cell in different electrolytes.

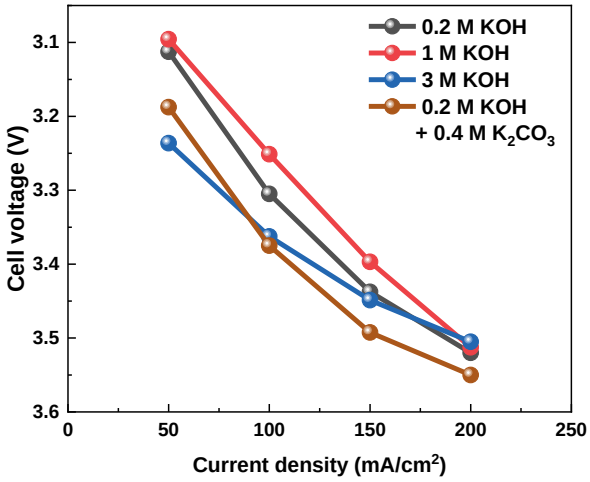

Figure C.6: Ohmic resistance corrected cell voltage as function of current density in a BPMEA cell in different electrolytes.

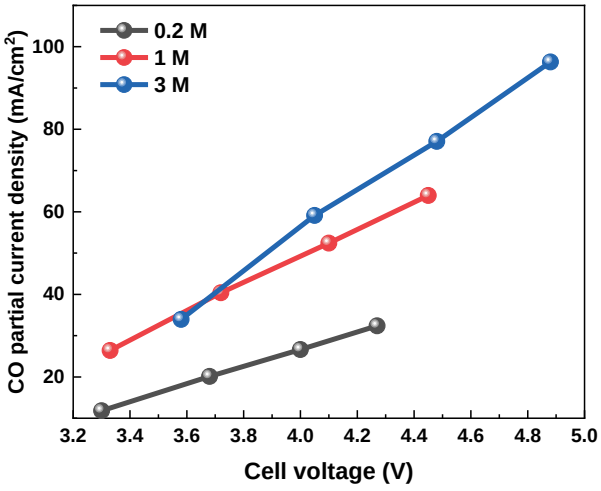

Figure C.7: Partial current density of CO as function of cell voltage in different electrolytes.

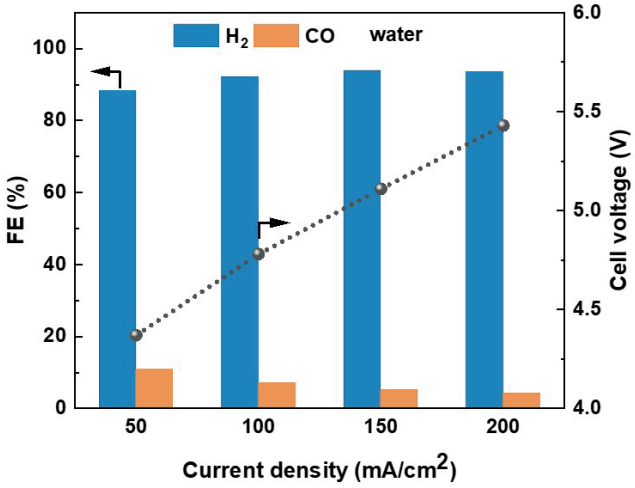

Figure C.8: Faradaic efficiency and cell voltage as function of current density using water as anolyte in a BPMEA.

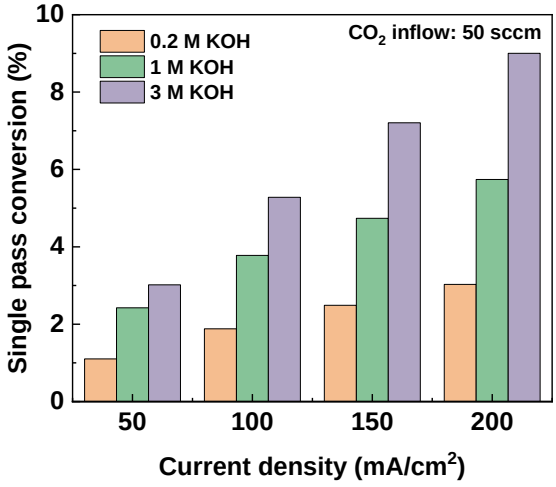

Figure C.9: Single pass conversion of CO_2 reactant in a BPMEA cell.

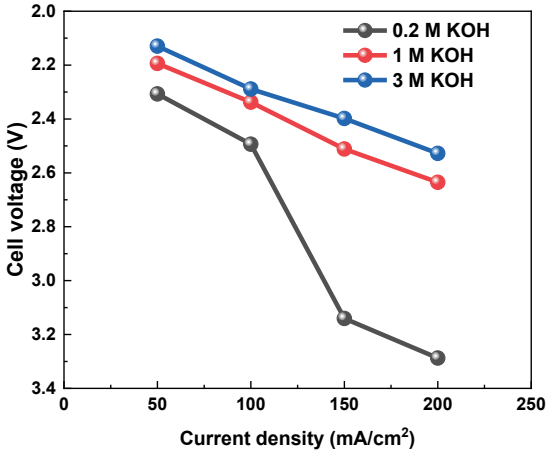

Figure C.10: Ohmic resistance corrected cell voltage as function of current density in a AEMEA cell in different electrolytes.

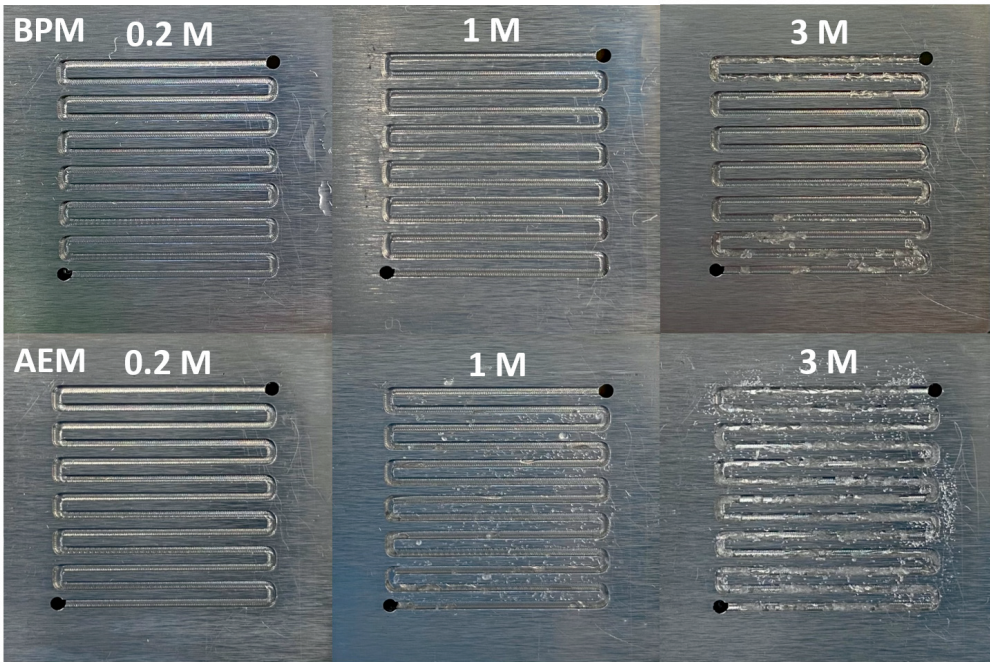

Figure C.11: CO_2 flow field after ECO2R in both BPMEA (80 min) and AEMEA cells (60 min) with varying current density from 50 mA/cm^2 to 200 mA/cm^2 in different KOH concentration electrolytes.

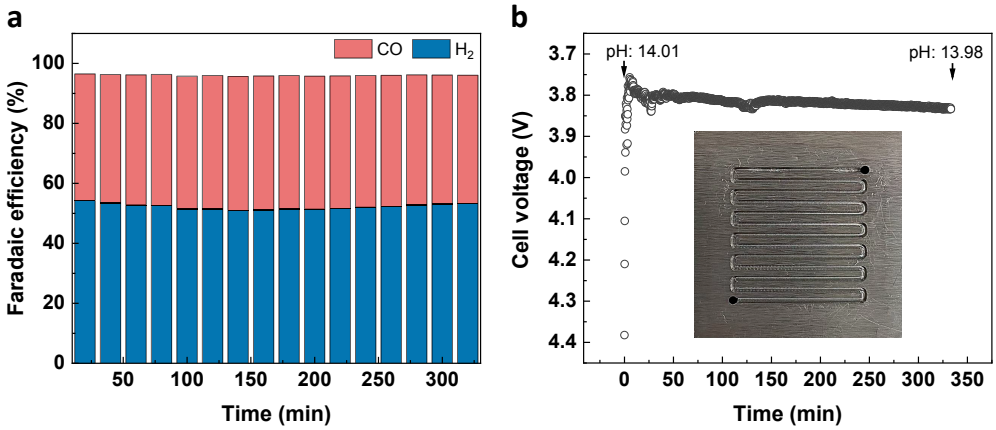

Figure C.12: CO and H_2 Faradaic efficiency at 100 mA/cm^2 current density during 5.5 hours operation in a BPMEA. Inserted in figure b) shows the gas channel after CO_2 reduction test.

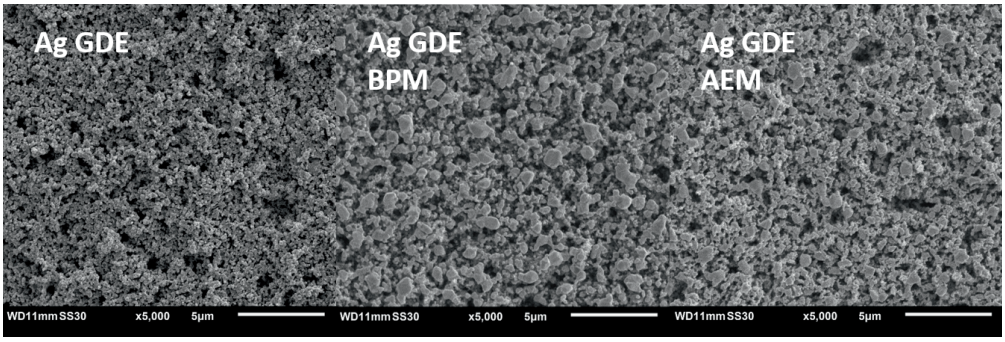

Figure C.13: SEM image of Ag GDE before and after ECO2R in both BPMEA and AEMEA cells with varying current density from 50 mA/cm^2 to 200 mA/cm^2 in different KOH concentration electrolytes.

Summary

The concept and necessity of an "energy transition" has become well-known as the general public acknowledges the severe consequences of climate change. As a side effect of industrial revolution, which has brought advances to modern society by burning fossil fuels, pollutants and greenhouse gases are also released to the atmosphere. As a result, the liveability of earth has dropped substantially, and there exists an urgent need to address decarbonization and energy transition. As a society, we must achieve net-zero by mid of this century to prevent major disasters from happening.

The majority of public efforts towards an energy transition has been to seek renewable energies as alternatives for energy demand, such as wind, solar, hydro power, biomass energies etc. Electricity is the main product from these renewable energies and its price (generated from solar and wind) can already compete with fossil fuel based power plant. With such low cost in favour, industrial processes already powered by electricity can replace this electricity with renewable electricity. Additionally, access to cheap and clean electricity has led some industrial processes to focus on process electrification. For processes which are extremely difficult to electrify, fossil fuels can still be used as long as the generated carbon can be sufficiently removed from the atmosphere. In this regard, carbon capture, usage and storage (CCUS) also plays an essential role and needs to be further investigated.

As discussed in this thesis, electrochemistry provides the potential to fill in the gaps between electricity storage, chemical fuels usage and carbon removal. For example, captured carbon dioxide and nitrogen can be electrochemically reduced to chemicals or fuels, using renewable electricity, to power industrial sectors. Among the proposed electrochemical processes, carbon dioxide reduction has attracted major attention due to its relative mature technological achievements. Mechanism studies in the past decades have provided insight into fundamentals of CO_2 electrolysis both from microscale and macroscale. Besides the discovery of effective catalysts, the system design has also been improved based on deeper understandings.

Electrochemical CO_2 reduction (ECO2R) originated from a conventional H-cell. In an H-cell the concepts of high local pH and low local CO_2 concentration are widely known, due to the mechanism of electrochemical reactions and sluggish mass transport which confines operation to liquid-dominated diffusion regimes. In the first work of this thesis, we sought to increase the CO_2 concentration at the reaction interface by using strong phosphate buffer solutions to mitigate the high local pH, thus enhancing CO_2 reduction activities in such liquid systems. Firstly we measured the in situ local pH and CO_2 concentration by surface enhanced infrared absorption spectroscopy (SEIRAS) and later verified the experimental results with a computational model. Furthermore, we tested the activity and selectivity of electrochemical CO_2 reduction in the buffer solution on Cu electrodes in a actual liquid cell system. Results from SEIRAS, model and ECO2R all showed that buffer solution only functioned to enhance hydrogen evolution reaction (HER). At similar potential, excessive amount of hydroxide ions (OH^-) produced from HER in a stronger buffer still caused the

rise of pH near the reaction interface, thus low CO_2 concentration. This work showed reaction rate of CO_2 electrolysis cannot attain the commercially relevant value due to mass transport limitations in aqueous cell at ambient pressure and temperature. With this consideration, separating the CO_2 gas with liquid electrolyte feed such as using a gas diffusion electrode (GDE) serves as a viable solution to boost the reaction rate.

Employing gas diffusion electrode in a flow cell has improved the mass transport of CO_2 significantly. In the meantime, alkaline electrolytes can be used to favour ECO2R and suppress HER. Activity has been increased by more than one order of magnitude higher, with high selectivity to desired products. However, gas and liquid balance at the reaction interface should be taken into extra considerations, as flooding is a well-known phenomenon in such GDE flow cells. Among all the mechanisms proposed in literature, the second work of this thesis hypothesized that flooding might be related to the electrochemical reaction of CO_2 reduction on catalyst layer (CL) , in relation to the electrochemical reactions happening on carbon-based gas diffusion layer (GDL). We tested the electrochemical activity of CO_2 reduction and hydrogen evolution on bare carbon GDL, Ag GDL, Cu GDL, Au GDL and Pt GDL. The fact of long stability reached on Pt for HER, and Cu for ECO2R compared with Ag demonstrated that the potential applied to the carbon support is the critical factor causing flooding, as compared to the catalyst directly. The non-ideal kinetics of ECO2R on current catalysts requires high overpotential, which leads to the high cathodic potential that induces electrowetting, thus liquid can wet the hydrophobic surface of GDE more easily. When this happens, liquid enters and wets the pores inside of carbon GDL. With the favourable potential, carbon can perform HER which leading to unstoppable flooding and quick failure of the system. Exploring new catalysts with better activity as well as designing GDL specifically for ECO2R should be again emphasized in the field.

With high selectivities and elevated current densities being acheived, a new challenge identified in CO_2 electrolysis is loss of CO_2 to (bi)carbonate, which makes the gaseous CO_2 electrolyzer less commercially feasible due to low energy efficiency and instability induced by (bi)carbonate salts. ECO2R in acidic media has attracted attention as a possible means to avoid (bi)carbonate formation, with a proton from the catholyte or membrane supplied to negate hydroxide formation. Such approaches have significantly increased CO_2 utilization with decent activity by mediating the local environment. Membrane based alternative has the advantage of linking the H^+ concentration with current density. Bipolar membrane (BPM) serves as good candidate. BPMs can not only provide H^+ under reversed bias, but also allow the use of alkaline anolyte, thus earth-abundant catalysts as anode. However the reported membrane electrode assembly couple with BPM showed low activity towards ECO2R. In the final work of this thesis, we hypothesized that this might be caused by the low cation concentrations on the catalyst surface, as cations were proved necessary to initiate ECO2R. On the contrary BPM can effectively prevent ion crossover, thus the cation cannot create a favourable electric field at the reaction interface to favor CO_2 reduction. We then increased the cation availability by concentration gradient induced diffusion and migration, and observed 3 time higher Faradaic efficiency to CO in such system. While comparing the CO_2 utilization of using BPM with common anion exchange membrane (AEM) in a MEA, we also achieved 2-3 times higher efficiency. We demonstrated that BPMEA can function as an effective system for high CO_2 conversion with proper engineering of cathode and cation source in future.

Overall the electrochemical reaction induced high local pH and the unavoidable competing HER have introduced complexity to CO_2 electrolysis. This thesis provides fundamental understanding of the local chemistry during ECO2R in different electrolyzers: aqueous cell, GDE flow cell and MEA cell, and gives insight into solutions and suggestions regarding the challenges mentioned. Together with the work from other researchers in this field, I am positive that all the challenges will be overcome one by one. With continued advancements occurring at the rates of recent years, electrochemical CO_2 reduction will be an important part in the process of energy transition and de-carbonation.

Samenvatting

Het concept van een “energie transitie” en de noodzaak ervan wordt breed gedragen sinds men de gevaarlijke consequenties van klimaatverandering erkent. Als een neven-effect van de industriële revolutie, welke voor vooruitgang en welvaart heeft gezorgd in onze moderne maatschappij door het verbranden van fossiele brandstoffen, zijn er vervuilende stoffen en broeikasgassen vrijgekomen in onze atmosfeer. Het resultaat daarvan is dat de leefbaarheid van onze planeet onder druk is komen staan, wat op haar beurt de urgentie creëert om met “de-carbonization” en de energie transitie aan de slag te gaan. Als maatschappij moeten we halverwege deze eeuw CO_2 neutraal zijn geworden om ernstige rampen, als gevolg van de opwarming van de aarde, te voorkomen.

Het overgrootte deel van de publieke inspanningen voor het maken van de energie transitie richt zich op het ontwikkelen van hernieuwbare energiebronnen als alternatief voor fossiele energie, zoals wind, zon, waterkracht en biomassa. De meeste hernieuwbare energiebronnen produceren elektriciteit en de prijs (voornamelijk uit zon en wind) is al economisch competitief in vergelijking met elektriciteitsproductie uit energiecentrales die gebruik maken van fossiele brandstoffen. Met dusdanige lage elektriciteitsprijzen, kan voor huidige elektrische industriele processen de elektrische energievraag eenvoudig vervangen worden door groene stroom. Bovendien is de beschikbaarheid van goedkope groene stroom een drijfveer voor investeren in elektrificatie van andere industriele processen. Voor processen waarbij het een zeer grote uitdaging is om ze te elektrificeren, kan voorlopig nog gebruik gemaakt worden van fossiele brandstoffen, zolang de geemitteerde CO_2 in voldoende mate kan worden verwijderd uit de atmosfeer. Oplossingen als CCS, Carbon Capture and Storage (of Usage; CCU) kunnen een essentiële rol spelen hierin en moeten verder worden onderzocht.

Zoals in deze thesis besproken wordt, elektrochemie kan in potentie een oplossing bieden voor opslag van elektrische energie, maken (en gebruiken) van chemische brandstoffen (elektrofuels) en verwijderen van CO_2 uit de atmosfeer. Afgevangen CO_2 kan bijvoorbeeld elektrochemisch gereduceerd worden tot bruikbare chemicaliën of brandstoffen, hierbij gebruik makend van hernieuwbare elektriciteit. Onder de voorgestelde elektrochemische processen, heeft elektrochemische CO_2 reductie de meeste aandacht getrokken vanwege zijn vergevorderde technologische ontwikkeling. Studies naar de mechanismen in de afgelopen decennia hebben inzichten verschaft in de fundamentele principes achter CO_2 elektrolyse, zowel op microschaal als macroschaal. Naast de ontdekking van effectieve katalysatoren, is ook het systeem zelf verbeterd door het betere begrip ervan.

Elektrochemische CO_2 reductie is ontstaan uit een conventionele H-cell. In een H-cell de concepten van hoge lokale pH en lage lokale CO_2 concentratie zijn breedgedragen theorieën door het mechanisme van elektrochemische reacties en traag massa transport welke een vloeistof diffusie regime laten domineren. In het eerste werk van dit proefschrift, is geprobeerd te zoeken naar een methode om de CO_2 concentratie aan het reactie interface

te verhogen door gebruik te maken van sterke fosfaat buffer oplossingen, welke de hoge lokale pH moeten bestrijden, waardoor de CO_2 reductie activiteit in het vloeistof systeem verhoogd wordt. Als eerste is de in situ lokale pH en CO_2 concentratie gemeten door gebruik te maken van "surface enhanced infrared absorption spectroscopy (SEIRAS), vervolgens zijn deze metingen geverifieerd met een model. Verder zijn de activiteit en selectiviteit van elektrochemische CO_2 reductie (ECO2R) in de buffer oplossing bij Cu (koper) elektrodes in een vloeistof cell systeem gemeten. De resultaten van SEIRAS, het model, en ECO2R lieten allen een vergelijkbaar beeld zien dat de buffer oplossing alleen werkt om de hydrogen evolution reaction (HER) te stimuleren. Bij gelijke potentialen, een overdaad aan hydroxide ionen (OH^-) die vrijkomen door de productie van waterstof (als gevolg van HER) in een sterkere buffer laat alsnog een verhoging van de lokale pH bij de reactie interface zien, en dus een lage CO_2 concentratie. Dit werk laat zien dat de reactie snelheid van CO_2 elektrolyse niet in de buurt komt van commercieel levensvatbare waardes door de problemen met massa transport limitaties in aqueous cells (H-Cell) bij normale temperatuur en druk. Met deze kennis, is het scheiden van het CO_2 gas van het vloeibare elektrolyt, bijvoorbeeld door gebruik te maken van een "Gas Diffusie Elektrode" (GDE) een mogelijke uitweg om de reactie snelheid een "boost" te geven.

Het gebruik van een gas diffusie elektrode in een "flow cell" heeft het massatransport van CO_2 naar het reactie oppervlak significant verbeterd. In de tussentijd wordt alkaline elektrolyten gebruikt om de ECO2R te bevorderen ten opzichte van de HER, die juist wordt onderdrukt in basisch milieu. De activiteit is met een ordegrootte verbeterd, met daarbij hoge selectiviteit naar de gewenste producten. Echter, de gas en vloeistof balans bij de reactie interface moet nauwlettend in de gaten worden gehouden, omdat "flooding" een veelvoorkomend probleem is. Na alle mechanismen die worden voorgesteld in de literatuur, wordt in het tweede werk van dit proefschrift een hypothese toegevoegd die stelt dat het probleem van "flooding" mogelijk oorzaak heeft door de elektrochemische reactie van CO_2 reductie op de katalyse laag, in relatie tot de elektrochemische reacties die verlopen op de carbon-based gas diffusie laag (GDL). In het onderzoek is de elektrochemische activiteit van CO_2 reductie en waterstof evolutie (HER) onderzocht op "kale" carbon GDL substraat, zilver(Ag) geladen GDL, koper(Cu) geladen GDL, goud(Au) geladen GDL en platina(Pt) geladen GDL. Het feit dat lange stabiliteit werd behaald op Pt geladen GDL voor de HER, en Cu geladen voor de ECO2R, in vergelijking met Ag laat zien dat de toegepaste potentiaal op het carbon substraat een kritische factor is in de mate waarop flooding optreed, in vergelijking met de katalysator direct. De niet-ideale kinetiek van ECO2R op huidige katalysatoren vereist een hoge overpotentiaal, wat leidt tot de hoge kathodische potentiaal die elektrowetting induceert, waardoor vloeistof het hydrofobe oppervlak van GDE gemakkelijker kan bevochtigen. Wanneer dat gebeurt kan de vloeistof (het elektrolyt) makkelijker de poriën indringen en de GDL steeds verder naar binnen toe bevochtigen. Met het juiste potentiaal kan koolstof zelf ook de HER faciliteren wat leidt tot versterken van ''flooding" en een snel falen van het systeem. Het ontwikkelen van nieuwe katalysatoren met hogere activiteit in combinatie met het ontwerpen van GDL die specifiek geschikt zijn voor ECO2R moeten opnieuw meer aandacht krijgen in het wetenschappelijke veld.

Nu hoge selectiviteit en verbeterde current densities bereikt zijn, ligt er een nieuwe uitdaging in de wereld van CO_2 elektrolyse. Het verlies van CO_2 door de reactie tot (bi)carbo naat, wat de gas diffusie CO_2 elektrolyse minder commercieel interessant maakt door de lagere energie efficiëntie en instabiliteit die wordt veroorzaakt door de vorming van (bi)carbonaat

zouten. ECO2R in zure milieus heeft de aandacht getrokken door de mogelijkheid tot het voorkomen van (bi)carbonaat vorming. In zuur milieu voorkomen de protonen afkomstig van de catholyte of het membraan de vorming van hydroxide ionen. Deze aanpak heeft de benutting van CO_2 gas significant verbeterd met als gevolg verhoogde activiteiten, door het behouden van het lokale pH milieu. Het op het gebruik van een membraan gebaseerde alternatief heeft als voordeel dat de H^+ concentratie gekoppeld wordt aan de current density. Een bipolair membraan (BPM) dient als een goede kandidaat. BPMs kunnen niet alleen H^+ leveren onder "reversed bias" (omgekeerd potentiaal). Maar staan ook het gebruik van alkaline anolyte toe, en daarmee goedkope veelvoorkomende katalysatoren als anode. Echter, de gerapporteerde membraan electrode assembly (MEA) waarbij gebruik wordt gemaakt van een BPM liet vooralsnog een lage activiteit zien voor de ECO2R. In het laatste deel van het werk uit deze thesis wordt de hypothese gesteld dat dit mogelijk het gevolg is van lage kationen concentraties aan het katalysator oppervlak. Aangezien eerder werd aangetoond dat kationen noodzakelijk zijn om de ECO2R te initiëren. Daartegenover staat dat een BPM goed in staat is om ion-crossover tegen te gaan, dus het kation kan geen wenselijk elektrisch veld aan het reactie oppervlak creëren wat CO_2 reductie zal bespoedigen. Daarna is de kation beschikbaarheid vergroot door concentratie gradiënt geïnduceerde diffusie en migratie, waarbij een drie keer hogere Faradaic efficiëntie naar CO is geobserveerd in het systeem. Vergelijken van de CO_2 benutting van het gebruik van BPM met gemeenschappelijk AEM (anionic exchange membrane) in een MEA laat zien dat de efficiëntie twee tot drie keer hoger is. In dit werk wordt aangetoond dat een BPMEA systeem kan functioneren als een effectieve methode voor hoge CO_2 omzetting met een zorgvuldig ontworpen kathode met kationen bron in de toekomst.

Over het algemeen hebben de elektrochemische reactie geleid tot een hoge lokale pH en de onvermijdelijke concurrerende HER hebben de CO_2-elektrolyse complexer gemaakt. Het beschreven werk in deze thesis geeft een fundamenteel begrip van de lokale chemie tijdens de ECO2R in verschillende typen elektrolyzers: de 'normale' (aqueous) H-Cell, de GDE flow cell en de MEA cell, en geeft inzichten in oplossingen en suggesties voor de genoemde uitdagingen. Samen met het werk van andere onderzoeksgroepen in dit werkveld, ben ik positief gestemd dat alle uitdagingen uiteindelijk zullen worden overwonnen. Met een voortgang van de snelheid van progressie zoals die afgelopen jaren is gegaan zou elektrochemische CO_2 reductie een belangrijke rol kunnen spelen in het proces van energie transitie en werken naar een CO_2 arme energie voorziening.

Acknowledgements

To be honest, I never thought I could finish my PhD when I started it. And now here I am, writing the very last part of my thesis. It would not be complete without looking back of course. When I look back, there were so many people I am grateful for, who have helped me to deliver this very thesis to your hands. So no particular order, I would like to thank:

Dr. Wilson Smith. Thank you for hiring me and inviting me to this lovely country and group. It has been a life-changing experience for me. You were always so positive and supportive of our work, which had given us the motivation to move forward. Later after being a supervisor myself, I realized how "risky" hiring was, putting a group of people together in harmony and letting them grow together as a scientist and a person. Yet you did it! Very successfully! Perhaps you had the "vision". **Dr. Tom Burdyny**. As my co-promotor, you have made my PhD journey much smoother despite all changes that have happened. I enjoyed all the projects I did together with you, all the scientific discussions, and all the conversations we had. You guided me to become a better researcher who enjoyed science more. Your rational and logical thinking changed my way of dealing with things. I am a better scientist, presenter, supervisor and person now all because of you. If I ever wanted to be a teacher, it must have been because of you - "Teacher of the Year"!

Prof. Bernard Dam. I would not be here if it was not for you either. You forwarded my application to Wilson, and that led to everything that happened afterward. I had so much to learn from you especially during our regular meetings. You taught me to reflect on things with a helicopter view, which is not only important for science, but also for personal development. **Prof. Hans Geerlings**. Thank you for being the committee member of all my master students' defenses. **Prof. Fokko Mulder** and **Prof. Andreas Schmidt-Ott**. Thank you for your valuable comments and feedback during MECS group meetings. **Joost** and **Herman**. The first two colleagues I met when Wilson gave me the lab tour. Then later **Bart**. Since then, the three trustworthy technicians have been there supporting my science. I enjoyed the all coffee breaks and borrel with you. **Roos**, thank you for all the support for administrative matters.

Dr. Recep Kas. I could not express how grateful I am to you. You were my colleague. We worked closely together for 3 years, even after you left TUD. You were so knowledgeable and yet so generous with your knowledge. You shared all the information that I ever asked for, but with more. Without you, there would be definitely no this doctor to be. You are my dear friend. We had so many interesting discussions about science, human, nature, culture, food and everything. You broadened my eyes, you made me more open-minded. You were also my mentor. You were there guiding and supporting me when I doubted myself. **Anirudh**, my angel, we sat together for 4 years. I still remember the big smile on your face when you saw me entering our office the first time. You are so sweet, knowledgeable and wise. I feel lucky that I could sit together with you during those years. Although our research didn't overlap much, we could always discuss our science for hours. I spilled all my troubles and complaints to you, amazingly you could always make me feel much better. **Mark**, so sweet

and caring. You always look after the newcomers and make them feel welcome. Thanks to you I quickly adapted to the life here. One can always have so much fun with you, you are the treasure of the group. **Sanjana** and **Marijn**. You came on the same day. Half a month later after me. Together with Ani, we spent our adventurous 4 years together. Thank you Sanjana for hearing out my troubles and showing support in those years. And one valuable thing I learned from Marijn was the "Dutch attitude". (Or you call it Belgian?) Confident, direct and decisive.

Now some relatively new P3T members. **Hugo**, maybe I shouldn't put you here. You were already here way before me. And **Sid**. Thank you two for being such lovely colleagues and critical scientists. What a summer school we had in Athens together with Sanjana! I would never forget that. Then some real doctors: **Aaron**, **Erdem** and **Maryam**. Thank you all for contributing your knowledge to this group and helping around! Aaron, you are so open to discussing and sharing knowledge, I learned a lot from you already although you just came here several months ago.

Giorgio, "the sweetest person on earth" said Recep. He was right, you are indeed so sweet and considerate. Lucky to share one office with you too! Here I also would like to thank all the other office mates I had: **Marco**, **Bartek**, **Dowon**. Dowon, your sense of humour and coolness always lighted my mood. **Martin**, I still don't know how we became good colleagues and friends, but it just happened. I think we share more commonality than we realized. I dream of us working together and becoming future entrepreneurs. **Robin**, being a German, you have so much humour in you, and it always made me laugh. **Davide**, I really enjoyed our conversations and discussions. You are a good listener with a sweet heart, and a great scientist. **Diana**, we co-supervised the 4 amazing LO2 students. That has left me some really nice memories. **Bernhard**, **Mark W**, **Pranav**, **Dylan**, **Peter**. Thank you for being such creative scientists and supportive colleagues. Dylan and Peter I couldn't hear enough of your conversations with Mark S.

Some people already left, but I still owe them my gratitude. **Fahimeh**, a girl full of positive energy. Thank you for supporting me through my difficult times. **Divya**, I enjoyed all our chitchat because your mind is full of interesting ideas. **Ming**, **Kai**, **Steffen**, **Nate**, **Nienke**, **Audrey**, thank you all for the company during the journey. There were also tons of master/bachelor students with who I worked together for months, I couldn't mention them all here, but I do would like to mention several who have made a difference in my life. **Nitin** and **Piyush**, you two master students taught me and trained me a lot when I just started in the lab. Thank you for making me a good start to my PhD study. I didn't want to thank **Nick**, you argued that you giving me mental support for a year during the process was worth an honourable mentioning. While I totally forgot all the fun time we had in the lab and coffee corners. But science remembers it for us instead, our young and beautiful figures, together with **Boaz** (Thank you too) will be on the ACS Energy Letters paper forever. My master students **Goncalo**, **Gaurav** and **Shiyu**. Thank you all for teaching me how to be a better supervisor and scientist. Gaurav and Shiyu, I am so proud of you two and I can't say that enough.

I also would to thank my dear colleagues and friends who were not from MECS group, but had been there for me. **Benjamin**, I learned how to make sushi from this German. **Ali**, **Jiashang**, **Zimu**, **Bowen**, **Guotai**, **Wenjun**, **Chuncheng**, **Kui**. Thank you all for the company, and the lunch breaks. My neighbours: **Alice (Qiyao)**, **Roger (Zhe)**, **Kimi (Yancong)** and

Xiujie. You are all my dear friends who I can always trust and count on. Our regular gathering for eating and gaming had added so much fun to my PhD life. Alice thank you for all the food and cakes you made for us, they were truly amazing. **Huanhuan** and **Meiqi**, I am grateful that you two girls were there with me during those years, cheering me up. You two are so special and have had a positive influence on me that I would never forget. **Pan**, thank you for your great company during the difficult corona time. Our dinners always made my day after work. My badminton community: **Jie R.**, **Xuan T.**, **Meng W.**, **Zhi H.**, also Alice and Roger, playing badminton with you guys was more fun than attending parties. My trainer and badminton partner **Master**, we just clicked! You always laughed at my jokes and thought I was super funny. That was great encouragement because I thought I seemed actually super boring to most people. And friends I met while learning Dutch. **Nicholas**, an American who is good at German, Dutch and appreiciating food and people. Cooking and eating together with you was always a feast. **Laura**, thank you so much for sharing with me thoes Dutch culture and stories. They have helped me to know better about Dutch people and this land. I always look forward to our next meetup and talking all kind of interesting topics with you.

4 years ago, **Chengyu**, **Shirong**, **Min**, **Peikai**, and I graduated from the same university, then came to this land together. Oh I can't forget the one in ETH Zürich, **Fuze** (NOT the founder of Fuze tea). You are all my dear friends, I know we are there for each other whenever needed. **Chengyu**, we have known each other for more than 7 years now. I owe you all the sweetness and understanding you gave me. I would also like to acknowledge my supervisor during my master study, **Prof. Jun Lin** and my colleague **Jia**. Thank you for setting me the road to where I am now. Words can't express my great gratitude to **Dr. Peng Wang**. You helped me and changed my life, twice. I wish I could also have a kind heart like yours. Finally, **Kayiu** and his family, thank you for making my life easier and making me happy. it means more than it sounds actually because even I can't do that for myself. You have made the Netherlands more home to me.

Some special thanks to **Congfei**, **Xuping**, **Yaxian**, **Dan**. I know you all for more than 10 years. I am so grateful that we maintained our friendship throughout the years even when we are spread out in different cities. You are the friends that even without seeing you or talking to you for years, I know I would feel we are never apart when we see each other again. Finally my dear family. Thank you **baba** and **mama**, you have always tried to be supportive of my decisions. I know that is not easy for you. But don't worry, I'm making all the right choices for myself. Thank you **Qin**, for keeping baba and mama company while I was abroad. And be a good kid! Thank you all, my **aunts**, **uncles**, **cousins**, **nephews** for putting such a lovely family together. Last but not least, I thank myself, **Kailun**! Past years were not always easy. I am very proud that I have progressed so much and have come this far, becoming the person I like more. I wish I could find more challenges and joy in the years to come!

Kailun
Delft, February 2022

List of Publications

10. R. Kas, **K. Yang**, G. P. Yewale, A. Crow, T. Burdyny, W. A. Smith. Modelling the local environment within porous electrode during electrochemical reaction of bicarbonate. *I&EC research*, 2022, under review.

9. M. Sassenburg, R. de Rooij, N.T. Nesbitt, R. Kas, S. Chandrashekar, N. J. Firet, **K. Yang**, K. Liu, M. A. Blommaert, M. Kolen, D. Ripepi, W. A. Smith, T. Burdyny. Characterizing CO_2 reduction catalysts on gas diffusion electrodes: comparing activity, selectivity and stability of transition metal catalysts. *ACS Appl. Energy Mater.*, 2022, under review.

8. **K. Yang**, M. Li, S. Subramanian, W. A. Smith, T. Burdyny. Cation driven increases of CO_2 utilization in a bipolar membrane electrode assembly for CO_2 electrolysis. *ACS Energy Lett.*, 2021, 6, 12, 4291-4298.

7. M. A. Blommaert, S. Subramanian, **K. Yang**, W. A. Smith, D. A. Vermaas. High indirect energy consumption in AEM-based CO_2 electrolyzers demonstrates the potential of bipolar membranes. *ACS Appl. Mater. Interfaces*, 2021, 14, 1, 557-563.

6. R. Kas, A. G. Star, **K. Yang**, T. Van Cleve, K. C. Neyerlin, W. A. Smith. Along the channel gradients impact on the spatioactivity of gas diffusion electrodes at high conversions during CO_2 electroreduction. *ACS Sustainable Chem. Eng.*, 2021, 9, 3, 1286–1296.

5. **K. Yang**, R. Kas, W. A. Smith, T. Burdyny. Role of the carbon-based gas diffusion layer on flooding in a gas diffusion electrode cell for electrochemical CO_2 reduction. *ACS Energy Lett.*, 2021, 6, 1, 33–40.

4. R. Kas, **K. Yang**, D. Bohra, R. Kortlever, T. Burdyny, W. A. Smith. Electrochemical CO_2 reduction on nanostructured metal electrodes: fact or defect? *Chem. Sci.*, 2020, 11, 1738-1749.

3. **K. Yang**, R. Kas, W. A. Smith. In situ infrared spectroscopy reveals persistent alkalinity near electrode surfaces during CO_2 electroreduction. *J. Am. Chem. Soc.*, 2019, 141, 40, 15891–15900.

2. **K. Yang**, J. Li, Y. Peng, J. Lin. Enhanced visible light photocatalysis over Pt-loaded Bi_2O_3: an insight into its photogenerated charge separation, transfer and capture. *Phys. Chem. Chem. Phys.*, 2017, 19, 251-257.

1. S. Han, J. Li, **K. Yang**, J. Lin. Fabrication of a β-Bi_2O_3/BiOI heterojunction and its efficient photocatalysis for organic dye removal. *Chinese J. Catal.*, 2015, 36, 2119–2126.

Curriculum Vitæ

Kailun Yang was born on December 18, 1991 in Handan, China. She received her Master degree of Engineering in Applied Chemistry from Renmin University of China in June 2017. Same year in September, she joined the Materials for Energy Conversion and Storage (MECS) group as a PhD student under the supervision of Dr. Wilson Smith and Dr. Tom Burdyny, at the Chemical Engineering department of TU Delft. Her research focuses on the fundamental understanding and system study of electrochemical carbon dioxide reduction reactions. Most results of her doctoral research are presented in this dissertation.